Syracuse University

SURFACE

Dissertations - ALL

SURFACE

August 2019

Carboxylic Acid Hydrodeoxygenation over Supported Noble Metal Catalysts

Joshua Gopeesingh
Syracuse University

Follow this and additional works at: https://surface.syr.edu/etd

Part of the Engineering Commons

Recommended Citation

ABSTRACT

Carboxylic acid hydrodeoxygenation (HDO) over supported noble metal catalysts was carried out in order identify the main challenges associated with supported monometallic catalysts and identifying solutions that may increase the practicality of these high activity metals. Using propionic acid as a probe molecule, it was found that supported platinum (Pt) and ruthenium (Ru) catalysts have two main issues: selectivity and stability. Both metals are quite unselective towards HDO products, multiple chemistries occur over the catalysts that lead to a myriad of undesired products. Decarbonylation (DCN) is the most selective pathway over Pt catalysts, while both DCN and methanation chemistries are heavily dominant over Ru catalysts. The high selectivity to DCN products for both catalysts snowballs into the second issue which is the lack of stability, carbon monoxide is a product of DCN which has an inibitive characteristic on the active metal sites; it essentially poisons the catalyst.

The addition of an oxophilic promoter metal, Tin (Sn), drastically improves the catalytic properties. PtSn bimetallic catalysts showed to be only selective to HDO products, and it also demonstrated a resistance to carbon monoxide poisoning. Investigations into PtSn catalysts using chemical adsorption, shows than Sn reduces the irreversible uptake capabilities of carbon monoxide onto Pt sites, which is indicative of the binding characteristics being altered. We developed a microkinetic model that sucessfully represents propionic acid HDO activity over Pt, while also being able to accurately provide useful kinetic parameters. Through applying microkinetic modelling, the energies associated with the species' interactions on the catalyst surface of both mono- and bi- metallic systems can be compared in order to pin point the source of what alters the catalyst behaviour.

Carboxylic Acid Hydrodeoxygenation over Supported Noble Metal Catalysts

by

Joshua Levi Emmanuel Judah Gopeesingh

B. Sc., Hampton University, 2014

Dissertation

Submitted in partial fulfillment of the requirements for the degree of

Doctor of Philosophy in Chemical Engineering

Syracuse University

August 2019

ACKNOWLEDGMENTS

taken care of me and assumed the role as my family when I was adjusting to being away from my parents.

I'd like to thank all the faculty and staff at Syracuse University. Professors Sureshkumar and Hasenwinkely, thank you for adopting me for the summer of 2013, it's an experience that made me feel at home being apart of the SU family; an experience that has brought me back for my doctorate. I'd also like to thank the staff in the office (past and present) for feeding me whenever free food was available in the office. I'd like to thank my thesis committee: Dr. Nangia, Dr. Hosein, Dr. Cybulskis, Dr. Tavlarides and Dr. Johnson for being apart of this final stretch of my journey at SU.

To the Bond Group, thank you for all contributing to experience, from giving advice to being there when I needed to talk about nonsense. I'd like to give special thanks to Christian, Omar and Argy, who were my first lab mentors when I was a naïve and bright eyed first year student, you've helped me through the initial stages of the PhD hurdles that had a lot to do with not giving up and being resilient; and even after you graduated, you have all continuted to mentor me to this point.

To my advisor, Dr. Jesse Bond, we were mean't to be from the moment I heard that you like rap music. You've taken me under your wing for the past 5 years, and showed me how to be a mentor to others. I believe that the environment you've created in your group is what makes it feel like a family, there's no feeling of intimidation to come in everyday and you've made yourself extremely approachable. I've never felt uncomfortable to express my anxiety during our interactions, and you've always been empathatic to how difficult the PhD journey can be for someone. As I close this chapter of my life, I hope we meet again on the outside. Maybe I might treat you to coffee since I won't be on a graduate student salary anymore.

TABLE OF CONTENTS

LIST OF TABLES

LIST OF FIGURES

CHAPTER 1

Introduction

1.1 Overview

The 19th century saw the industrial evolution which impacted the society for generations to come in ways that were unimaginable at the time; scientists realized that natural resources outside of woody biomass existed, that also had higher energy densities[1]. The world witnessed the birth and expansion of different markets as processes became more efficient through machinization. Coal and iron ore were the most common resources to meet the energy demands of a rapidly growing societal landscape, but little did the scientists know at the time that the main resource that fueled the industrialization at the time was just a stepping stone. The 20th century chaperoned the oil industry, oil became a resource so powerful that it affected the geographical, environmental and political landscape of the entire world[2]. This "black gold" had almost double the energy density of coal and a diverse composition that made it a building block for majority of the chemical industry today. Oil's reign (and fossil fuels as a whole) as the greatest resource was unquestioned until society started paying attention to the environment and found fossil fuel-related activities as major sources of pollution[3].

In a time of environmental awareness, studies have highlighted the roll of greenhouse gases on global warming and climate change (Figure 1.1). Greenhouse gases include carbon dioxide, methane, nitrous oxides and fluorinated gases; the species are listed in order of decreasing emissions based on a 2016 U.S. survey[4].
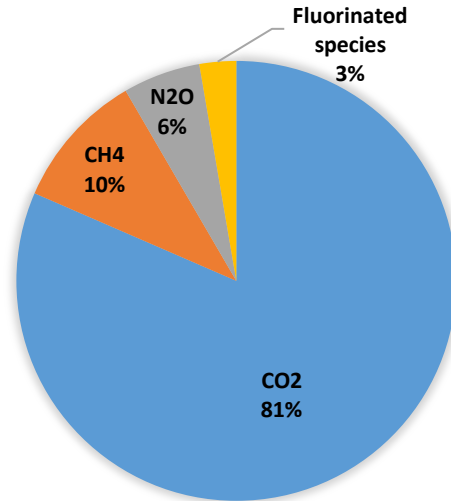
Figure 1.1: Contribution of different gasses to collective greenhouse emissions in the atmosphere[4].

The large amount of carbon dioxide emitted were mostly attributed to fossil fuel combustion and non-energy use of fuels from the sectors: transport, agriculture, industry, electricity and commercial and residential. While there has been developments on reducing emissions through carbon dioxide capture technology and exhaust filtering of industrial plants, solving the problem became non-trivial as two other aspects came to a forefront. The first is that fossil fuels are described as non-renewable resources; this means that current reserves cannot continue to sustain society's development indefinitely and would require expansion onto new and undiscovered reserves. The second aspect is that pollution by greenhouse gas emissions is only one dimension of fossil fuel's negative environmental impact; there are also many issues with waste management as well as land and water pollution. Different international agreements[5] have been set up to urge participating countries to take active roles in reducing its carbon footprints. To this end, countries are working towards diversifying their economies through incorporating renewable and "greener" resources[6].

There are many ways in which renewable resources can potentially infiltrate the energy landscape to meet societal needs. In terms of fuel, hydrogen and uranium have shown a far higher energy density than traditional gasoline, Table 1.1 below compares the energy densities of different fuel types[7].

Table 1.1: Energy densities of various fuels.

Resource	Energy Density (MJ/kg)
Wood	22.5
Coal	24
Bioethanol	26.8
Gasoline	47
Hydrogen	142
Uranium	79,390,000

Generating power can also be approached through different avenues from renewable resources; this sector of energy consumption has the most variety of resources because of technological advancement. It is becoming less and less trivial to harness the energy of "mother nature" into power for electricity; such forms of energy include solar, wind, hydroelectric and geothermal. The caveat is that for such natural occurrences, the energy is not constant as there are fluctuations depending on the weather and other environment conditions; this motivates the need for proper energy storage. As it stands, efficient batteries for storing energy from these types of resources make up the current limiter on advancements in energy generation from renewable resources. The U.S. energy consumption in 2017 (Fig. 1.2) shows that there is still a long way to go in lessening society's dependence on fossil fuels, non- renewable resources account for 80% of total energy consumption[4]. These statistics for energy consumption varies depending on country as seen for France (Fig. 1.2), where nuclear energy holds the majority for energy consumption; a country's

investment into non-fossil fuel resources drives these energy statistics. For example, 100% of Iceland's power is generated from renewable resources, a combination of geothermal and hydroelectric power sources.
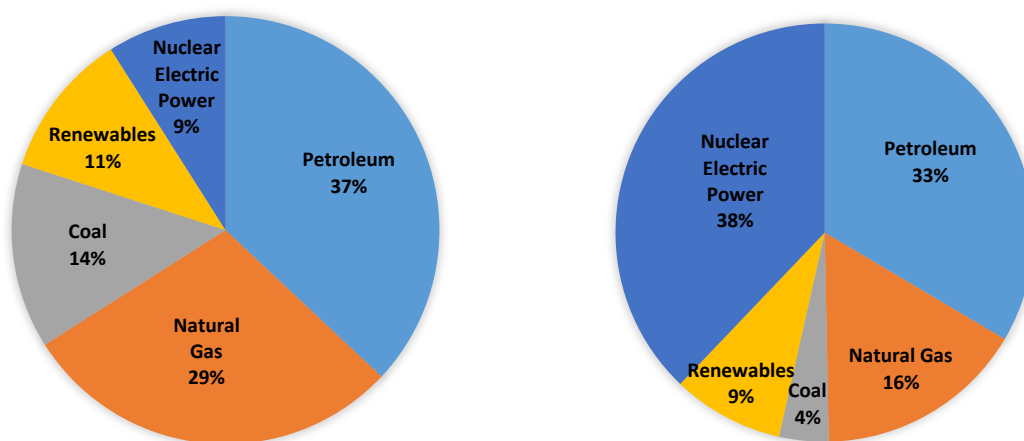
Figure 1.2: 2017 Energy consumption in the USA [4](left) and France [8](right).

While there are multiple alternative resources for energy, the industrial sector also relies heavily on fossil fuel derived feedstocks; there are very few renewable alternatives to plastics and solvents, thus feedstocks should ultimately come from renewable carbon- biomass. The alkanes, alkenes, and aromatic species present in crude oil and natural gas confer high energy density, which makes them attractive industrial feedstocks. In contrast, due to its high atomic percentage of oxygen, biomass has a low energy density, which impacts feedstock sourcing, transportation, and upgrading to industrial commodities[1,9]. From a technical perspective, it is generally possible to convert biomass into various liquid fuels, and many such processes—based on pyrolysis, gasification and catalytic conversion of sugars and/or lignins—have been explored. Unfortunately, the excessive hydrogen demand of lignocellulosic biofuel production alongside the present cost of fossil resources makes it difficult for "advanced biofuels" to compete in the present landscape. In

this context, we note that there are potential niche markets within the petrochemical industry where biomass might offer a competitive advantage. A good example is the production of polyoxygenated hydrocarbons, which are used in producing many industrial commodities but are typically challenging to prepare from crude oil (due to the difficulty of selectively activating alkanes under oxidizing conditions)[10].

A system that can be examined is the market surrounding maleic anhydride (MA). MA is petroleum derived and used as the raw material in the production of tetrahydrofuran (THF), gamma butyrolactone (GBL) and 1,4-butanediol (BDO)- the BDO market size is one of the fastest growing in chemicals over the past few years and is expected to continue upwards in growth[11]. The hydrolyzed structure of MA is maleic acid (MAc), which is functionally similar to succinic acid (SAc); the difference between MAc and SAc is that the C_2-C_3 in SAc is fully hydrogenated, whereas the C_2-C_3 bond in MAc is unsaturated (i.e., an alkene). The three species are interconvertible through hydration/dehydration (MA/MAc) and hydrogenation/dehydrogenation (MAc/SAc) (Figure 1.3), this is why SAc is just as viable as a feedstock as MA. The ray of light in this scenario is that SAc can be produced through anaerobic fermentation of lignocellulosic biomass[9]. Hydrodeoxygenation (HDO) chemistry of these types of bio-derived acids for producing specialty chemicals such as THF, BDO and GBL is an insightful area of research as a driving force for renewable resources. Targeted oxygen removal by hydrogen on SAc, can be envisioned as a plausible route to the mentioned industry chemicals (Figure 1.4).
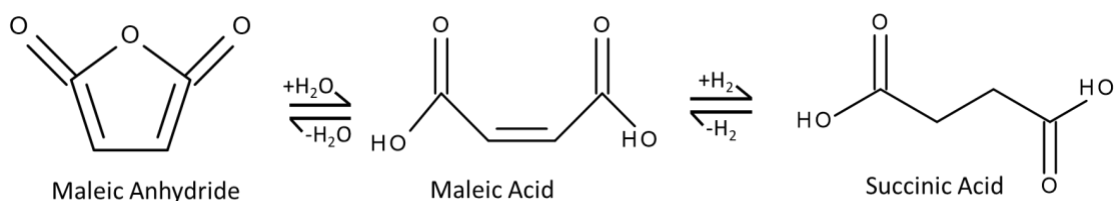
Figure 1.3: Chemical similarity between maleic anhydride and succinic acid.
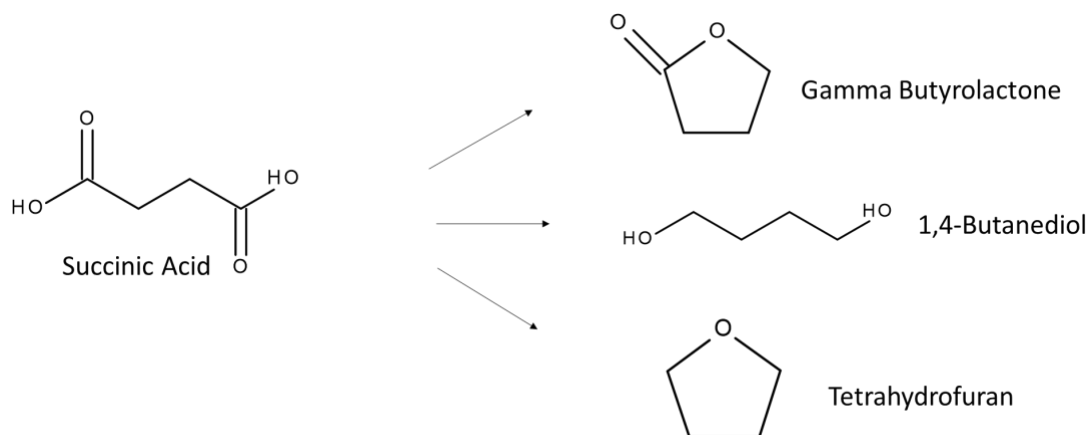
Figure 1.4: Targeted oxygenated products form succinic acid.

In the bio-refining landscape, carboxylic acid HDO comprises an important family of reactions involved in upgrading pyrolysis oils and derivatives of sugar hydrolysis[9]. Carboxylic acid HDO can deliver aldehydes, alcohols, alkanes, and alkenes[12-15]; however, controlling the product distribution is non-trivial. Catalysts that activate carboxylic acids for HDO are also generally active for multiple parallel and sequential side reactions, some of which lead to low value products. Supported noble metals, such Pt, Ru, Pd, Rh and Ni are active catalysts for carboxylic acid hydrodeoxygenation[12,13,15,16]; however, such catalysts have high activity for many other reactions as well[17]. It can therefore be expected that in addition to HDO chemistry, noble metals will facilitate other undesired reactions such as decarbonylation, methanation and hydrogenolysis[18-21], which are kinetically facile over many noble metals and thus may be prevalent at high conversions. This limits the practicality of these systems. The interaction between noble metals and reactant species can be adjusted by making changes to the catalyst; such changes may include type of support or adjusting the oxophilicity of the surface by adding a promoter metal.

This dissertation focusses on carboxylic acid hydrodeoxygenation over metal catalysts. In order to understand fundamental aspects of this system, we consider gas-phase HDO of propionic acid as a tractable model system. It approaches catalyst activity from a reaction engineering and a surface science perspective, by making use of both experimental and computational techniques for an all-encapsulating understanding of the system. Monometallic catalyst systems will be used to understand the reaction pathways that are involved during catalytic activity using a carboxylic acid feedstock; a reaction mechanism will be proposed along with kinetic parameters for the pathways involved in the mechanism. Carboxylic acid HDO will then be observed over bimetallic catalysts, and possible conclusions will be made on the role of a secondary metal during carboxylic acid HDO over noble metals.

1.2 Current State of Knowledge

1.1.1 Biomass Upgrading

Biomass is any material derived from the remains of plants and animals; it may be classified as forestry, agriculture, industry and waste. Trees and plants are the main biomass contributors. Trees are primarily made of cellulose, hemicellulose, lignin, starch and proteins, while plants are composed of lignin and carbohydrates/sugars[1,10]. The end use of biomass determines characteristics that would be deemed attractive and whether biomass can be a feasible option. Biomass for fuel may require focus on energy and moisture content, while biomass for chemicals would play closer attention to chemical composition. A collaboration between National Renewable Energy Laboratory and Pacific Northwest National Laboratory put forth a list of the top value added chemicals from biomass[22]:

- Four Carbon 1,4 Diacids (Succinic, Fumaric and Malic)
- 2,5- Furan dicarboxylic acid

- 3-Hydroxy propionic acid

- Aspartic acid

- Glucaric acid

- Glutamic acid

- Itaconic acid

- Levulinic acid

- 3-Hydroxybutyrolactone

- Glycerol

- Sorbitol

- Xylitol

As this dissertation is modelled after upgrading succinic acid, we tune our scope to the chemistries involving four carbon 1,4 diacids. The main derivatives achieved through reduction are members of the 1,4-butaniediol, tetrahydrofuran and gammabutyrolactone family. The technical barriers of succinic acid upgrading include selective reductions, catalyst life and operating at mild conditions[22,23].

1.1.2 Current Commercial Production Routes to GBL, BDO & THF

There are four industrial precursors to production of BDO, with THF and GBL as byproducts. The first, and oldest, technology is the Reppe process developed in the 1930's; this involves reacting acetylene and formaldehyde to give 1,4-butynediol, that is then hydrogenated to BDO[24].

$$HC \equiv CH + 2CH_2O \rightarrow HOCH_2C \equiv CCH_2OH$$

$$HOCH_2C \equiv CCH_2OH + 2H_2 \rightarrow HOCH_2CH_2CH_2CH_2OH$$
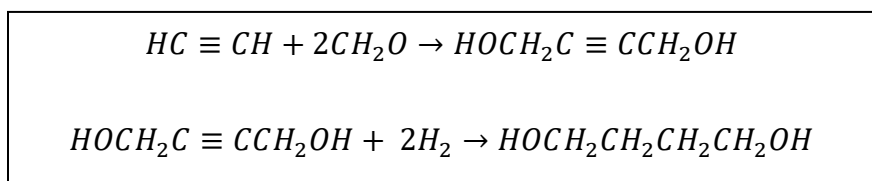
Figure 1.5: Reppe Process.

Mitsubishi Chemical later developed a second BDO route from butadiene through oxidative acetoxylation with acetic acid, the product is then hydrogenated and hydrolyzed to form BDO[25].
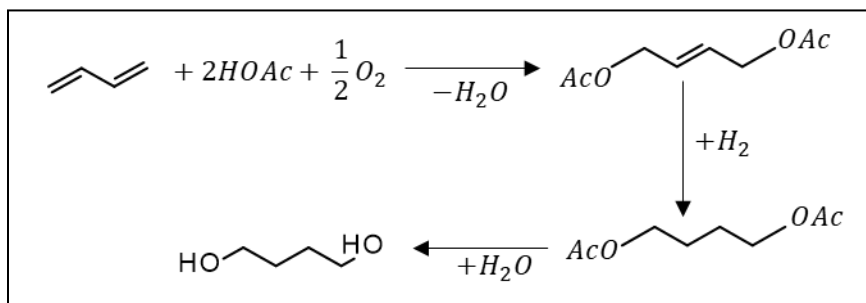
Figure 1.6: Oxidative Acetoxylation to form BDO.

The 90's brought forth the third route from propylene oxide developed by Arco Chemical. The propylene oxide is isomerized to allyl alcohol, then converted to 4-hydroxyburyaldehyde through hydroformylation with syn gas, and finally hydrogenated to BDO[26].
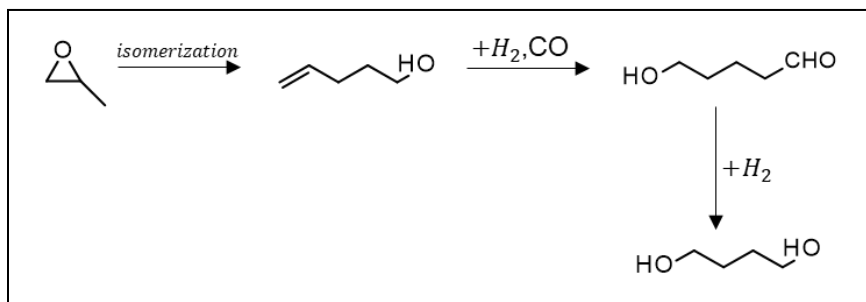
Figure 1.7: Propylene oxide route to form BDO.

The newest commercial route to BDO is through Davy Technology using maleic anhydride as the precursor. The maleic anhydride is esterified using methanol to form a diester, which is then hydrogenated to form GBL and BDO, this can be dehydrated to produce THF[27].
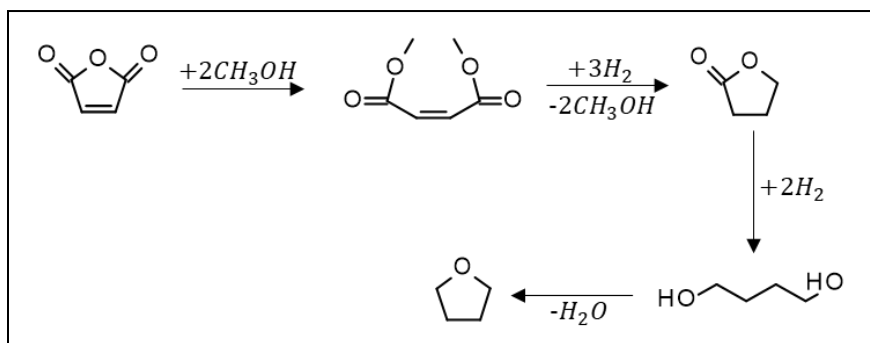
Figure 1.8: Maleic acid route to form BDO.

1.1.3 Carboxylic Acid Reactivity over Monometallic Catalysts

There has been different motivations for research into carboxylic acids, as the functional group allows for the privilege of choosing a product from a variety of potential product compositions. Metal and support types has shown to have large impact on dominant reactions involving carboxylic acids[17,28]. There has been a lot of work done on acetic acid probing the metal and support effects on reactivity. Rachmady and Vannice were among the first to dive deep into exploring HDO chemistry using acetic acid over different supported Pt catalysts[20]. Reactions observed included decomposition, hydrogenation, esterification and ketonization, with the pathway selectivities differing depending on the support. Pt/TiO_2 saw the highest selectivity towards hydrogenation products, acetaldehyde and ethanol. Al_2O_3 and SiO_2 supported Pt catalysts showed higher selectivity towards decomposition pathways that produced CO, CO_2 and methane.

Decomposition (Decarbonylation): $CH_3COOH + H_2 \rightarrow CH_4 + CO + H_2O$

Decomposition (Decarboxylation): $CH_3COOH \rightarrow CH_4 + CO_2$

Ketonization: $2CH_3COOH \rightarrow CH_3COCH_3 + CO_2 + H_2O$

Hydrogenation to propanal : $CH_3COOH + H_2 \rightarrow CH_3CHO + H_2O$

Hydrogenation to propanol: $CH_3COOH + 2H_2 \rightarrow CH_3CH_2OH + H_2O$

Esterification: $CH_3COOH + CH_3CH_2OH \rightarrow CH_3COOCH_2CH_3 + H_2O$

Further studies into acetic acid dissected the activity using Pt/SiO$_2$ as the catalyst, showing that the same decomposition products can be observed using acetic acid, acetaldehyde and ethanol; alluding to a system being more complicated than what was originally imagined[13,15,29]. The two-carbon nature of acetic acid can cause different types of C-C cleavage chemistries to be lumped, decoupling of such chemistries was possible during work that was done on longer chained molecules.

Propionic acid HDO over supported metals allowed for DCN/DCX pathways to be distinguished from methanation and water gas shift reactions that was also taking place during catalytic activity. The effects of metal and support effects was investigated for propionic acid HDO[17], it was found that the reaction activity followed the order: Pd > Ru > Pt > Rh > Ni. Pd supported catalyst showed selectivity to propanal at low conversions (below 300K), but was mostly selective towards C$_2$ species. The observed activity over Pt catalysts produced only C$_2$ products. Similarly, high C$_2$ selectivity was seen over Rh with small selectivity towards C$_3$ species, designated to either propylene or propane. Products observed during propionic acid HDO over Ru were C$_1$ and C$_2$ species, as well as diethyl ketone; low temperatures saw high selectivity towards C$_1$ products, while higher temperatures facilitated a change towards diethyl ketone selectivity being the most dominant. While Ni catalysts saw the same product diversity as Ru, C$_2$ products took up majority

of the selectivity at high conversions and temperatures[12]. Support effect experiments using propionic acid HDO saw similar observations to experiments mentioned previously using acetic acid; TiO_2 saw the highest selectivity towards oxygenated products compared to SiO_2 and carbons supports, however this observation only held valid at low conversions, higher conversions still saw selectivity dominance of C_2 species. Cu supported catalyst showed selectivity towards propanol and propanal at high conversions and temperatures; however when the turn over frequency (TOF) was compared to some noble metals, it had the lowest value regardless of support (TOF values: Pd/SiO_2=33 h^{-1}, Pt/SiO_2=3.3 h^{-1}, Cu/SiO_2=1.3 h^{-1})[14].

Metal and support effects carried on to carboxylic acids of higher chain lengths. Hexanoic acid HDO using Pt showed high selectivity towards oxygenated products when supported by TiO_2, however, an Al_2O_3 support showed a significant amount of saturated hydrocarbons[30]. Oleic acid HDO was investigated over Ru catalysts at high hydrogen partial pressures (5MPa) in an attempt to reduce unwanted reactions; the results were positive as both catalysts produced stearic acid and stearyl alcohol, but catalysts supported by SiO_2 produced stearyl alcohol at far lower rates compared to those supported by TiO_2[31].
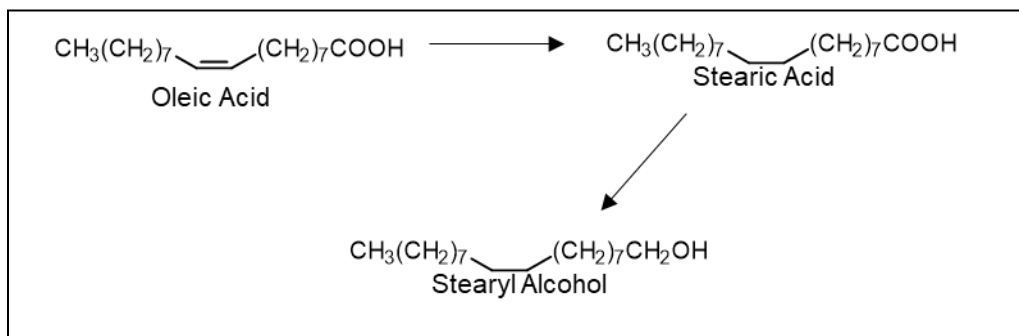
Figure 1.9: Oleic Acid Hydrogenation Pathway

Work was also done using oleic acid as a model compound for palm oil conversion to biodiesel over different gamma-alumina supported metals[18]. It was observed that there was a significant portion (>50%) of selectivity towards HDO products over Co catalysts, while Ni, Pt and Pd produced species that stemmed from mostly DCN/DCX chemistry. It was also observed that there were higher amounts of methane over Ni and Co catalysts, indicating that these catalysts were more active for the methanation reaction. Co was found to be the most active metal during oleic acid HDO, however a number of deactivation problems exist using Co such as sintering, carbon deposition and surface restructuring.

The National Renewable Energy Laboratory investigated succinic acid HDO over supported metal catalysts (Ru, Pt and Pd), which aligns well with this dissertation since succinic acid is molecule of focus for biomass upgrading[32]. Ru catalyzed reactions showed no selectivity towards oxygenated products. Pt had the lowest activity of the three metals, however the product streams had near equal amounts of GBL, BDO and THF. The most positive metal was Pd which had high activity and also significant selectivity towards the oxygenated products, with GBL occupying 49% of the product yield.

The disadvantages of majority of monometallic catalysts during carboxylic acid HDO have been established that the reaction is fairly unselective towards oxygenated products and some metals are prone to deactivation, this set the groundwork for investigations into adding secondary and tertiary metals in order to improve the stability and selectivity of catalyst performance[17,33,34].

1.1.4 Carboxylic Acid Activity over Bimetallic Catalysts

The addition of secondary metals have been use to improve catalytic activity before investigations into carboxylic acids became popular. Reactions involving alcohols and aldehydes have set the precedence on increased selectivity of oxygenate products using promoter metals[35]. In commercial

environments, secondary metals have been used to increase the stability of catalysts so that reactor beds would have longer lives. In the hydrotreatment of diesel, CoMo is a common bimetallic catalyst being employed; because of harsh deactivation of monometallic Co in the presence of sulfur compounds, Mo was added to increase the catalyst's resistance to poisoning. Cu-Cr catalysts are commercially used in the conversion of fatty acid esters to alcohols, however, the toxic nature of Cr and also the harsh environments required (high temperature and pressure) has pushed for less toxic and also more active metals[36]. The use of secondary metals to naturally more active noble metals showed positive results when carried out in investigations involving carboxylic acid HDO and hydrogenation experiments.

Propionic acid HDO over PdRe/SiO$_2$ showed 100% selectivity to oxygenated products, the distribution between propanal and propanol varied depending on conversion as well as reactor conditions[37]. The addition of Mo to supported Ru catalysts also showed an increase in selectivity towards propanol during propionic acid HDO. The Pd-Re combination has also been tested in the hydrogenation of fatty acids and showed to have high selectivity (>90%) towards alcohols at 433K, the fatty acids tested were: stearic, palmitic, myristic, lauric, capric, octanoic, hexanoic and stearic acids[18,38]. Hexanoic acid HDO over Pt-Re also showed high selectivity towards alcohols, it was also pointed out that the ratio between the two metals have an effect on selectivity distribution as well as the reaction rate[30,39]. Ratios of Re/Pt between 1-2 had the highest reaction rates when compared to the ratios both higher and lower.

Pentadecanoic acid hydrogenation experiments over monometallic Rh, Ru, and Pt metals showed a large increase in the yield of oxygenated products when paired with any of the promoter metals, Re, W and Mo; these experiments were carried out at low conversions. Aliphatic and aromatic acid hydrogenation to alcohols (yield in brackets) using a Sn promoted Ru catalyst was

demonstrated to be a successful catalyst for the compounds hexanoic acid (86%), lauric acid (94%), 2-ethylhexanoic acid (67%), cyclohexanecarboxylic acid (74%), oleic acid (76%) and benzoic acid (94%)[16,40,41]. The Ru-Sn experiments also highlighted that the catalyst can selectively hydrogenate the C=O bond without hydrogenating the C=C bonds and aromatic groups.

Succinic acid HDO has been investigated over different types of bimetallic catalysts in efforts to find ways of increasing BDO yield[35,42]. The most popular secondary metal that has been added is Re, with numerous studies investigating catalytic performance. Re paired with Pt, Pd and Ru all showed increased selectivity towards BDO, these catalysts also showed very little in performance loss during reactions. The bimetallic catalyst performance during succinic acid can also be affected by the catalyst preparation method. Catalysts prepared by strong electrostatic adsorption was more active compared to those prepared by incipient wetness and sol gel methods. Using Sn as a promoter metal for Pd, Pt and Ru catalyzed HDO of succinic acid also showed high selectivity towards BDO[32]; this is especially promising since Sn is cheaper than Re. The ratio between active and promoter metals was shown to not only affect product selectivity, but the ratios affected each of the catalysts in different ways. A 1:1 ratio between active and promoter metals seemed to be ideal in all instances, with BDO occupying the highest selectivity. Pd-Sn catalyst maintained the same performance when the Sn weigh loading was doubled, the same could not be said for Ru and Pt; the conversion decreased upon increasing the Sn content on the Pt catalyst, while the Ru-Sn catalyst saw a significant decrease in BDO selectivity for the same change.

1.3 Research Overview

The experimental techniques used throughout the dissertation is described in Chapter 2, where the preparation, characterization and evaluation methods are thoroughly described. The investigation into propionic acid HDO over supported noble metals is then carried out over two different types

of monometallic catalysts. Monometallic Pt catalysts are used in Chapter 3, as we identify it's shortcoming as well as hypothesize ways of increasing its practicality. Sights were then turned on monometallic Ru catalysts in Chapter 4 repeating similar analysis procedures as what was carried out using Pt. After understanding the behavior of the monometallic catalysts, we created bimetallic catalysts through the addition of Sn to Pt catalysts in Chapter 5 where we explored how the secondary metal affected different catalysts properties. Upon realizing that investigations needed to be done on understand the nature of interactions between reactant species and the catalyst surface metals, we built a kinetic mode for propionic acid HDO over silica supported Pt catalysts in Chapter 6. The research was concluded in Chapter 7, where future work was proposed that would point towards the next step in the overarching theme of the work,

1.4 References

1 Wang, S., Dai, G., Yang, H. & Luo, Z. Lignocellulosic biomass pyrolysis mechanism: A state-of-the-art review. *Progress in Energy and Combustion Science 62*, 33-86 (2017).

2 Craig , J., Gerali , F., MacAulay, F. & Sorkhabi, R. Vol. 465 1-24 (Special Publications, Geological Society, London,, June 2018,).

3 Perera, F. Vol. 15 1 (Int J Environ Res Public Health, 2018).

4 Carmona, M., Feria, J., Golpe, A. & Iglesias, J. Energy consumption in the US reconsidered. Evidence across sources and economic sectors. *Renewable and Sustainable Energy Reviews 77*, 1055-1068 (2017).

5 Grubb, M. J., Fouquet, R. & Hope, C. Vol. 54 1-2 (Climatic Change, 2004).

6 Masjuki Hj. Hassan, M. A. K. An Overview of Biofuel as a Renewable Energy Source: Development and Challenges. *Procedia Engineering* **56**, 39-53 (2013).

7 Vincent K.M. Cheng, G. P. H. Life-cycle energy densities and land-take requirements of various power generators: A UK perspective,. *Journal of the Energy Institute* **90**, 210-213 (2017).

8 Petrova, V. *France brings online 2.8 GW of renewables in 2017*, 2018).

9 Gurbuz, E., Bond, J. Q., Dumesic, J. A. & Román-Leshkov, Y. in *The Role of Catalysis for the Sustainable Production of Bio-fuels and Biochemicals* 261-288 (Elsevier, 2013).

10 Simonetti, D. A. & Dumesic, J. A. Catalytic Production of Liquid Fuels from Biomass-Derived Oxygenated Hydrocarbons: Catalytic Coupling at Multiple Length Scales. *Catalysis Reviews 51*, 441-484 (2009).

11 Adom, F., Dunn, J. B., Han, J. & Sather, N. Vol. 48 14624−14631 (Environ. Sci. Technol, 2014).

12 Lugo-José, Y. K., Monnier, J. R., Heyden, A. & Williams, C. T. Hydrodeoxygenation of propanoic acid over silica-supported palladium: effect of metal particle size. *Catalysis Science & Technology 4*, 3909-3916 (2014).

13 Contreras-Mora, J. *et al.* Characterization and Evaluation of Carbon-Supported Noble Metals for the Hydrodeoxygenation of Acetic Acid. *Organic Process Research & Development 22*, 1628-1635 (2018).

14   Alotaibi, M. A., Kozhevnikova, E. F. & Kozhevnikov, I. V. Deoxygenation of propionic acid on heteropoly acid and bifunctional metal-loaded heteropoly acid catalysts: Reaction pathways and turnover rates. *Applied Catalysis A: General 447-448*, 32-40 (2012).

15   He, Z. & Wang, X. Required catalytic properties for alkane production from carboxylic acids: Hydrodeoxygenation of acetic acid. *Journal of Energy Chemistry 22*, 883-894 (2013).

16   Chen, L. *et al.* Aqueous-phase hydrodeoxygenation of carboxylic acids to alcohols or alkanes over supported Ru catalysts. *Journal of Molecular Catalysis A: Chemical 351*, 217-227 (2011).

17   Lugo-José, Y. K., Monnier, J. R. & Williams, T. C. Gas-Phase, catalytic hydrodeoxygenation of propanoic acid, over supported group VIII noble metals: Metal and support effects. *Applied Catalysis A: General 469*, 410-418 (2014).

18   Srifa, A., Faungnawakij, K., Itthibenchapong, V. & Assabumrungrat, S. Roles of monometallic catalysts in hydrodeoxygenation of palm oil to green diesel. *Chemical Engineering Journal 278*, 249-258 (2015).

19   Peng, B. *et al.* Comparison of kinetics and reaction pathways for hydrodeoxygenation of C3 alcohols on Pt/Al2O3. *Catalysis Today 183*, 3-9 (2012).

20   Rachmady, W. & Vannice, M. A. Acetic Acid Hydrogenation over Supported Platinum Catalysts. *Journal of Catalysis 192*, 322-334 (2000).

21   Shangguan, J., Olarte, M. V. & Chin, Y.-H. Mechanistic insights on CAO and CAC bond activation and hydrogen insertion during acetic acid hydrogenation catalyzed by ruthenium clusters in aqueous medium. *Journal of Catalysis 340*, 107-121 (2016).

22   Werpy, T. & Petersen, G. Top Value Added Chemicals from Biomass. (204).

23   Davis, R. *et al.*   (National Renewable Energy Laboratory, 2013).

24   Colborn, R. E. & Vollhardt, K. P. C. Mechanism of the Reppe cyclooctatetraene synthesis from ethyne: a labeling experiment. *J. Am. Chem. Soc* **103**, 20 (1981).

25   Moulijn, J. A., van Leeuwen, P. W. N. M. & van Santen, R. A. in *Studies in Surface Science and Catalysis* Vol. 79   Ch. Chapter 2, 23-67 (1993).

26   Zhang, Y., Liu, D. & Chen, Z. Production of C2-C4 diols from renewable bioresources: new metabolic pathways and metabolic engineering strategies. *Biotechnology for biofuels* **10**, 299 (2017).

27   Harris, N. & Tuck, M. W. Butanediol via maleic anhydride. *Hydrocarbon Processing* **69** (1990).

28   de Miguel, S. R., Román-Martínez, M. C., Cazorla-Amorós, D., Jablonski, E. L. & Scelza, O. A. Effect of the support in Pt and PtSn catalysts used for selective hydrogenation of carvone. *Catalysis Today* **66**, 289-295 (2001).

29   Gursahani, K. I., Alcalá, R., Cortright, R. D. & Dumesic, J. A. Reaction kinetics measurements and analysis of reaction pathways for conversions of acetic acid, ethanol, and ethyl acetate over silica-supported Pt. *Applied Catalysis: A General 222*, 369-392 (2001).

30   Aly, M. & Baumgarten, E. Vol. 210   1-12 (Applied Catalysis A: General, 2001).

31   Mendes, M. J., Santos, O. A. A., Jordão, E. & Silva, A. M. Hydrogenation of oleic acid over ruthenium catalysts. *Applied Catalysis A: General* **217**, 253-262 (2001).

32   Vardon, D. R. *et al.* Ru/Sn/Ac for the squeous phase reduction of succinic acidk to 1,4-butanediol under continuous process conditions. **7** (2017).

33   Alonso, D. M., Wettstein, S. G. & Dumesic, J. A. Bimetallic catalysts for upgrading of biomass to fuels and chemicals. *Chemical Society Reviews* (2012).

34   Merlo, A. B., Vetere, V., Ruggera, J. F. & Casella, M. L. Bimetallic PtSn catalyst for the selective hydrogenation of furfural to furfuryl alcohol in liquid-phase. *Catalyst Communications* **10**, 1665-1669 (2009).

35   He, D.-H., Wakasa, N. & Fuchikami, T. Hydrogenation of Carboxylic Acids Using Bimetallic Catalysts Consisting of Group 8 to 10, and Group 6 or 7 Metals. *Tetrahedron Letters 36*, 1059-1062 (1995).

36   Muegge, B. & Massoth, F. E. Comparison of Hydrotreating Catalyst Deactivation by Coking with Vacuum Gas Oil Vs. Anthracene. *Studies in Surface Science and Catalysis* **68**, 297-304 (1991).

37   Kammert, J. D. *et al.* Reduction of Propionic Acid over a Pd-Promoted ReOx/SiO2 Catalyst Probed by X-ray Absorption Spectroscopy and Transient Kinetic Analysis. *ACS Sustainable Chemistry & Engineering 6*, 12353−12366 (2018).

38   Wang, S., Guo, Z., Cai, Q. & Guo, L. Vol. 45   138-143 (Biomass and Bioenergy 2012).

39   Maynar, H. G. *et al.* Highly selective and efficient hydrogenation of carboxylic acids to alcohols using titania supported Pt catalysts. *Chemical Communications 46*, 6279-6281 (2010).

40   LoVoi, A. *Diesel vs. biodiesel vs. vegetable oil*, 2014).

41   Primo, A., Concepción, P. & Corma, A. Synergy between the metal nanoparticles and the support for the hydrogenation of functionalized carboxylic acids to diols on Ru/TiO2. *Chemical Communications 47*, 3613-3615 (2011).

42   Tomishige, K., Nakagawa, Y. & Tamura, M. Selective hydrogenolysis and hydrogenation using metal catalysts directly modified with metal oxide   species   *Green Chemistry* **19**, 2876 (2017).

CHAPTER 2

Experimental Techniques

2.1 List of Chemical Materials

Table 2.1 shows the chemicals involved in the various catalyst synthesis methods throughout the work. Tables 2.2 and 2.3 shows the chemicals and gases employed during various reactor experiments and catalyst characterization methods. Tables 2.4 and 2.5 show the chemicals and gases utilized in the characterization of the catalysts.

Table 2.1: Chemicals involved in catalyst synthesis procedure, this includes support and precursor compounds.

Chemical	Purity	Source
Gamma Alumina	97%	Strem
Amorphous Silica	99.8%	Sigma-Aldrich
Hydrogen Hexachloroplatinate(IV) Hydrate	38-40%Pt	Acros Organics
Ruthenium (III) Chloride Hexahydrate	35-40%Ru	Acros Organics
Tin(II) chloride dihydrate	98%	Acros Organics
Hydrocholoric Acid	Trace metal grade	Fisher Scientific
Sodium Hydroxide	>98%	Sigma-Aldrich
Water	resistivity>18Ωcm^{-1}	In House

Table 2.2: Liquid chemicals used in the reactor system for reactions and calibrations.

Chemical	Purity	Source
Propionic acid	99%	Acros Organics
1-Propanol	+99%	Acros Organics
Propanal	+99%	Acros Organics
Pentanone	99%	Alfa Aesar
Pentanol	98%	Alfa Aesar
Propyl Propanoate	+98%	Acros Organics

Table 2.3: Gases used in the reactor system for reactions, calibrations and characterizations.

Analysis Gas	Composition	Source
Hydrogen	99.999%	Airgas
Helium	99.999%	Airgas
Nitrogen	99.999%	Airgas
Carbon Monoxide	99.99%	Praxair
Oxygen	1% O_2, 0.99% Ar, 98% He	Airgas
Carbon Monoxide	0.99% CO, 0.99% Ar, 98% He	Airgas
Carbon Dioxide	0.97% CO_2, 0.99% Ar, 98% He	Airgas
Methane	0.05% CH_4, 0.99% Ar, 98.5% He	Airgas
Ethane	0.99% C_2H_6, 1. % Ar, 98% He	Airgas
Propane	1% C_3H_8, 1% Ar, 98% He	Airgas
Ethylene	1% C_2H_4, 1% Ar, 98% He	Airgas

2.2 Catalyst Preparation

The catalysts used in this dissertation were prepared by incipient wetness and strong electrostatic adsorption (SEA). Studies involving monometallic catalysis took advantage of the straightforward incipient wetness procedure. The work done using bimetallic catalysts required stronger control over metal adsorption on the support, which is typically characteristic of the SEA procedure.

2.2.1. Incipient Wetness

Monometallic Ru and Pt catalysts were prepared via incipient wetness onto an amorphous silica support[1]. This procedure takes advantage of a metal's affinity to be adsorbed onto the surface of a support; hence, the type of metal precursor salt used is very important. In this procedure, a solution of known concentration is made using a precursor salt, the weight percent of metal in a catalyst is usually leveraged by varying the concentrations of this precursor solution. The incipient volume of the silica support was measured using distilled water, this is a ratio of the volume of liquid required to fill all the pores of a mass of support; visually, the support appears to be at the point of saturation or "sappy." The incipient volume of the precursor solution is then added dropwise slowly to the desired amount of support material, this is typically done in a sonicator to ensure an even distribution of solution or that all of the pores of the silica support were filled. The catalysts were then left to stand at room temperature for an hour then placed in a furnace to be dried in air overnight. Catalysts were then transferred to a glass cell for post treatment procedures. The procedure contained alterations depending on the metal. Ru/SiO_2 catalysts were then reduced in H_2, however Pt/SiO_2 was first calcined in air before the reduction step. After reduction, all catalysts were passivated by flowing a 1% O_2 gas blend at room temperature to ensure safe handling outside of the glass cell. It is important to mention that between the reduction and passivation step, and also between the calcination and reduction step (for Pt), the cell was flushed with He at room

temperature to ensure that there was no mixing of reactive gases flowing over the catalysts at the same time. Table 2.4 shows further detail of the post treatment methods used for each metal,

Table 2.4: Post Treatment methods of the different supported metal catalysts.

Metal	Furnace Temperature (K)	Calcination Step	Reduction step
Ru	403	NONE	673 K for 6 hours
Pt	393	623 K for 3 hours	673 K for 4 hours

which consisted of a calcination step Ru catalysts were dried in a fuwere then reduced in flowing H_2 (100 ml min^{-1}) by ramping to 673 K at a ramp rate of 3 K min^{-1}, and held for 6 hours. Pt catalysts differed from Ru in that a calcination step preceded the reduction step, the catalysts were calcined in air (100 ml min^{-1}) at 623 K at a ramp rate of 3 K min^{-1}, and held for 3 hours. Pt catalysts were also only reduced in H_2 at 673 K for 4 hours.

2.2.2. Strong Electrostatic Adsorption (SEA)

The bimetallic study involved preparing catalysts via SEA to take advantage of the accuracy involved with the procedure[2]. In bimetallic procedures, there are instances where metals may leech or even not adsorb; catalysts prepared by SEA are typically guaranteed to display activity of adsorbed metals as opposed to incipient wetness where they may be metal oxides from precursor metal that did not adsorb onto the support surface. Adsorption of metals is affected by the pH of the precursor solution and the point of zero charge (PZC) of the support[3]. The PZX is the known as the pH at which the support has a zero electrical charge, pH's above or below the PZC will affect what type of metal complex will be ideal for the SEA method. In the instance of pH lower than the PZC, the support surface will have a positive charge, this means that metal complexes

with a negative charge would adsorb in this range, while positively charged complexed would be more suitable for environments with a pH higher than the PZC. Bimetallic catalysts were prepared sequentially. Pt was the first metal to be adsorbed, a precursor solution of the Pt salt with a concentration of 200 μg/mL and pH of 1; intuitively, it can be deduced that the precursor metal complex has a negative charge. The volume of precursor solution to be used was determined by the amount of available surface area on the designated mass of support, a surface loading of 1000 m^2/L was used as the ratio; this value can allude the fact that the volume of precursor solution was the limiting reagent. The support-solution mixture was allowed to mix for an hour on an orbital rotator set to 80 rpm. The post treatment procedure for the Pt catalysts made via SEA was the same as with those prepared using incipient wetness.

The addition of Sn required the Pt catalysts to be calcined an additional time in order to prevent leeching of the Pt into solution. The Sn precursor solution was made at a concentration of 300 μg/mL. Since the pH has a strong influence on the amount of metal adsorbed on the support, the desired wt% of Sn was leveraged by altering the pH of the precursor solution; Figure 2.1 below shows the uptake of Sn at different pH's. The synthesis SEA procedure and post treatment steps then followed same as what was carried out when adsorbing the Pt metal.
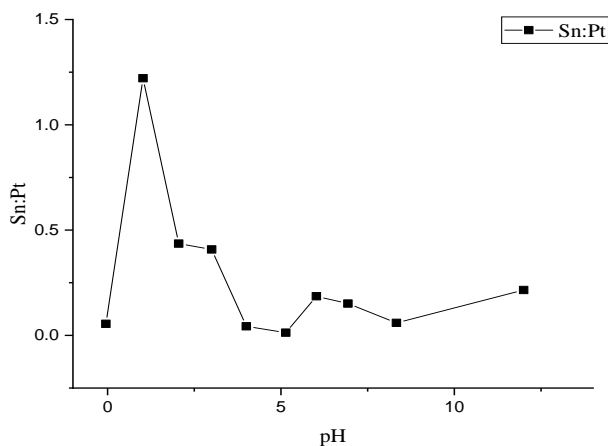
Figure 2.1: Sn uptake at different pH values.

2.3 Catalyst Characterization

2.3.1. N_2 Physical Adsorption

The catalyst support surface area and porosity was determined using N_2 adsorption. This was at 77K using a commercial instrument (Micromeritics ASAP 2020). Surface areas were determined using Brunauer-Emmett-Teller (BET) analysis; micro/mesoporosity were assessed using t-plot analysis; pore volumes were computed as the cumulative volume of N_2 condensed at a relative pressure $(P/P_0) = 0.995$; and average pore diameters were estimated from Barett-Joyner-Halenda (BJH) analysis of the desorption branch of the isotherm. Prior to N2 dosing, samples were dried by evacuating to 500 μm Hg at 298K and then heated to 623 K (240 min hold, 10 K min^{-1} ramp).

2.3.2. Metal Site Titration

In exploring the performance/activity of catalysts, it is important to know specific details about the exposed metal active sites on a support such as: concentration, dispersion and particle diameter. Gas titrants would typically adsorb onto metal sites, and the molar quantity of adsorbed titrant would be used as a correlation of the exposed sites per gram of catalyst; titrant gases may have

different stoichiometric factors with metal sites. It is also important to note that titrant gases are very specific on the metal with which adsorption is experienced. Carbon monoxide, oxygen and hydrogen were the titrant gases that were dosed over the catalyst surface[4].

Chemical Adsorption was therefore used to interrogate the Pt surface area available for reaction using a Micromeritics ASAP 2020 instrument. Prior to titrant dosing, samples were dried by evacuating to 10 µm Hg at 298K and subsequently heating to 373 K (30 min hold, 10 K min^{-1} ramp). Samples were then exposed to flowing oxygen and the cell temperature was increased to 673K (10 K min^{-1}, 30 min hold). The cell was then evacuated to 5 µm Hg at 673K, held under vacuum for 15 minutes, cooled under vacuum to 373K, and then exposed to H_2 flow The cell was then heated under continuous H_2 flow to 673K (10K min^{-1}, 4 h hold). Finally, the cell was evacuated to 5 µm Hg at 673K to remove chemisorbed hydrogen (30 min) and cooled to 308K under vacuum. A titrant uptake isotherm was then collected at 308K at varying dosing pressures, the sample cell was evacuated for 60 min to remove physisorbed titrants, and a second titrant uptake isotherm was collected at 308K. Irreversible titrant uptake was calculated as the difference in titrant uptake between the two isotherms. This was done for CO, O_2 and H_2. The irreversible uptake of titrant and known mass of catalyst was used to describe some of the concentration of exposed metals on the surface. Quantifying exposed monometallic Ru and Pt sites were fairly straightforward, as the titrants only had to be normalized by a stoichiometry factor, however, it is still unclear how titrant gases behave in the presence of Sn promoted Pt. Using the site density and assuming a spherical metal shape, the average diameter of the nanoparticle as well as the dispersion of the metal can be calculated using the following equations.

$$d_p = \frac{6}{S * \rho} \hspace{5cm} \text{Equation 2.1}$$

$$S = N_M N_a A_m \qquad\qquad\qquad\qquad \text{Equation 2.2}$$

$$D = \frac{N_M * M}{W} \qquad\qquad\qquad\qquad \text{Equation 2.3}$$

Where d_p is the average particle diameter, S is the surface area of metal sites per gram of catalyst, ρ is the density of the metal atom, N_M is the site density from titrant uptakes, N_a is Avogadro's constant, A_m is the cross sectional area of the metal atom, D is the dispersion of exposed metal on the surface, M is the mass of catalyst and W is the weight percent loading of the metal on the support.

2.3.3. Inductively Coupled Plasma Mass Spectrometry (ICP-MS)

Samples first had to be digested in aqua regia before ICP-MS analysis[5]. The aqua regia solution consisted of a mixture of 7 mL hydrochloric acid and 3 mL nitric acid. Digestion was carried out in a round bottom flask kept in a mineral oil bath at 373K and stirred constantly, a reflux system kept at 288 K was incorporated to prevent the escape of any gases; digestions were allowed to occur for 12 hours. After digestion, the solution was diluted to 25 ml using DI water, then further diluted in 1% nitric acid for ICP-MS using a Perkin Elmer Elan 6100 instrument. The metal responses were compared to a curve made from calibrations using high purity commercial standards.

2.4 Catalyst Activity Testing

The reactor system used for all catalytic activity tests is illustrated in Figure 2.2. Gases are introduced to the system at controlled flowrates using digital mass flow controllers (Brooks). Reactors always operated under gas phase conditions, but many of our feeds were introduced to the system as liquids using a syringe pump (Cole Parmer). Specifically liquids were fed through a PEEK capillary (130 μm, IDEX) into a home-built, temperature-controlled vaporizer, where they

were combined with pre-heated gas feeds. To increase surface area for gas-liquid contact, the vaporizer was packed with quartz granules (850-2000 μm, Aldrich). To ensure complete vaporization, partial pressures of condensable species were maintained below 90% of their vapor pressure at a given reaction condition. After leaving the vaporizer, the process stream flowed through a 6-port valve, which was used to direct flow either to the reactor or to the bypass. During startup, the reactor was bypassed until we observed steady state feed concentrations via Gas Chromatography. Once the reactor feed stream reached steady state, flow was diverted to the reactor.

The packed bed reactor operated in an upflow configuration. It was constructed from ½" stainless steel tubing (McMaster). The catalyst bed was placed between two quartz wool plugs in the center of the tube, and the void volume upstream of the reactor was packed with quartz granules. The reactor temperature was monitored at the external of the wall using a type-K thermocouple, and the external wall temperature was regulated using a PID controller (LOVE 16A 3010). A second type-K thermocouple was placed inline and used to monitor reactor temperature immediately downstream of the catalyst bed. Data reported in this manuscript reflect the inline temperature measurement. The reactor effluent was transferred, via heat-traced stainless steel tubing, to a pair of online gas-chromatographs (HP 5890) for quantitative resolution of the product mixture. The first GC was equipped with dual inlets leading, respectively, to an HP-PONA column paired with a flame-ionization detector (FID) and a Restek ShinCarbon ST Micropacked column paired with a thermal conductivity detector (TCD). In general, propionic acid, propanal, propanol, propane, ethylene, and ethane were resolved and quantified using the PONA/FID system, while methane, CO, and CO_2 were resolved and quantified using the ShinCarbon/TCD system. The second GC was configured with a single inlet and a Restek ShinCarbon ST Micropacked column leading to a

Methanizer/FID detector. This system was used for quantifying CO, CO_2, and methane concentrations that were below TCD detection limits. Species were qualitatively identified using standards prepared from commercial samples.

Figure 2.2: Schematic of packed bed reactor setup.

Reactions were run over various catalysts, temperatures, reactant partial pressures, and contact times, and species production rates were quantified at 15-minute intervals. Unless otherwise noted, reported rates reflect steady state operation. Typically, after startup, reactors were allowed to reach steady state species production rates under a well-defined, "reference" condition. This typically took less than 1 hour. After reaching steady state, production rates for all species were quantified. Subsequently, a single perturbation in temperature, partial pressure, or contact time was introduced, and the system was allowed to evolve to a new steady state, where effluent flowrates of all species were again quantified. Metal catalysts employed for oxygenate processing are

generally susceptible to various modes of deactivation, which can obscure kinetic trends. Accordingly, after quantifying the impact of each perturbation on species flowrates, the system was returned to the reference condition and allowed to reach steady state. This provided a rigorous benchmark for assessing catalyst deactivation. Under most of our operating conditions, deactivation was relatively mild. There is one exception: we have observed that high pressures of propanal induce severe deactivation of Pt, which is consistent with prior reports. In general, high propanal pressures were encountered when feeding propanal or 1-propanol into reactors (the latter readily dehydrogenates over Pt to form propanal). In systems with pronounced deactivation, it is difficult to define meaningful reaction rates from steady state measurements as the available catalytic surface area is generally changing as a function of time on stream. In these systems, initial production rates were estimated by extrapolating the deactivation profile to zero-time-on-stream. During typical startup and between experiments (e.g., changing the feed molecule), the catalyst bed was reduced under flowing H_2 at 673K (10 K min^{-1}, 4h), which was sufficient to restore the initial activity of the catalyst after most experiments. However, a reducing treatment alone was not able to restore activity after exposure to high propanal pressures. In these experiments, it was instead necessary to calcine catalysts in flowing air prior to reduction.

Species production rates are reported here as site time yields:

$$STY_j = \frac{F_j}{N_{Pt}}$$
Equation 2.4

Where Fj is the total molar flowrate of species j in the reactor effluent and N_{Pt} is the total molar quantity of surface Pt atoms in the catalyst bed as estimated by CO chemisorption. Feed conversion was defined on a carbon basis and computed based on product flowrates:

$$X_i = \frac{\sum\limits_{j \neq i} F_j \cdot C_{n,j}}{F_{i,0} \cdot C_{n,i}}$$

Equation 2.5

Where F_j is the molar flowrate of reaction products, j, in the reactor effluent, $F_{i,0}$ is the inlet flowrate of the reacting species, i, and C_n is the number of carbon atoms in a given molecule. Selectivity to a specific reaction product, k, is defined in terms of molar flowrates of all reaction products, j:

$$S_k = \frac{F_k}{\sum\limits_{j} F_j}$$

Equation 2.6

2.5 References

1   Sietsma, J. R. A., Jos van Dillen, A., de Jongh, P. E. & de Jong, K. P. Application of ordered mesoporous materials as model supports to study catalyst preparation by impregnation and drying. *Studies in Surface Science and Catalysis* **162**, 95-102 (2006).

2   Tengco, J., Lugo-José, Y. K., Monnier, J. R. & Regalbuto, J. R. Chemisorption–XRD particle size discrepancy of carbon supported palladium: Carbon decoration of Pd. *Catalysis Today* **246**, 9-14 (2015).

3   Samad, J. E., Keels, J. & Regalbuto, J. R. A Comparison of Pt(II) and Pt(IV) Chloride Precursors for Strong Electrostatic Adsorption Synthesis of Pt/Alumina and Pt/Carbon Catalysts. **146**, 157-162 (2015).

4   Doyen, G. & Ertl, G. Theory of carbon monoxide chemisorption on transition metals. *Surface Science* **43**, 197-229 (1974).

5   Bulska, E. & Wagner, B. Quantitative aspects of inductively coupled plasma mass spectrometry. *Philos Trans A Math Phys Eng Sci* . **374**, 2079 (2016).

CHAPTER 3

Carboxylic Acid Hydrodeoxygenation over Supported Pt Catalysts

3.1.   Introduction

A roadblock in understanding reaction chemistries over catalysts with high activities is that the desired reaction is seldom the only reaction occurring over the catalyst. Hydrodeoxygenation (HDO) chemistry, for example, has received a lot of attention because of its potential to convert heavily oxygenated bio-derived feedstocks to specialty chemicals[1,2]; this creates an avenue to diversify the industrial feedstock landscape as it can alleviate the burden on fossil fuel derived feedstocks. There has been significant work studying carboxylic acid HDO/hydrogenation over different types of metal supported catalysts, noble metals such as Pt, Ru, Pd and Ni have stood out as having the highest activity. The caveat in employing noble metal catalysts is that a key observation over such catalysts in a monometallic state is the dominance of C-C cleavage products at higher conversions, which is indicative of decarbonylation (DCN), decarboxylation (DCX) and hydrogenolysis reactions[3]. Bimetallic catalysts through the addition of oxophilic promoters to noble metals have shown significant promise in tuning the selectivity toward oxygenated products during HDO[4-6]. While bi-functionality is an important iteration towards selective catalysts for HDO, there is still room for better understanding monometallic catalytic activity of noble metals to contribute to the current overall picture that has been set forth by past studies. There has been a wide array of work done over Pt catalysts exhibiting its ability to facilitate different types of reactions in addition to the ones mentioned previously (DCN, DCX, HDO and hydrogenolysis) such as (de)hydrogenation, methanation, and water-gas shift[7-17]. During carboxylic HDO, one can expect the desired products to include either an aldehyde or alcohol functional group, however Pt

catalyzed HDO has shown to mainly result in DCN and trace DCX products for a short and long chain carboxylic acids tested in the literature. A large portion of insight provided on carboxylic acid HDO over Pt has been done using acetic acid[3,18-20] as the probe molecule because of its simplicity, which is an asset in analyzing non-trivial catalytic activity; such studies have proposed mechanisms to govern some of the observations made during experiments. Work has been done towards increasing the complexity of reactants for HDO such as longer molecules or more than one functional group, however, the active chemistries remained the same regardless of the nature of the reactant. The drawback with using a C_2 carboxylic acid for HDO is that it may be hard to decouple methane derived from C-C cleavage and methanation pathways. Propionic acid (PAc) can act as a good probe molecule to decouple a wider range of reactions than acetic acid since the products formed would be a bit more distinct depending on the pathway occurring. A study was published by Lugo-Jose, Monnier and Williams[21] on PAc HDO over different noble metals; it was found that there was 100% selectivity towards ethane over Pt, indicating DCN to be the dominant pathway. Reactivity over active catalysts such as Pt can be fickle and largely dependent on reaction conditions such as partial pressures, temperatures and contact time. The anticipated (and desired) partially oxygenated hydrocarbons prepared by propionic acid HDO are propanal and propanol. Direct DCN of PAc will yield carbon monoxide, ethylene, and water; C=C hydrogenation is both kinetically facile and (nearly) thermodynamically irreversible; accordingly, if ethylene is formed, it is not expected to be directly observable. Instead, it would be rapidly hydrogenated to form ethane. Decarboxylation of propionic acid can also take place, which will yield CO_2 and ethane. The equations of the expected reactions mentioned are:

Hydrodeoxygenation 1: $C_2H_5COOH + H_2 \rightarrow C_2H_5CHO + H_2O$

Hydrodeoxygenation 2: $C_2H_5COOH + 2H_2 \rightarrow C_2H_5CH_2OH + H_2O$

Decarbonylation + Hydrogenation: $C_2H_5COOH + H_2 \rightarrow C_2H_6 + CO + H_2O$

Decarboxylation: $C_2H_5COOH \rightarrow C_2H_6 + CO_2$

In this study, the reactions involved during HDO of PAc over Pt supported catalysts will be explored by also incorporating observations using the products of HDO as feedstocks for further probing catalyst activity. An expansive mechanism will be proposed by taking into consideration experimental observations as well as those published by past studies. Using data collected over a wide range of conditions as well as different reactants, the system will be modelled in order assess the capability of Pt catalysts to operate in regimes for high HDO selectivity.

3.2. Materials and Methods

3.2.1. Reagents

Air (Airgas, zero grade); amorphous silica (481.2 m^2/g, 48-90 μm mesh size, Aldrich, 99.8%); chloroplatinic acid (Acros, 99.9%); CO (Praxair, 99.99%); CO/He (Airgas: 0.991% CO, 0.996% Ar, 98% He); ethane Airgas: 0.994% C_2H_4, 1. % Ar, 98% He); ethylene (Airgas: 1% C_2H_4, 1% Ar, 98% He); He (Airgas, 99.999%); H_2 (Airgas, 99.999%); N_2 (Airgas, 99.999%%); O_2/Ar/He (1% O_2, 1% Ar, 98% He); propane (Airgas: 1% propane, 1% Ar, 98% He); 1-propanol (Acros Organics, 99+%); propanal (Acros Organics, 99+%) and propionic acid (Acros Organics, 99%) were employed for catalyst synthesis, catalyst characterization, and reactor operation. Each was used as supplied from commercial vendors. Water (Type II, 18.0 MΩcm^{-1} resistivity) was prepared in house (Spectrapure).

3.2.2. Catalyst Preparation

Pt/SiO_2 catalysts were prepared by incipient wetness impregnation of an aqueous chloroplatinic acid solution into amorphous silica (1.8 grams of chloroplatinic acid solution per gram of silica). Concentrations of chloroplatinic acid were varied as necessary to achieve desired mass loadings of platinum. Catalysts were then dried overnight in static air at 393K. Subsequently, samples were loaded into a quartz flow cell, calcined in air (100 ml min^{-1} Air, 3 K min^{-1} ramp rate) at 623 K for 3 hours, then reduced at 673K under H_2 flow for 4 hours (100 ml min^{-1} H_2, 3 K min^{-1} ramp rate), and cooled to 298K under H_2. Prior to exposure to ambient air, samples were passivated at 298K by purging the cell volume with He for 30 minutes and then exposing the cell to 1% O_2 in 1% Ar 98% He for 30 minutes.

3.2.3. Catalyst Characterization

Catalyst surface area and porosity were assessed with N_2 physisorption at 77K using a commercial instrument (Micromeritics ASAP 2020). Surface areas were determined using BET analysis; micro/mesoporosity were assessed using t-plot analysis; pore volumes were computed as the cumulative volume of N_2 condensed at a relative pressure $(P/P_0) = 0.995$; and average pore diameters were estimated from BJH analysis of the desorption branch of the isotherm. Prior to N2 dosing, samples were dried by evacuating to 500µm Hg at 298K and then heated to 623 K (240 min hold, 10 K min^{-1} ramp).

We used CO chemisorption to interrogate the Pt surface area available for reaction (Micromeritics ASAP 2020). Prior to CO dosing, samples were dried by evacuating to 5 µm Hg at 298K and subsequently heating to 373 K (30 min hold, 10 K min^{-1} ramp). Samples were then exposed to flowing oxygen and the cell temperature was increased to 673K (10 K min^{-1}, 30 min hold). The

cell was then evacuated to 5 μm Hg at 673K, held under vacuum for 15 minutes, cooled under vacuum to 373K, and then exposed to H_2 flow. The cell was then heated under continuous H2 flow to 673K (10K min^{-1}, 4 h hold). Finally, the cell was evacuated to 5 μm Hg at 673K to remove chemisorbed hydrogen (30 min) and cooled to 308K under vacuum. A CO uptake isotherm was then collected at 308K, the sample cell was evacuated to remove physisorbed CO, and a second CO uptake isotherm was collected at 308K. Irreversible CO uptake was calculated as the difference in CO uptake between the two isotherms. Pt particle size was estimated assuming that Pt has a shape factor of 6, an atomic cross sectional area of 0.08 nm^2 and a density of 21.450 g cm^{-3}. The average diameter of the nanoparticle as well as the dispersion of the metal can be calculated using Equations 2.1-2.3:

3.2.4. Catalyst Activity Testing

The reactor system used for all catalytic activity tests is illustrated in Figure 2.2. Gases introduced to the system at controlled flowrates using digital mass flow controllers (Brooks). Reactors always operated under gas phase conditions, but many of our feeds were introduced to the system as liquids using a syringe pump (Cole Parmer). Specifically liquids were fed through a PEEK capillary (130 μm, IDEX) into a home-built, temperature-controlled vaporizer, where they were combined with pre-heated gas feeds. To increase surface area for gas-liquid contact, the vaporizer was packed with quartz granules (850-2000 μm, Aldrich). To ensure complete vaporization, partial pressures of condensable species were maintained below 15% of their vapor pressure at a given reaction condition. After leaving the vaporizer, the process stream flowed through a 6-port valve, which was used to direct flow either to the reactor or to the bypass. During startup, the reactor was bypassed until we observed steady state feed concentrations via Gas Chromatography. Once the reactor feed stream reached steady state, flow was diverted to the reactor.

The packed bed reactor operated in an upflow configuration. It was constructed from ½" stainless steel tubing (McMaster). The catalyst bed was placed between two quartz wool plugs in the center of the tube, and the void volume upstream of the reactor was packed with quartz granules. The reactor temperature was monitored at the external wall using a type-K thermocouple, and the external wall temperature was regulated using a PID controller (LOVE 16A 3010). A second type-K thermocouple was placed inline and used to monitor reactor temperature immediately downstream of the catalyst bed. Data reported in this manuscript reflect the inline temperature measurement. The reactor effluent was transferred, via heat-traced stainless steel tubing, to a pair of online gas-chromatographs (HP 5890) for quantitative resolution of the product mixture. The first GC was equipped with dual inlets leading, respectively, to an HP-PONA column paired with a flame-ionization detector (FID) and a Restek ShinCarbon ST Micropacked column paired with a thermal conductivity detector (TCD). In general, propionic acid, propanal, propanol, propane, ethylene, and ethane were resolved and quantified using the PONA/FID system, while methane, CO, and CO_2 were resolved and quantified using the ShinCarbon/TCD system. The second GC was configured with a single inlet and a Restek ShinCarbon ST Micropacked column leading to a Methanizer/FID detector. This system was used for quantifying CO, CO_2, and methane concentrations that were below TCD detection limits. Species were qualitatively identified using standards prepared from commercial samples. Where necessary, unknown species were identified by injection of gas samples into an offline GC-MS (Agilent 7890 + 5975C MSD). Carbon balances for all conditions reported here closed to 95% or greater.

Reactions were run over various catalysts, temperatures, reactant partial pressures, and contact times, and species production rates were quantified at 15-minute intervals. Unless otherwise noted, reported rates reflect steady state operation. Typically, after startup, reactors were allowed to reach

steady state species production rates under a well-defined, "reference" condition. This typically took less than 1 hour. After reaching steady state, production rates for all species were quantified. Subsequently, a single perturbation in temperature, partial pressure, or contact time was introduced, and the system was allowed to evolve to a new steady state, where effluent flowrates of all species were again quantified. Metal catalysts employed for oxygenate processing are generally susceptible to various modes of deactivation, which can obscure kinetic trends. Accordingly, after quantifying the impact of each perturbation on species flowrates, the system was returned to the reference condition and allowed to reach steady state. This provided a rigorous benchmark for assessing catalyst deactivation. Under most of our operating conditions, deactivation was relatively mild. Differences in zero time production rates and steady state production rates measured at the reference condition throughout the experiment showed less than 10% loss in activity; accordingly, steady state rates were not corrected for deactivation. There is one exception: we have observed that high pressures of propanal induce severe deactivation of Pt, which is consistent with prior reports. In general, high propanal pressures were encountered when feeding propanal or 1-propanol into reactors (the latter readily dehydrogenates over Pt to form propanal). In systems with pronounced deactivation, it is difficult to define meaningful reaction rates from steady state measurements as the available catalytic surface area is generally changing as a function of time on stream. In these systems, initial production rates were estimated by extrapolating the deactivation profile to zero-time-on-stream. During typical startup and between experiments (e.g., changing the feed molecule), the catalyst bed was reduced under flowing H_2 at 673K (10 K min^{-1}, 4h), which was sufficient to restore the initial activity of the catalyst after most experiments. However, a reducing treatment alone was not able to restore activity after exposure

to high propanal pressures. In these experiments, it was instead necessary to calcine catalysts in flowing air prior to reduction.

Species production rates are reported here as site time yields:

$$STY_j = \frac{F_j}{N_{Pt}}$$

Equation 3.1

Where Fj is the total molar flowrate of species j in the reactor effluent and N_{Pt} is the total molar quantity of surface Pt atoms in the catalyst bed as estimated by CO chemisorption. Feed conversion was defined on a carbon basis and computed based on product flowrates:

$$X_i = \frac{\sum_{j \neq i} F_j \cdot C_{n,j}}{F_{i,0} \cdot C_{n,i}}$$

Equation 3.2

Where F_j is the molar flowrate of reaction products, j, in the reactor effluent, $F_{i,0}$ is the inlet flowrate of the reacting species, i, and C_n is the number of carbon atoms in a given molecule. Selectivity to a specific reaction product, k, is defined in terms of molar flowrates of all reaction products, j:

$$S_k = \frac{F_k}{\sum_j F_j}$$

Equation 3.3

3.3. Results

3.3.1. Propionic Acid

From the expected reactions mentioned previously, one can expect the anticipated reaction network as summarized in Figure 3.1. The trends associated with propionic acid HDO will be

observed by these expected pathways as a means of not overcrowding figures, this will allow a

clearer focus on product behaviors.
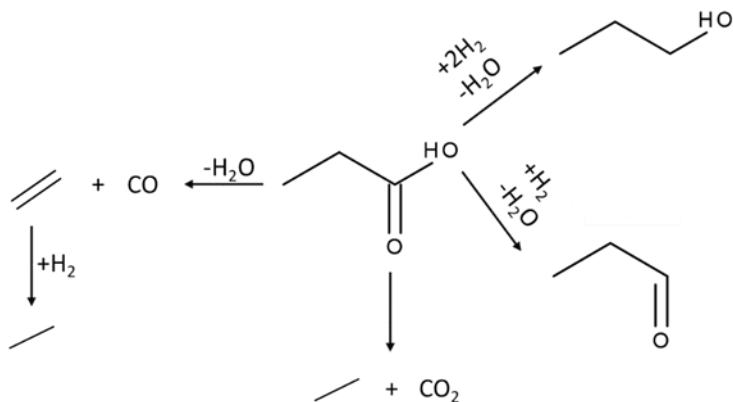
Figure 3.1: Anticipated reaction pathways for propionic acid HDO over Pt.

Here we first explore how the yield of each anticipated species varies as a function of contact

time, this allows us to gauge the selectivity of HDO products in relation to other undesired

products; we can also extract reaction rates and observe whether any of the reactions are

equilibrated. Theoretically, the slope of a *'yield vs contact time'* graph should represent the rate

of the reaction. The yield of the anticipated species –only taking into consideration proposed

pathways- might plateau with contact time in the instance of a reaction approaching equilibrium.

Analyzing apparent rates become problematic when operating in regions where yield finds itself

behaving non-linearly with contact time as it means that the 'rate values' may be influenced by

reaction equilibrium. It is important to note that for very short contact time regimes, the yield of

majority of the species are fairly linear with contact time. The yield of HDO 1 (propanal) and

HDO 2 (propanol) products over different contact times can be seen in Figure 3.2. The yield of

propanal increases at very short contact times then begins to decrease after a contact time of 20 s.

The yield of propanol shows a sharp increase at short contact times, after which the change in

yield is reduced as the experiment condition taken towards higher contact times.
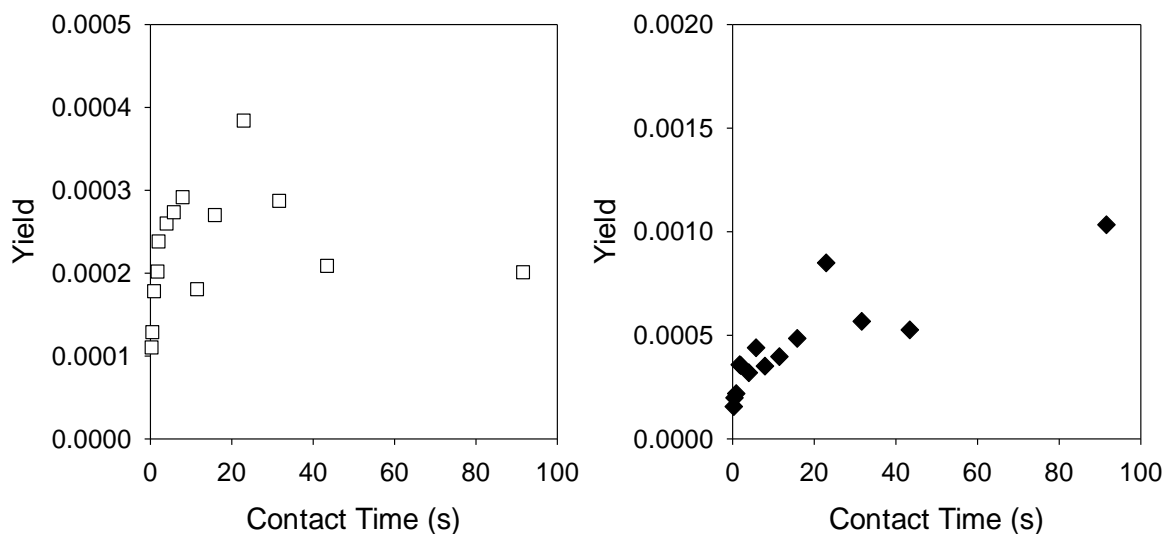
Figure 3.2: Effect of contact time on the yield of HDO 1 (left) and HDO 2 (right) products propanal and propanol respectively, at propionic acid and hydrogen partial pressure of 5 and 755 torr respectively at 448K over Pt.

Conversions in the displayed yield figures for HDO 1 and HDO 2 were less than 2%, yet they showed evidence of approaching a plateau, which is typically characteristic of a chemical reaction approaching equilibrium. The data for the HDO 1 and HDO 2 pathways were reworked in order to observe their proximity to equilibrium at the different contact times; this can be seen in Figure 3.3. The y-axis represents the ration between reaction quotient (Q) and theoretical equilibrium (K); a value of (or near) 1 would mean the reaction is constrained by equilibrium phenomenon. Propanal and propanol are orders of magnitude below the theoretical equilibrium, this means that the rates are decreasing for a non-equilibrium phenomena.
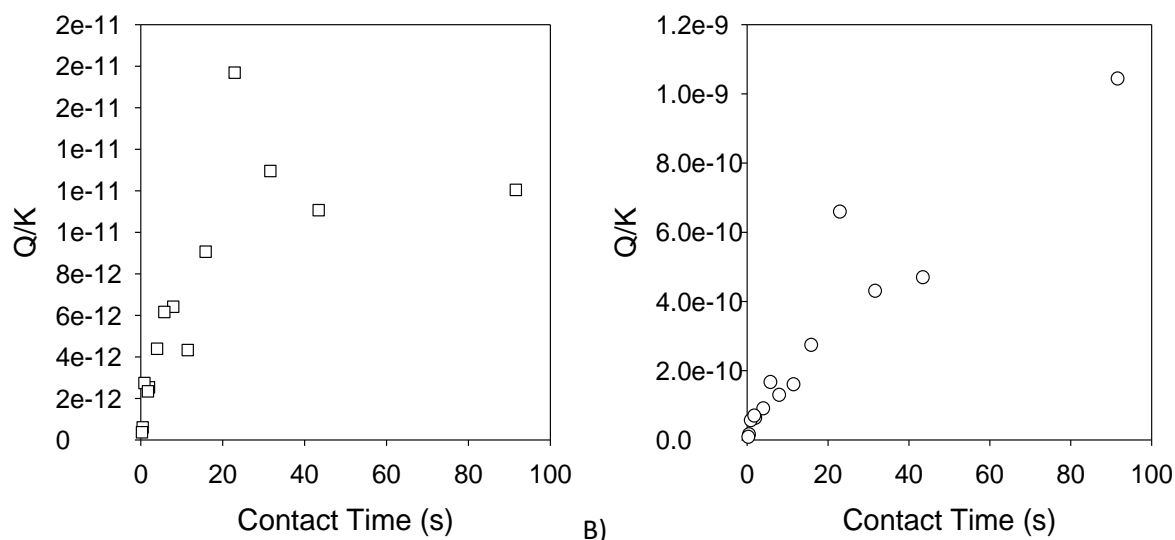
Figure 3.3: Proximity to equilibrium of the pathways HDO 1 (left) and B) HDO 2 (right) at propionic acid and hydrogen partial pressure of 5 and 755 torr respectively at 448K over Pt.

The yields of DCN products ethane and carbon monoxide are shown in Figure 3.4 (left). The yield of carbon monoxide and ethane are equal at contact times below 40s, after which the ethane yield becomes slightly higher than carbon monoxide's. The yield of carbon monoxide and ethane are linear at short contact times, but eventually show signs of "plateau-ing", which is indicative of a decrease in reaction rate. While ethane begins to approach a plateau, the carbon monoxide yield actually shows a slight decrease at higher contact times. The yield of DCX products carbon dioxide and ethane is illustrated in Figure 3.4 (right). The DCX reaction produces ethane and carbon dioxide in equimolar amounts; however, ethane's yield was significantly higher than the yield of carbon dioxide. The ethane trend was described previously, as it is also a product of DCN. Carbon dioxide had the lowest yield of all the anticipated products, the yield appeared to be stable across contact times below 40 s, but then shows a slight decrease. The observation that ethane's yield was closer to carbon monoxide than that of carbon dioxide is likely due to the fact the DCN pathway is more prevalent at these conditions compared to DCX; DCX appeared to be

the least favorable pathway. Products also appeared to plateau at higher contact times, this was

quickly investigated by observing their proximity to equilibrium for the DCN and DCX

pathways as seen in Figure 3.5
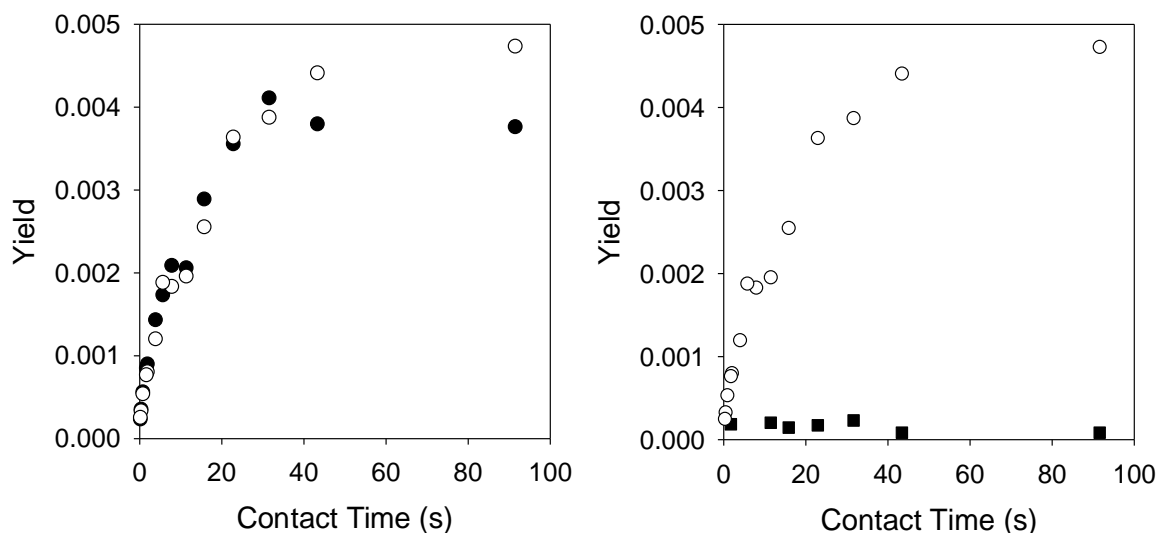
Figure 3.4: Effect of contact time on the yield of DCN (left) and DCX (right) products ethane (○), carbon dioxide (■) and carbon monoxide (●) at propionic acid and hydrogen partial pressure of 5 and 755 torr respectively at 448K over Pt.

As with the HDO 1 and 2 pathways, DCN nor DCN are even remotely close to their respective

theoretical equilibrium values, yet their rates are decreasing with contact time. Further

investigations into the decreasing rates during propionic acid HDO will be carried out later on in

this section.
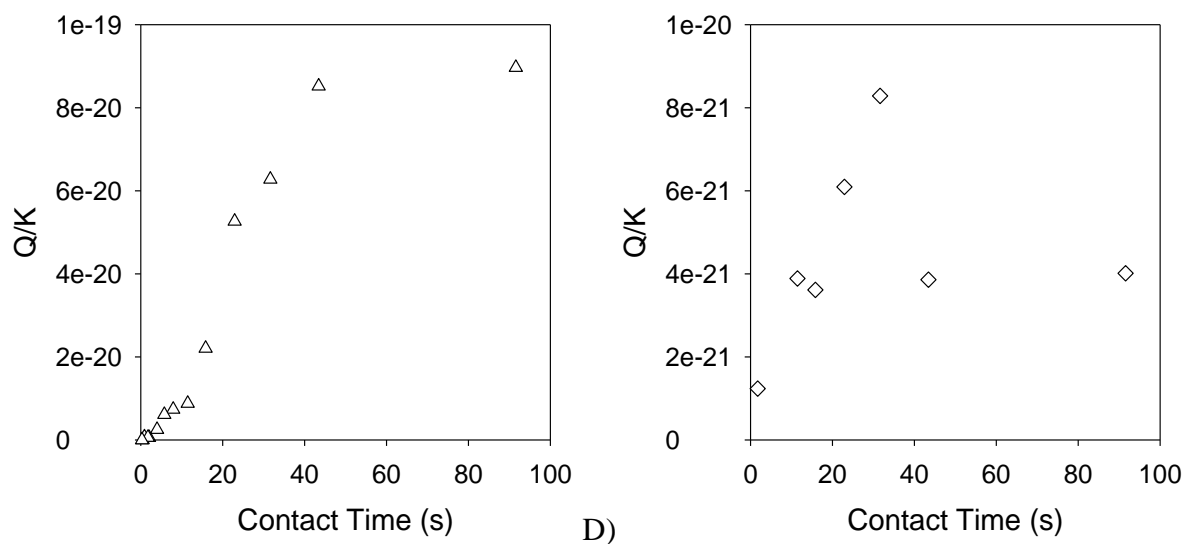
Figure 3.5: Proximity to equilibrium of the pathways DCN (left) and DCX (right) at propionic acid and hydrogen partial pressure of 5 and 755 torr respectively at 448K over Pt.

Taking into consideration the linear data at lower contact times, we can extract production rates as seen in Table 3.1. Ethane and carbon monoxide had the same production rate at the experimental conditions and also the highest production rates of all the observable species, this is because both products are formed in equimolar amounts through the DCN pathway, their high production rates also accounts for the yield of carbon monoxide and ethane being the highest. The rates of the propionic acid HDO 1 and HDO 2 products were an order of magnitude lower than DCN products, with propanol production rate slightly higher than that of propanal. Carbon dioxide production rate was the lowest; this quantity was calculated by taking the average of all the individual site-time yields since the slope of the yield would be negative.

Table 3.1: Production rates of anticipated species at propionic acid and hydrogen partial pressure of 5 and 755 torr respectively at 448K over Pt

Species	Production rate (s^{-1})
Ethane	0.0003
Carbon Monoxide	0.0003
Propanol	0.00004
Propanal	0.00003

Carbon Dioxide	0.00001

There were two products formed that was not as a result of the anticipated equations, propane and methane, these unanticipated products in addition to some product yields decreasing at higher contact time hits towards primary products being possibly consumed by secondary reactions. The effect of contact time on the yields of unanticipated products is shown in Figure 3.6. Apart from carbon dioxide, the unexpected products had yields far lower than most of the anticipated products. The yield of propane showed a sharp increase in the range of short contact times, but the rate shows to decrease at higher contact times. Methane shows a steady linear increase in yield across all contact times where the amounts were large enough for collectable data.
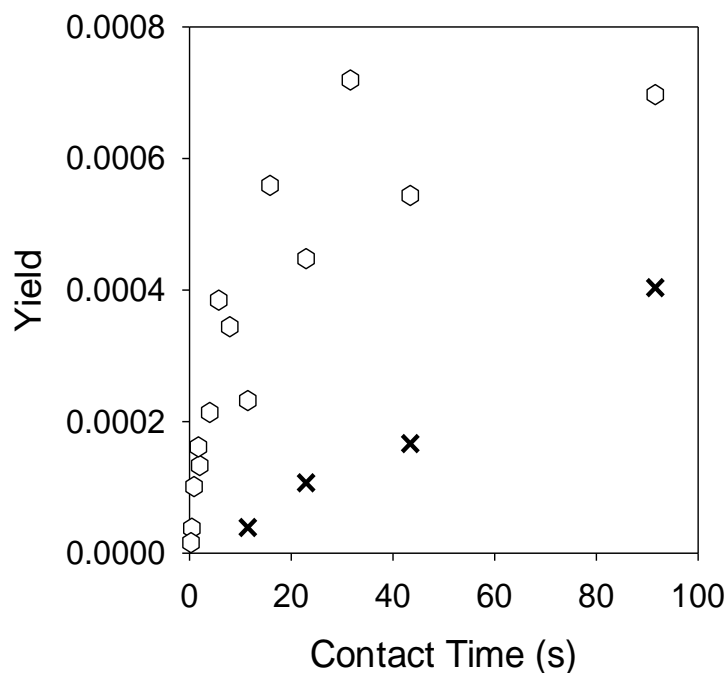
Figure 3.6: Effect of contact time on the yield of unanticipated products propane (○) and methane (**x**) at propionic acid and hydrogen partial pressure of 5 and 755 torr respectively at 448K over Pt.

The production rates of the unanticipated products is shown in Table 3.2. Methane production rate was the lowest of all species observed during propionic acid HDO at the experimental conditions. Propane was produced at a higher rate than the HDO products (seen in Table 3.2), propanol and propanal.

Table 3.2: Production rates of anticipated species at propionic acid and hydrogen partial pressure of 5 and 755 torr respectively at 448K over Pt

Species	Production rate (s^{-1})
Propane	0.00008
Methane	0.000004

Upon analyzing the yields of the various products, we have two main inquires: what are the actual pathways involved during propionic acid HDO? And also, why is the rate of the reaction pathways decreasing when operating so far from equilibrium?

In order to further discriminate between pathways leading to observed products, the molar selectivity experiments can be designed to discriminate between species formed as primary products during propionic acid HDO and those formed through sequential reactions that consume primary products. The goal in the selectivity experiments is to approach the zero-conversion limit for propionic acid HDO. The expectation is that, as propionic acid conversion approaches zero, so will the partial pressure of the primary products of propionic acid conversion. As the partial pressure of these species approaches zero, so does the driving force for secondary reactions; thus, in the zero conversion limit, only primary reaction products can be observed. Practically speaking, this means that products formed from non-primary pathways will approach zero selectivity in the zero conversion limit, whereas primary products will have a positive, non-zero selectivity in the zero conversion limit. As conversion increases, we generally can observe three distinct phenomena. First, species selectivity may remain constant as a function of feed fractional

conversion. This observation implies a stable product that does not undergo sequential reaction. Second, species selectivity may increase as a function of feed fractional conversion. In general, this implies that the species is formed through sequential (i.e., secondary or tertiary reaction pathways). Finally, species selectivity may decrease as a function of feed fractional conversion, which implies that a species is consumed by sequential reactions. Importantly, there is no restriction that prevents a single species from being formed in multiple reactions, and some species can exhibit characteristics of both primary and secondary products.

At a fixed temperature, as well as propionic acid and hydrogen partial pressures, the effect of conversion on selectivity was observed for the products formed during HDO experiments. The lowest conversion achieved was 0.08%, lower conversions were impractical as product resolution would become difficult with the current setup. The selectivity of HDO 1 product propanal as a function of conversion is shown in Figure 3.7. Propanal selectivity decreases (from a non-zero y-intercept) with conversion; its selectivity reduces by more than 90% over the 1% conversion range tested.
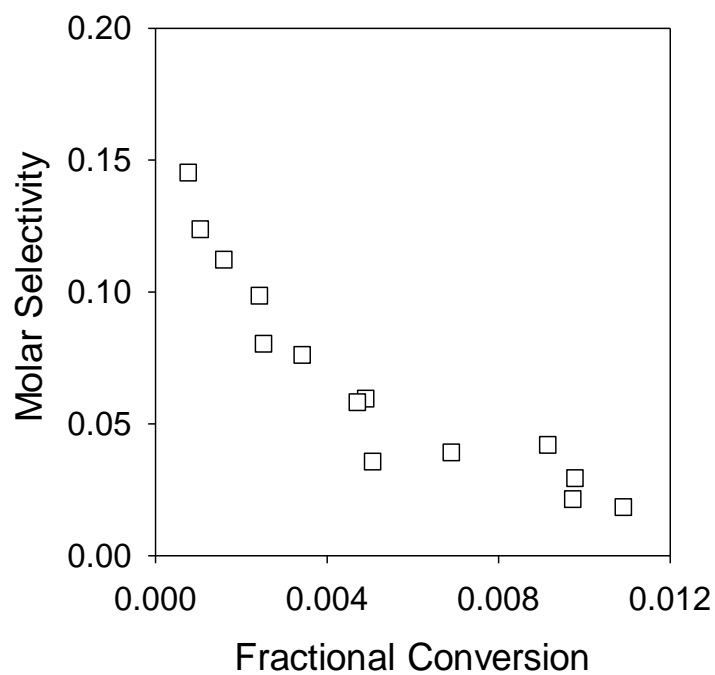
Figure 3.7: Effect of fractional conversion on the molar selectivity of HDO 1 product propanal at propionic acid and hydrogen partial pressure of 5 and 755 torr respectively at 448K over Pt.

The effect of conversion on the selectivity of HDO 2 product propanol ,as seen in Figure 3.8, behaves similar to propanal; there is a decrease in selectivty across the conversion tested, propanol also appears to have a non-zero selectivity towards the zero fractional conversion limit. The selectivity of propanol is slightly higher than that of propanol for all the data collected. As a contrast, propanol selectivity appears to be approaching a steady state while propanal showed no evidence of approaching a fixed selectivity.
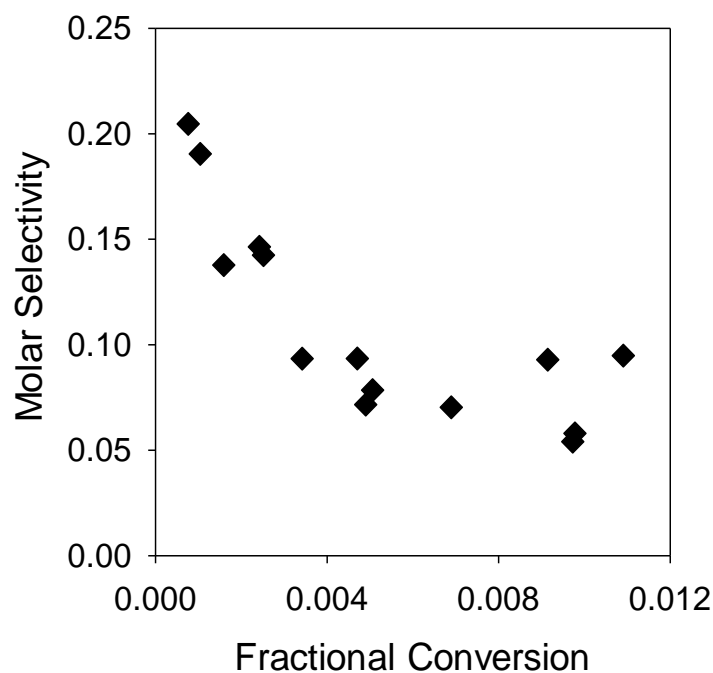
Figure 3.8: Effect of fractional conversion on the molar selectivity of HDO 2 product propanol at propionic acid and hydrogen partial pressure of 5 and 755 torr respectively at 448K over Pt.

The selectivity towards DCN products across different conversions is illustrated in Figure 3.9. Carbon monoxide and ethane expectedly appears in stoichiometric ratio as was pointed out previously when observing their yields. The selectivity of DCN products was consisently higher than the other observed products acoss all converstions tested, the selectivity also increased with conversion. The ratio between ethane and carbon dioxide in the yield data carried over into their selectivites as seen in Figure 3.10, which describes the effect of conversion on DCX products. Carbon dioxide showed a decrease in selectivity with conversion for the amounts that were large enough to be quantified accurately; as with yield, it also had the lowest selectivity of all the anticipated products. The molar selectivities of all the anticipated products (propanal, propanol, carbon monoxide, ethane and carbon dioxide) appeared to intercept the Y-axis at a nonzero values

towards the zero conversion limit; this confirms that all product are indeed formed from primary pathways.
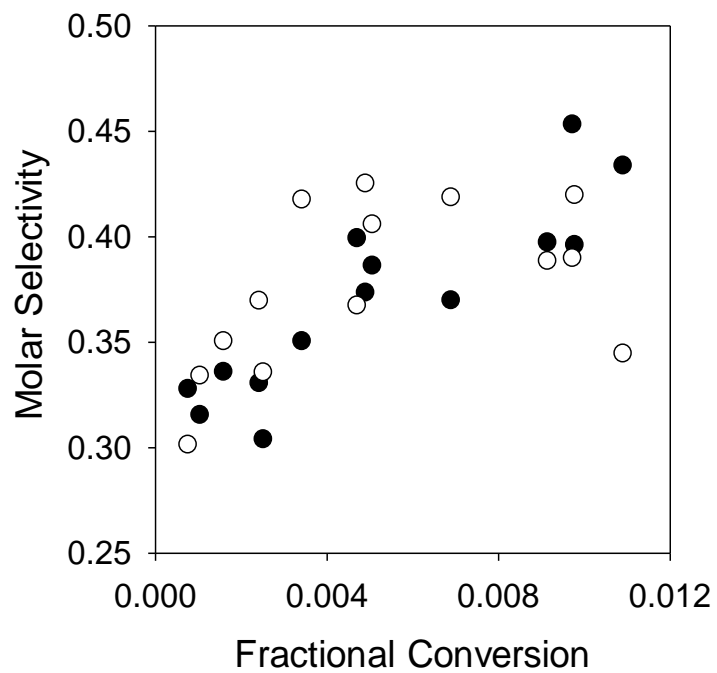
Figure 3.9: Effect of fractional conversion on the molar selectivity of DCN products ethane (○) and carbon monoxide (●) at propionic acid and hydrogen partial pressure of 5 and 755 torr respectively at 448K over Pt.
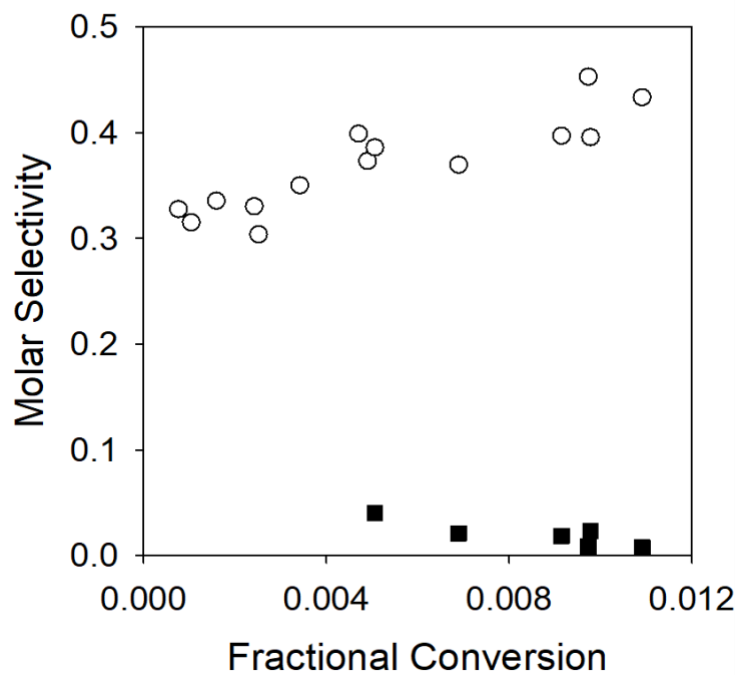
Figure 3.10: Effect of fractional conversion on the molar selectivity of DCX products carbon dioxide (■) and ethane (○) at propionic acid and hydrogen partial pressure of 5 and 755 torr respectively at 448K over Pt.

The molar selectivity of the unanticipated products, propane and methane, are illustrated in Figure 3.11. Both products appear to be increasing with conversion, with propane having the higher selectivity of the products, and they also intercept the y-axis at zero towards zero conversion, which means that these are not primary products.
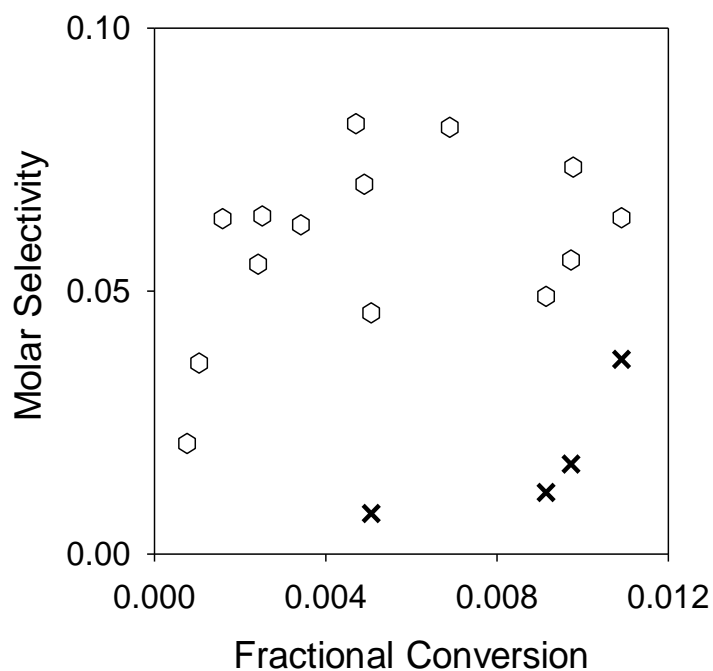
Figure 3.11: Effect of fractional conversion on the molar selectivity of the unanticipated products propane (○) and methane (**x**) at propionic acid and hydrogen partial pressure of 5 and 755 torr respectively at 448K over Pt.

Carbon monoxide, ethane, methane and propane all show increasing selectivity as a function of conversion, which suggests they are formed by non-primary reactions; and carbon dioxide, propanol and propanal decrease in selectivity as a function of conversion, suggesting they are both consumed by sequential reactions.

In addition to the molar selectivities of all products, the rate of conversion was also observed at different fractional conversions during propionic acid HDO, this is illustrated in Figure 3.12. The rate of conversion showed a large decrease (>90%) over the fractional conversion range tested. The rate of conversation observation reflects the "plateau-like" characteristics of the product yields, this point towards some sort of rate inhibition that is destroying catalytic activity.
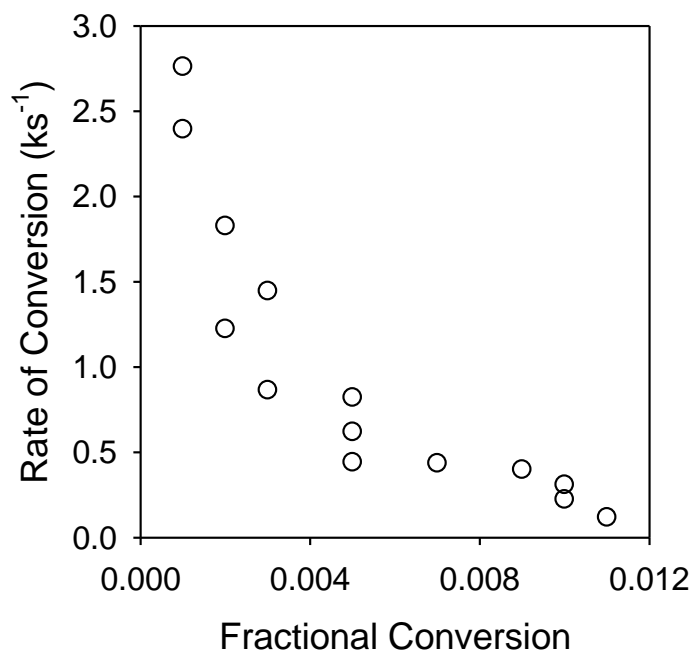
Figure 3.12: The rate of conversion of propionic acid at different fractional conversions during propionic acid HDO at propionic acid and hydrogen partial pressure of 5 and 755 torr respectively at 448K over Pt.

In order to further resolve contributions from primary and secondary reactions, we analyzed effect of fractional conversion on the product selectivities formed from each of the primary products when they are used as reactants in a hydrogen rich environment over Pt. We also monitored the rate of conversions while probing these non-primary pathways; this would allow us to pinpoint the main culprit for the observed product inhibition in Figure 3.12.

3.3.2. Propanal

A survey of the literature provides a source for anticipated reaction pathways that might take place feeding propanal and hydrogen over Pt[14,22]. Aldehydes can be hydrogenated to form an alcohol, in this instance, propanol would be the anticipated product. It is also expected that DCN can take place; this C-C bond cleavage of propanal would form ethane and carbon monoxide. It is already being seen that there are possible pathways that may interfere with rates that were

measured previously during propionic acid HDO. We have avenues for propanal consumption that include routes that may produce propanol, ethane and carbon monoxide.

Hydrogenation: $C_2H_5CHO + H_2 \rightarrow C_2H_5CH_2OH$

Decarbonylation: $C_2H_5CHO \rightarrow C_2H_6 + CO$
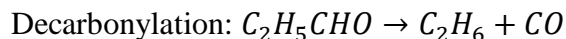
This anticipated primary reaction network is summarized in Figure 3.13.
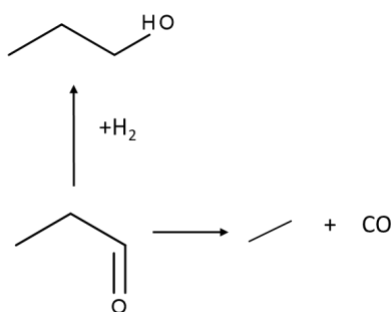
Figure 3.13: Anticipated primary reaction pathways for propanal over Pt.

The effect of conversion on the molar selectivity of propanol and ethane are shown in Figures 3.14 and 3.15 respectively. The presence of the anticipated products confirmed the hydrogenation and DCN pathways proposed. Propanal hydrogenation to form propanol has the highest selectivity, this decreases as conversion is increased. The quantity of DCN products were too low for carbon monoxide to be observed because of detector sensitivity, therefore ethane was the only DCN product that was able to be observed in the reactor outlet. The molar selectivity of ethane was constant across all the fractional conversions tested; ethane also had the lowest molar selectivity of all observed products during propanal HDO experiments. Propanol and ethane had non-zero molar selectivities towards zero conversion, confirming the DCN and hydrogenation primary pathways. Ethane is seen as a stable species, indicating that it is neither formed nor consumed by

non primary pathways. Propanol is the only product that is decreasing in selectivity, this means that it is being consumed by a non-primary reaction.
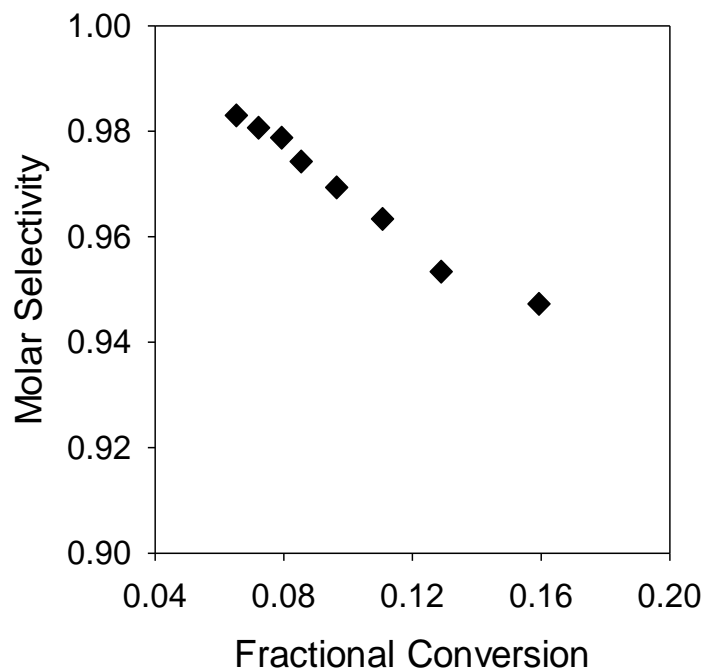
Figure 3.14: Effect of fractional conversion on the molar selectivity of the Hydrogenation product propanol at propanal and hydrogen partial pressure of 2.6 and 757 torr respectively at 311K over Pt.

The molar selectivity towards propane is shown in Figure 3.16. Propane selectivity increased with fractional conversion; it was the only observed product to show an increase. The selectivity of propane also appears to intercept the y-axis at zero. Since the decrease in propanol is almost proportional to the increase in propane, it is likely that the reaction consuming propanol is the also the reaction producing propane, this will be further elaborated on in the discussions on propanol pathways, as selectivity figures can only differentiate between primary and non-primary pathways.
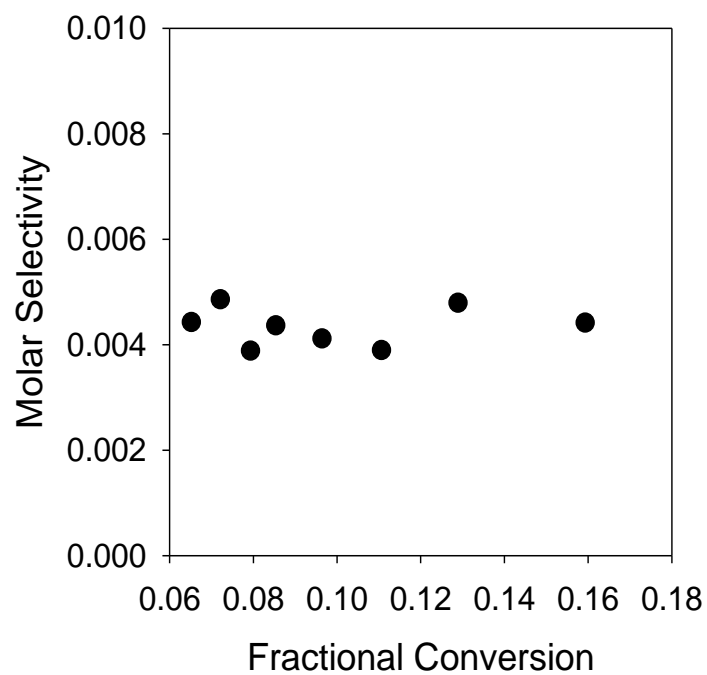
Figure 3.15: Effect of fractional conversion on the molar selectivity of DCN product ethane at propanal and hydrogen partial pressure of 2.6 and 757 torr respectively at 311K over Pt.
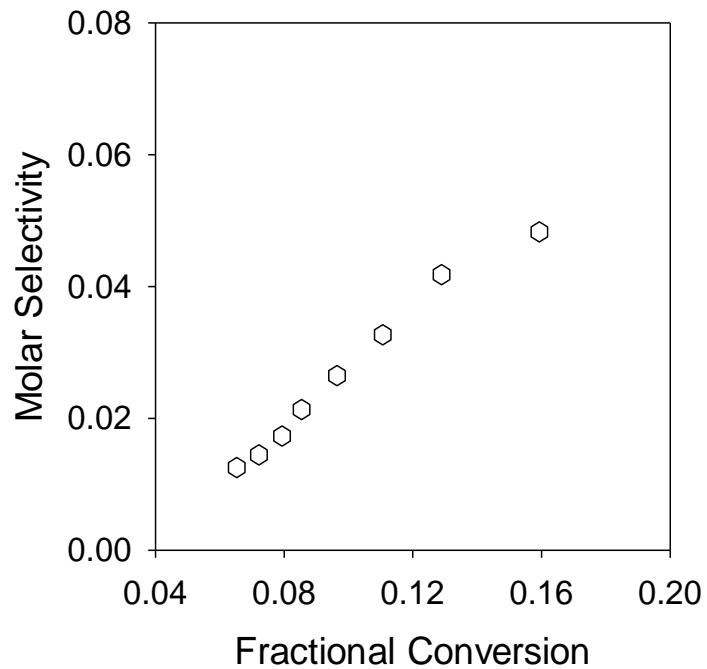
Figure 3.16: Effect of fractional conversion on the molar selectivity of the unanticipated product propane at propanal and hydrogen partial pressure of 2.6 and 757 torr respectively at 311K over Pt.

3.3.3. Propanol

Propanol is expected to undergo dehydration to form propylene as a primary product, however, we speculate that the hydrogen excess environment would rapidly hydrogenate the unsaturated bond to form propane[6]; this can be visualized as a one-step hydrogenolysis reaction. Propanol over most metals can also undergo dehydrogenation to form propanal[22,23].

Hydrogenolysis: $C_2H_5CH_2OH + H_2 \rightarrow C_3H_8 + H_2O$

Dehydrogenation: $C_2H_5CH_2OH \rightarrow C_2H_5CHO + H_2$
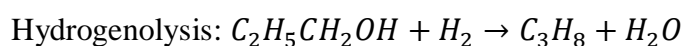
This anticipated reaction network is summarized in Figure 3.18.
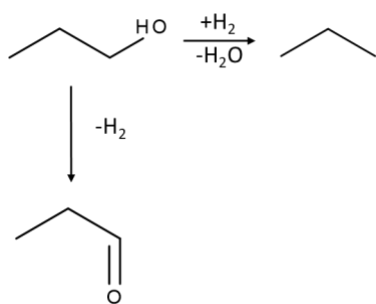
Figure 3.18: Anticipated primary reaction pathways for propanol over Pt.

The effect of fractional conversion on the molar selectivity of hydrogenolysis and dehydrogenation products are shown in Figures 3.19 and 3.20 respectively. The molar selectivity of the hydrogenolysis product propane is fairly constant across all the fractional conversions tested; at low conversions it was the least selective product, which changed at higher conversions because of the propanal trend. Propane's stability means that it was not consumed by a secondary pathway. The dehydrogenation pathway, as represented by propanal, decreased in molar

selectivity as the conversion increased, eventually being the least selective observed product towards higher conversions; this means that propanal is being consumed rapidly by a secondary pathway. Both propane and propanal had non-zero y intercepts towards the zero conversion limit, confirming both products being formed through their anticipated primary pathways.
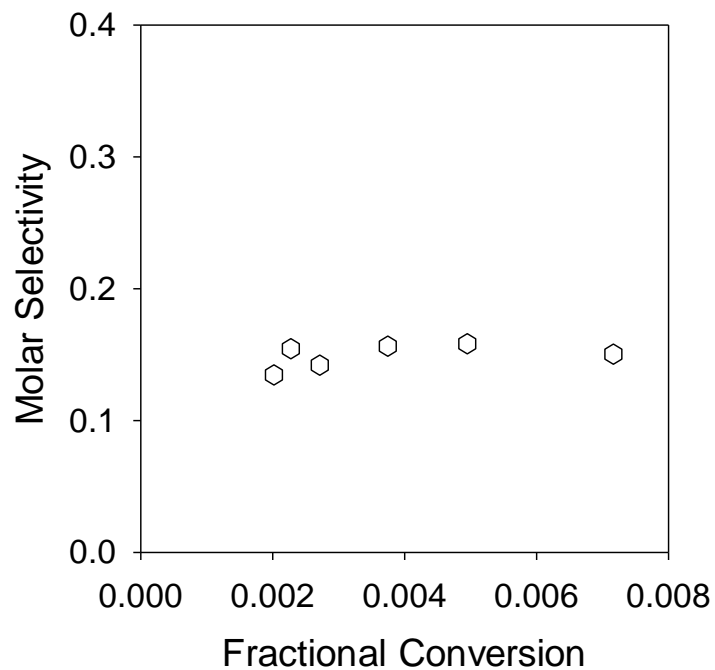
Figure 3.19: Effect of fractional conversion on the molar selectivity of the Hydrogenolysis product propane at propanol and hydrogen partial pressure of 5 and 755 torr respectively at 458K over Pt.
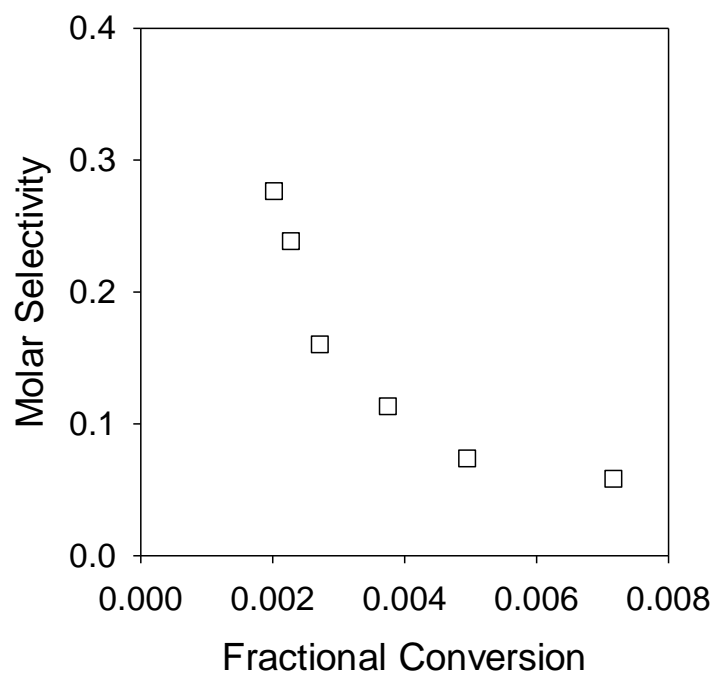
Figure 3.20: Effect of fractional conversion on the molar selectivity of the Dehydrogenation product propanal at propanol and hydrogen partial pressure of 5 and 755 torr respectively at 458K over Pt.

The molar selectivities of the unanticipated products as a result of changes in fractional conversion are illustrated in Figure 3.21. The first major observation is that carbon monoxide and ethane are formed in near equal amounts. The molar selectivity of both products also appear to be increasing with fractional conversion. It is unclear whether the products would eventually intercept the y-axis at a zero or non-zero value, but based on the experimental data presented in Figure 3.21, it appears to have the primary product characteristic of a non-zero value.
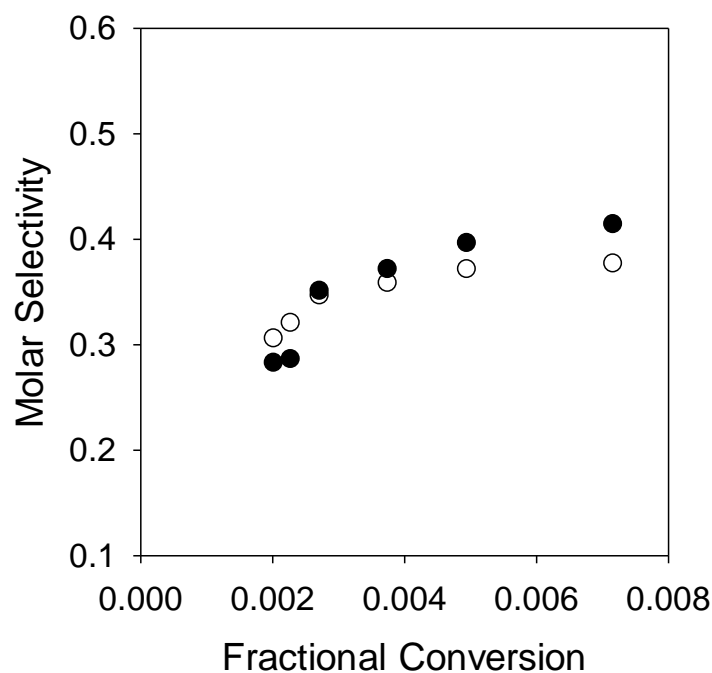
Figure 3.21: Effect of fractional conversion on the molar selectivity on products of unanticipated primary reactions, ethane (○) and carbon monoxide (●) at propanol and hydrogen partial pressure of 5 and 755 torr respectively at 458K over Pt.

We revisited DCN products from propanal because of the observations in Figure 3.21; this is because there is no reported direct DCN of propanol[24,25]. We probed propanal reactivity at 311K, whereas we generally benchmark propanol reactivity at significantly higher temperatures. We observe that direct decarbonylation of propanal occurs with a STY (molar species production rate per unit mole of active site) of 0.0118 min^{-1} at 311K at propanal and hydrogen partial pressures of 2.6 and 757.4 torr respectively. Over Pt, we do not observe comparable site time yields for propanol dehydrogenation (to form propanal) until roughly 410K at propanol and hydrogen partial pressures of 5 and 755 torr respectively. Here, we observe a propanal STY of 0.015 min^{-1}. Practically speaking, the observation that, for similar oxygenate partial pressures, aldehyde decarbonylation rates at 311K are comparable to alcohol dehydrogenation rates at

410K suggests that, over Pt, aldehyde decarbonylation is intrinsically facile relative to alcohol dehydrogenation.

While comparing propanal and propanol experiments, another important observation from propanal HDO is that the rate of aldehyde hydrogenation (3.2 min-1 at 311K) is rapid relative to observed total rate of propionic acid conversion at 437K (0.079 min-1). This may suggest that the apparent co-production of propanal and propanol as primary products during propionic acid HDO (Figures 3.7 and 3.8) is an artifact of rapid aldehyde hydrogenation. This was further investigated by taking the quantities of propanol and propanal formed during propionic acid HDO and observing its proximity to equilibrium considering the products only as a result of the aldehyde hydrogenation pathway (illustrated in Figure 3.22). In addition to propanal hydrogenation to form propanol being a facile reaction, it seems that there is a high possibility that the reaction is equilibrium controlled from its proximity to the theoretical equilibrium under the experimental conditions.
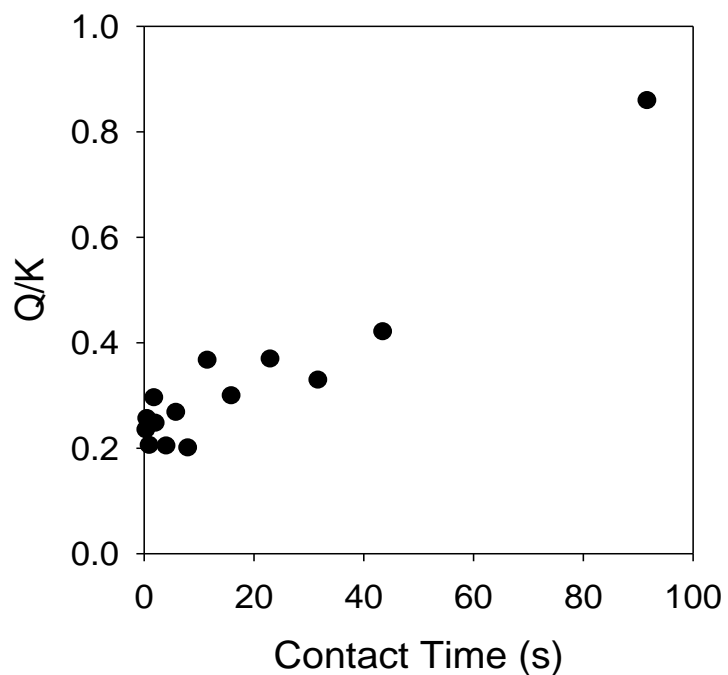
Figure 3.22: Proximity to equilibrium considering propanol formed through propanal hydrogenation during propionic acid HDO experiments at propionic acid and hydrogen partial pressures of 5 and 755 torr respectively at 448K over Pt.

The effect of fractional conversion on the rate conversions is illustrated in Figure 3.23. The rate of conversion decreases rapidly across the fractional conversion range tested, this observation is similar to the occurrence during propionic acid HDO in Figure 3.12. At this point, propanol and propionic acid showed a decrease in rate of conversion, while both having high selectivity to DCN products during reactivity.
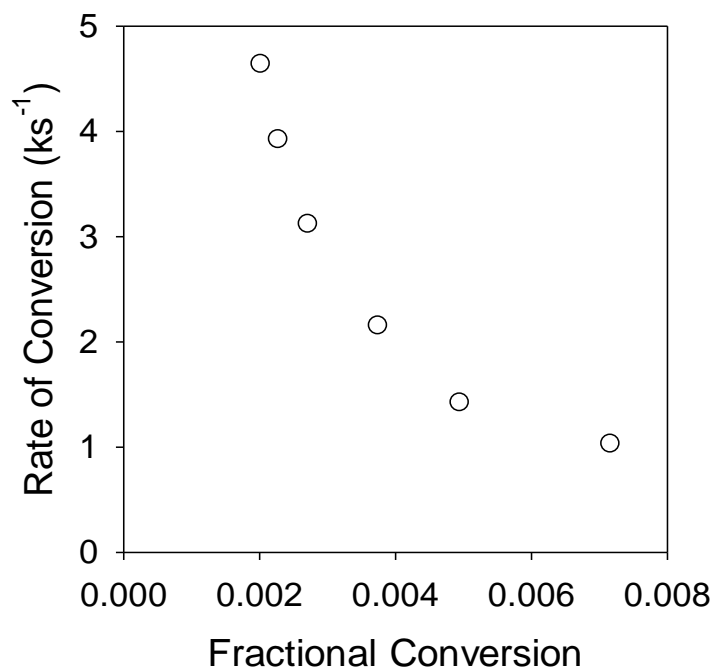
Figure 3.23: The rate of conversion of propanol at different fractional conversions at propanol and hydrogen partial pressure of 5 and 755 torr respectively at 458K over Pt.

3.3.4. Carbon Monoxide

Here we probe possible reactions involving carbon monoxide as reported throughout the literature[17,26-29]: methanation, water-gas shift, and the Boudouard reaction under characteristic operating conditions; this meant low CO partial pressures in a hydrogen rich environment.

Methanation: $CO + 3H_2 \rightarrow CH_4 + H_2O$

Boudouard Reaction: $CO + CO \rightarrow CO_2 + C$

Water-Gas Shift: $CO + H_2O \rightarrow CO_2 + H_2$
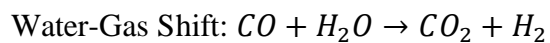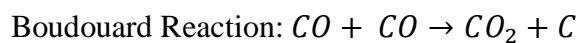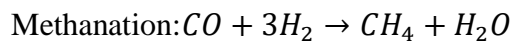
CO methanation was tested as over a range of conditions that include partial pressures of 0.5-60 torr and temperatures of 450-550K. In general, we observe that CO undergoes methanation to an appreciable extent under our reaction conditions, which indicates that CO methanation is a primary source of methane in our system. It is also worth mentioning that propane and ethane showed no evidence of hydrogenolysis over Pt, which allows us to exclude consideration of propane and ethane hydrogenolysis as potential methane sources under our experimental conditions. Carbon dioxide was observed as a product during propionic acid HDO when carbon monoxide product partial pressures were in the range of 0.003 - 0.11 torr, this range was troublesome to attain as 0.5 torr was the lowest achievable partial pressure given the materials available. The Boudouard reaction showed no observable activity at a CO partial pressure of 0.5 torr in the temperature range of 450-550K; however, carbon dioxide formation rates were seen above 600K. Water-gas shift reaction is a well-documented reaction over Pt catalysts; further control experiments also showed this chemistry to be active in conditions as close to those during propionic acid HDO. Water-gas shift experiments include cofeeding in trace amounts of water that would typically be formed during HDO. A key takeaway from carbon monoxide experiments is Figure 3.24, which shows the rate of conversion of carbon monoxide as a function of fractional conversion. The rate of carbon monoxide conversion decreased with fractional conversion, which follows the trends seen in Figures 3.12 and 3.24. Since DCN cannot occur with carbon monoxide as a reactor feed, the characteristic that ties all reactant species together is the amount of carbon monoxide on the surface during reactions.
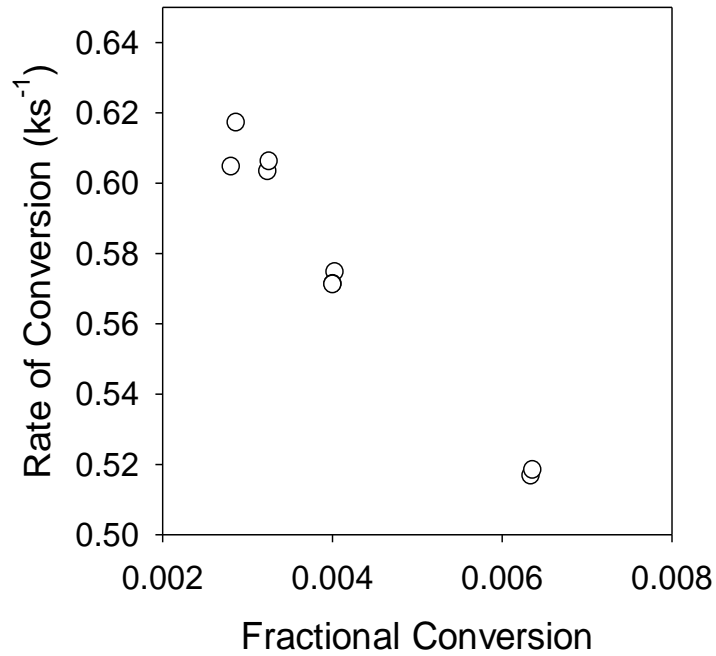
Figure 3.24: Effect of fractional conversion on the rate of conversion of carbon monoxide in water-gas shift. The partial pressures of CO, water and helium were 7, 21 and 732 torr respectively, and the temperature was held at 465K.

Hydrogen was cofed to the reactor to closer simulate conditions during propionic acid HDO, the results of this experiment is shown in Figure 3.25. As with the principles of equilibrium, hydrogen partial pressures reduced the favorability of carbon dioxide formation rates; the site time yield (STY) decreased as higher partial pressures of hydrogen were cofed to the reactor.
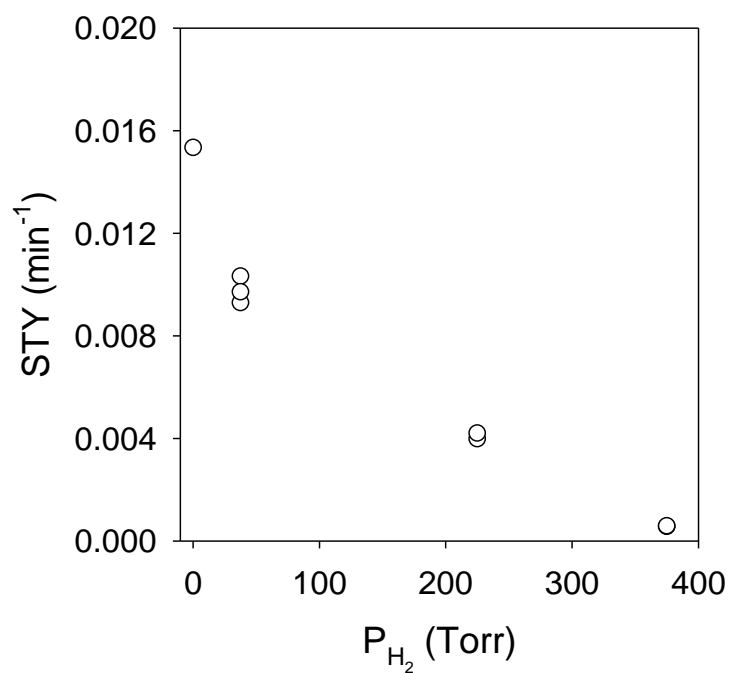
Figure 3.25: Effect of hydrogen cofeeding on the STY of carbon dioxide formation in water-gas shift. The partial pressures of CO and water were kept at 3.7 and 10 torr respectively; He was used to balance the total pressure at 760 torr. The temperature was held at 465K.

The proximity to equilibrium was then observed for the water gas shift reaction for the PAc HDO data collected; this is illustrated in Figure 3.26. It is highly likely that the reaction is controlled by equilibrium; the caveat in this idea is that it would be difficult to decouple the carbon dioxide formed from decarboxylation and the amount formed from water gas shift.
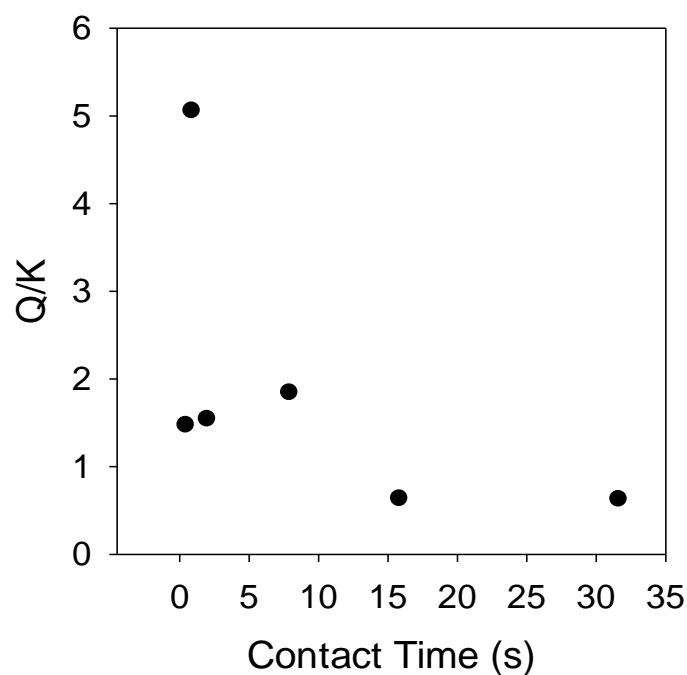
Figure 3.26: Proximity to equilibrium at different contact times assuming all carbon dioxide from Propionic acid HDO was formed through WGS pathway

3.4. Discussion

The yield of the observed products allowed for initial insights on propionic activity over Pt/SiO2.

Some of the observations were aligned with expected trends while others left room for further

investigation. A key observation was the linearity of the figures in each of the anticipated

pathways; conversions in the displayed figures were less than 2%, yet some figures showed

evidence of approaching a plateau, which is typically characteristic of a chemical reaction

approaching equilibrium. Each of the anticipated reactions was orders of magnitude below the

theoretical equilibrium, this meant that the rates were decreasing for a non-equilibrium

phenomena. Using the primary equations, the Gibbs free energy of the anticipated reactions are

shown in Table 3.3:

69

Table 3.3: Gibbs free energy of anticipated pathways.

Reaction Pathway	Gibbs Free Energy (KJ)
HDO 1 (Propanal)	-28
HDO 2 (Propanol)	-18
DCN	-89
DCX	-105

From the Gibbs free energy calculated using the gas phase equations, the spontaneity of the reactions can be predicted. DCX chemistry appears to be the most spontaneous of all the anticipated pathways, however over Pt, yet it was the least favorable reaction; this hints towards DCX chemistry may actually not be occurring.

In addition to the appearance of an approach to equilibrium, another peculiar observation mentioned was the yield of some products (propanal and carbon monoxide) decreasing with contact time. This led to the exploration of rate inhibition and reaction pathways using molar selectivity and rate of conversion trends.

3.4.1. Propionic Acid Pathways

During Propionic acid HDO (Figures 3.7-3.10) over Pt, five species exhibit characteristics of primary products. Carbon monoxide, carbon dioxide, ethane, propanol and propanal all show non-zero y-intercepts. CO, ethane, methane and propane all show increasing selectivity as a function of conversion, which suggests they are formed by non-primary reactions; and carbon dioxide, propanol and propanal decrease in selectivity as a function of conversion, suggesting they are all consumed by sequential reactions. The selectivity of CO and ethane are always observed in a 1:1 molar ratio, suggesting that these species are co-evolved through the DCN pathway. It was also discovered that the partial pressures of carbon monoxide and carbon dioxide produced indicated a strong possibility that the water-gas shift is being controlled by equilibrium.

3.4.2. Propanal Pathways

From the effect of conversion on molar selectivity data for propanal (Figures 3.14-3.16), we deduced the primary reactions. The primary products observed during propanal HDO are ethane and propane; ethane is seen as a stable species, while propanol is being consumed by a non-primary reaction. Propane's increase in molar selectivity along with propanol's decrease hints propane hydrogenolysis of the alcohol taking place.

3.4.3. Propanol Pathways

Figures 3.19-3.21 reveals that all four products show a non-zero y-intercept, indicating that CO, ethane, propanal, and propane are all *apparent* primary products of 1-propanol conversion. Primary formation of propanol and propane are consistent with the expectations for this system, specifically that propanol can undergo either dehydrogenation (to form propanal) or hydrogenolysis (to form propane). However, we know of no direct pathway for decarbonylation of 1-propanol to yield CO and ethane (whereas decarbonylation of propanal is reportedly facile [4,15,25]). Accordingly, we hypothesized that propanal formed by propanol dehydrogenation undergoes rapid decarbonylation, giving it the appearance of a primary product in the range of experimentally tractable contact times. The high propanal activity for DCN carried over towards creating the hydrogenation hypothesis that the propanol formed during propionic acid HDO is not actually a primary HDO pathway, but formed via propanal hydrogenation occurring at extremely fast rates.

3.4.4. Carbon Monoxide Pathways

We observed in Section 3.3.4 that carbon monoxide can undergo methanation and water gas shift, this is likely the main source of methane observed during propionic acid HDO experiments. A possible issue arose involving the water gas shift reaction; during the hydrogen cofeeding experiments (Figure 3.25), where the STY dropped with increasing hydrogen partial pressure, a hypothesis was formed that the water gas shift reaction might be at equilibrium during the propionic acid HDO experiments. It is highly likely that the reaction is controlled by equilibrium; the caveat in this idea is that it would be difficult to decouple the carbon dioxide formed from decarboxylation and the amount formed from water gas shift; this may not be necessary as DCX chemistry is theoretically the most favorable, yet practically it is the least.

3.4.5. Pathway Summary

The main reaction pathways expected to have occurred during propionic acid HDO experiments are illustrated in Figure 3.27. To avoid cluttering, redundant chemistries were not included: such as multiple methanation and water gas shifts routes.
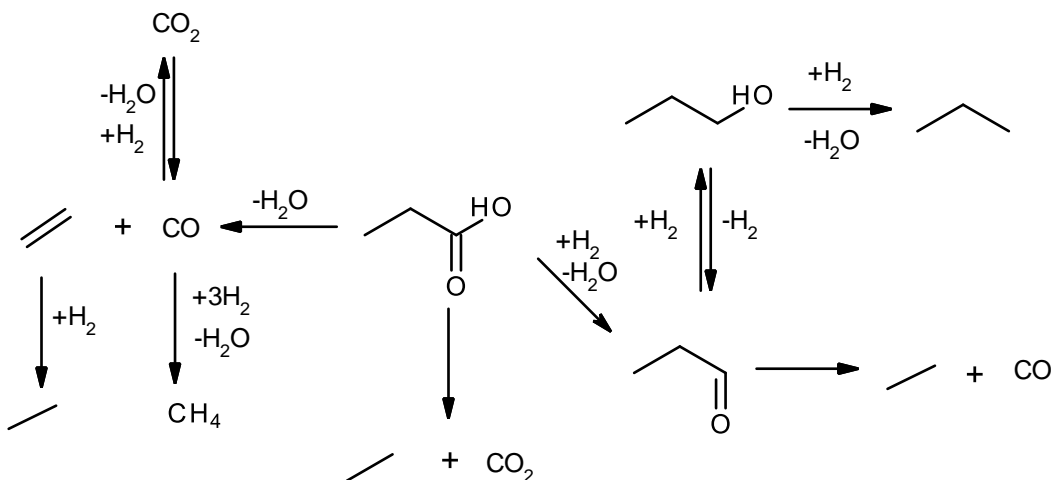
Figure 3.27: Reaction schematic after taking into account results from selectivity experiments.

3.4.6. Rate Inhibition

Since it was proven that the pathways are not close to equilibrium, the decrease in rate of conversion is likely as a result some sort of rate inhibition. In fact, this rate inhibition was seen in experiments with most of the different reactant species. Specially, propionic acid, propanol and carbon monoxide feed experiments exhibited rate inhibition, while propanal experiments seemed to be absent of any sort of inhibition. Carbon monoxide is known to poison Pt sites[30,31], which may explain why the rates of conversion decreased; as carbon monoxide was formed, it covered the catalyst surface and prevented other reactions from taking place. This product inhibition phenomenon can be observed by taking a closer look at the partial pressures of carbon monoxide and its relation to conversion.

The partial pressure of carbon monoxide on the catalyst surface during propionic acid HDO increases with fractional conversion (Figure 3.28), this constant buildup of carbon monoxide is conversely decreasing rate of conversion. Also, taking rate of propanal formation an indication of the rate of propionic acid HDO, this rate is inversely proportional to the partial pressure of CO

73

present over the catalyst bed (Figure 3.29); this means that propanal rates are only high when the fraction conversion of propionic acid HDO is low, this is the only reactor regime where the partial pressures of carbon monoxide are low. An inconsistent rate with contact time and fractional conversion also means that the partial pressures of the species are changing across the reactor bed. Analyzing rates must therefore take into consideration multiple secondary and tertiary reactions while also accounting the rate changing across the reactor bed as a result of product inhibition by carbon monoxide.
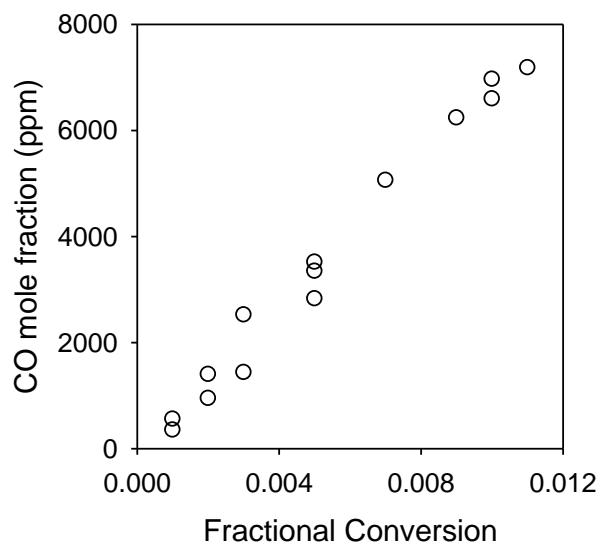
Figure 3.28: Formation of carbon monoxide in relation to the fractional conversion of propionic acid over Pt.
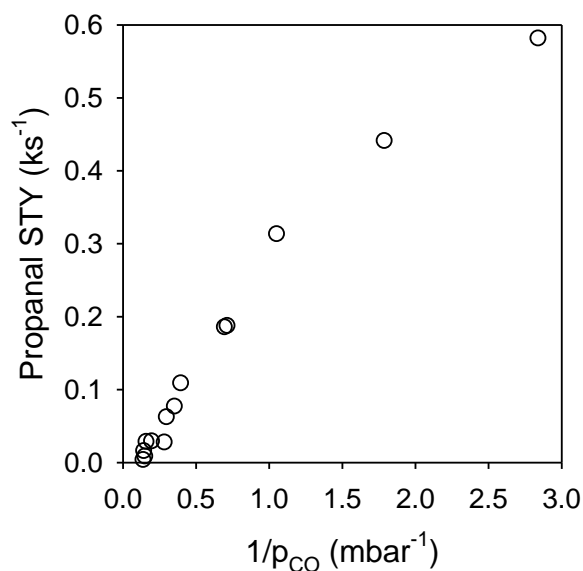
Figure 3.29: The relationship between rate of propionic acid HDO and partial pressure of CO over Pt.

3.4.7. Modeling Propionic Acid HDO over Pt

Because of the complex reaction network(s) occurring during propionic acid HDO over Pt, it is difficult to anticipate and thus optimize selectivity toward the desired oxygenated intermediates. In order to elucidate the connection between selectivity and reactor operation conditions, we aim to develop a kinetic model that captures the relative rate of each reaction observed in the network. This observed reaction network comprised of roughly 8 *overall*, macroscopic reactions.

1. $C_2H_5COOH + H_2 \rightarrow C_2H_5CHO + H_2O$
2. $C_2H_5COOH \rightarrow C_2H_6 + CO_2$
3. $C_2H_5COOH + H_2 \rightarrow C_2H_6 + CO + H_2O$
4. $C_2H_5CHO + H_2 \leftrightarrow C_3H_7OH$
5. $CO + H_2O \leftrightarrow CO_2 + H_2$
6. $C_2H_5CHO \rightarrow C_2H_6 + CO$
7. $C_3H_7OH + H_2 \rightarrow C_3H_8 + H_2O$
8. $CO + 3H_2 \rightarrow CH_4 + H_2O$

List of Equations used in MATLAB model.

In theory, each of these can be described with a multi-step mechanism that might form the basis of a microkinetic analysis; this will be the focus of another study. This effort is ongoing through a collaboration jointly funded with our experimental work; however, it remains in development, and we presently employ a more empirical approach. Accordingly, we have taken a semi-empirical approach based on the conventions of Langmuir-Hinshelwood surface kinetics. For preliminary analysis, we have assumed that the rate of each reaction has a first order dependence on the *coverage* of the reactants that participate in the overall reaction. Species coverages are then computed by assuming that the adsorption/desorption of each stable, gas-phase reactant and/or is equilibrated. This allows us to broadly capture inhibitive effects of certain species (like carbon monoxide) which was observed during the experimental section, where the rate of conversion decreased across the reactor bed. The main governing equations of the model are as follows:

$$k_i = k_m \cdot e^{\frac{-E_A}{R\Delta T}}$$

$$K_j = K_m \cdot e^{\frac{-DH}{R\Delta T}}$$

$$\theta_* = \frac{1}{1 + \sum K_j \cdot p_j}$$

$$\theta_j = K_j \cdot p_j \cdot \theta_*$$

$$r_i = k_i \cdot \prod \theta_j$$

Where DH is the binding enthalpy, E_A is the activation energy, θ_j is the species coverage, k_m is the mean rate constant, K_m is the mean binding constant, K_j is the binding constant, k_i is the rate constant and r_i is the rate of the reaction. The mean rate constants and mean binding constants are

use in order to regress the model parameters with experimental values. The parameters that undergo regression in order to fit the data include the activation energies, mean rate constants, and the mean binding constants and enthalpies for the non-terminal species.

Species production rates in this system are computed by modeling our experimental reactor as an idealized packed bed, which requires that we integrate species balances over the number of active sites present in a given reactor at a given set of experimental conditions. Doing so, we are able to adequately capture trends in experimental production rates over Pt as seen in Figure 3.30.
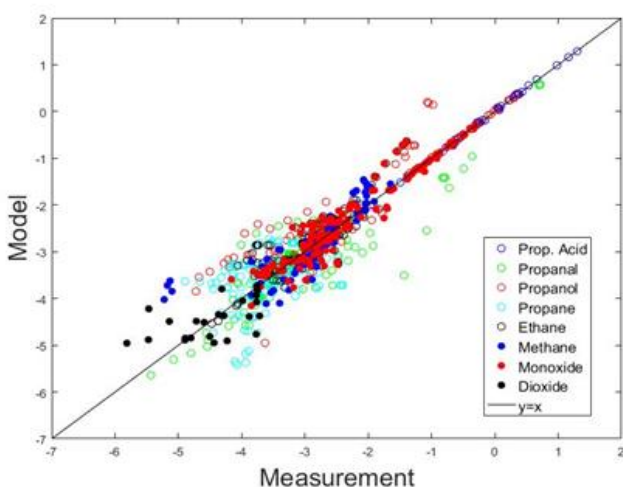
Figure 3.30: Parity plot of the natural logarithm of experimental rates versus theoretical rates for all species involved in reactions proposed for Pt.

This allows us to tentatively extrapolate results to inaccessible experimental conditions (within the constraints of our equipment), which allows us to predict HDO selectivities over a large range of temperatures, pressures, and operating conditions. In addition, while it is generally impossible to observe propionic acid HDO under truly differential conditions in the laboratory (because secondary reactions are so facile), it is possible to simulate reactor performance at an infinitesimal contact time, which helps us to resolve the primary contributions of propionic acid HDO, DCN, and DCX to observed product formation rates.

Figure 3.31 illustrates predicted trends in selectivity of the desired carboxylic acid HDO products (propanol and propanal specifically) over Pt. We observe that the highest HDO selectivity is at temperatures above 450K and low residence times. Around 475K, there is a wider range of residence times (10^{-4} sec to 10^{-2} sec) available to achieve 100% HDO selectivity; higher temperatures reduce the upper end of that range. At low residence time ($>10^{-3}$), the ideal ratio of propionic acid to hydrogen partial pressures lie in the 10^{-1} to 10^{1} range. The major limit in practicality of Pt is that, invariably, one only observed high selectivity at very short residence times. Consistent with our experimental observations, this implies that good HDO selectivity is only attainable at very low conversions, suggesting that the yield of target oxygenates will be prohibitively low over monometallic Pt during single pass operation. If monometallic catalysts are to be employed, reactors will only deliver good HDO yields if operated very low per pass conversion and very high recycle ratios. While the model does capture trends, the parameters do not hold much meaning because of over-parameterization; a black box was essentially created. In order to accurately extract rates and kinetic parameters, a micro kinetic model would need to be constructed.
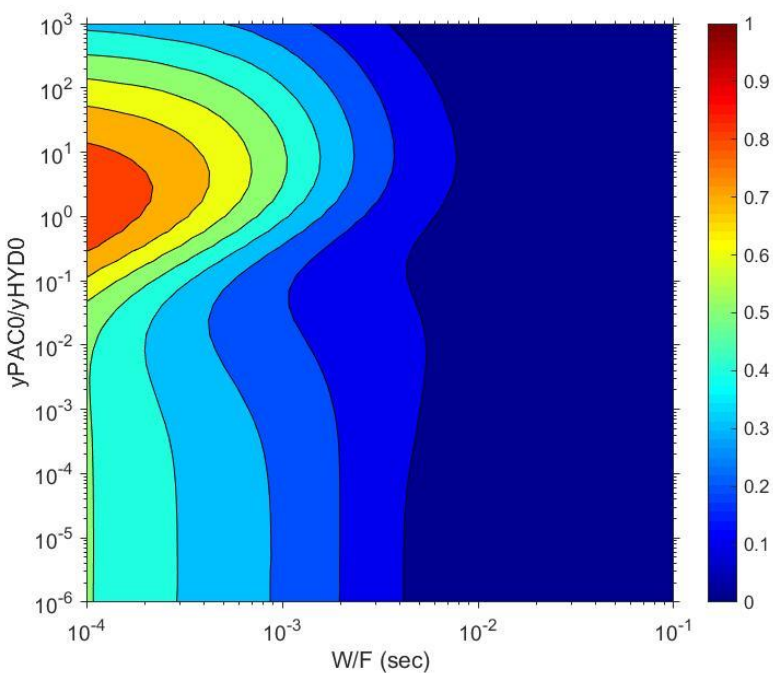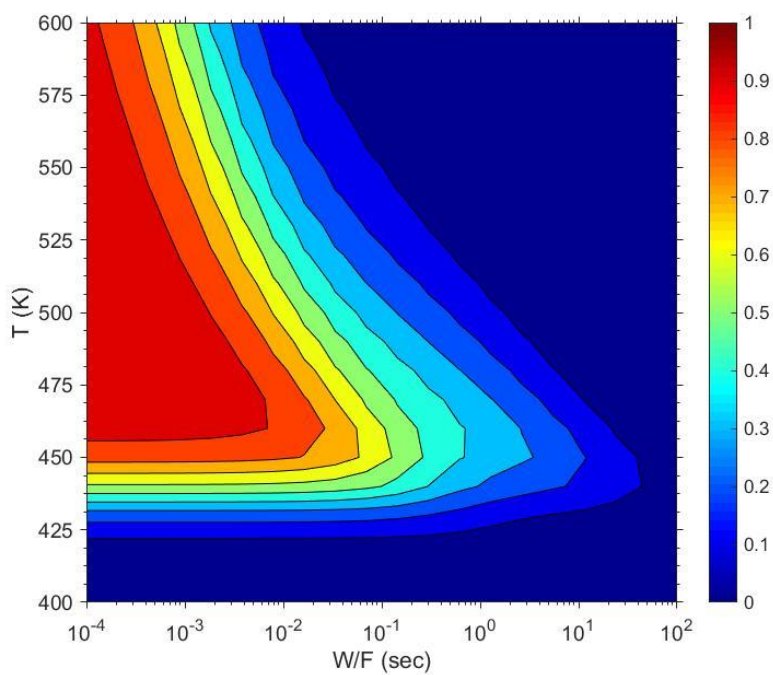
Figure 3.31: (Top) Effect of temperature and propionic acid residence time on the selectivity of HDO products at a ratio of propionic acid to hydrogen partial pressure of 10^{-2} over Pt. **(Bottom)** Effect of the ratio of propionic acid to hydrogen partial pressure and propionic acid residence time on the selectivity of HDO products at 523K over Pt.

3.5.   Conclusion

Propionic acid HDO over Pt catalysts showed major selectivity problems which is as a result of two main issues: multiple pathways, rate inhibition. The most active pathway occurring during HDO experiments was DCN, which produced carbon monoxide and ethane that consistently dominated product selectivities. In addition to the DCN pathway being facile, carbon monoxide also poisons the Pt active sites as it is being formed. Other unwanted (but minor) pathways include methanation, water gas shift and hydrogenolysis. A MATLAB model was used in an attempt to identify experimental regimes that may facilitate higher selectivity towards HDO products, it was identified that low pass conversion and high recycle ratios would be required, which is not economically feasible in terms of monometallic Pt being used in a more practical setting. Homogeneous gas phase equations used when modelling the monometallic network is not adequate when determining rates and kinetic parameters because of the tendency to establish too many parameters; a micro kinetic model is inevitable when analyzing reaction rates of specific pathways. Experimental conditions is not enough for increasing HDO selectivity over monometallic catalysts, other avenues should be explored in tuning catalytic activity such as using bimetallic systems though the addition of oxophilic promoters.

3.6. References

1   Wu, L., Moteki, T., Gokhale, A. A., Flaherty, D. W. & Toste, F. D. Production of Fuels and Chemicals from Biomass: Condensation Reactions and Beyond. *Chem* **1**, 32-58 (2016).

2   Gurbuz, E., Bond, J. Q., Dumesic, J. A. & Román-Leshkov, Y. in *The Role of Catalysis for the Sustainable Production of Bio-fuels and Biochemicals*   261-288 (Elsevier, 2013).

3   Rachmady, W. & Vannice, M. A. Acetic Acid Hydrogenation over Supported Platinum Catalysts. *Journal of Catalysis 192*, 322-334 (2000).

4   Englisch, M., Ranade, V. S. & Lercher, J. A. Hydrogenation of crotonaldehyde over Pt based bimetallic catalysts. *Journal of Molecular Catalysis A: Chemical* **121**, 69-80 (1997).

5   He, D.-H., Wakasa, N. & Fuchikami, T. Hydrogenation of Carboxylic Acids Using Bimetallic Catalysts Consisting of Group 8 to 10, and Group 6 or 7 Metals   *Tetrahedron Letters* **36**, 1059-1062 (1995).

6   Murillo, L. E. & Chen, J. G. Adsorption and reaction of propanal, 2-propanol and 1-propanol on Ni/Pt(111) bimetallic surfaces. *Surface Science 602*, 2412-2420 (2008).

7   Peng, B. *et al.* Comparison of kinetics and reaction pathways for hydrodeoxygenation of C3 alcohols on Pt/Al2O3. *Catalysis Today 183*, 3-9 (2012).

8   de Miguel, S. R., Román-Martínez, M. C., Cazorla-Amorós, D., Jablonski, E. L. & Scelza, O. A. Effect of the support in Pt and PtSn catalysts used for selective hydrogenation of carvone. *Catalysis Today* **66**, 289-295 (2001).

9   Santori, G. F. *et al.* Hydrogenation of aromatic ketones with Pt- and Sn-modified Pt catalysts. *Applied Catalysis A: General* **269**, 215-223 (2004).

10   Maynar, H. G. *et al.* Highly selective and efficient hydrogenation of carboxylic acids to alcohols using titania supported Pt catalysts. *Chemical Communications 46*, 6279-6281 (2010).

11   Gao, X., Heyden, A., Abdelrahman, O. A. & Bond, J. Q. Microkinetic analysis of acetone hydrogenation over Pt/SiO2. *Journal of Catalysis* **374**, 183-198 (2019).

12   Vannice, M. A. & Sudhakar, C. A Model for the Metal-Support Effect Enhancing CO Hydrogenation Rates over Pt-Ti02. Catalysts. *Journal of Physical Chemistry* **88**, 2429-2432 (1984).

13   Castaño, M. G., Reina, T. R., Ivanova, S., Centeno, M. A. & Odriozola, J. A. Pt vs. Au in water–gas shift reaction. *Journal of Catalysis* **314** 1-9 (2014).

14   Gursahani, K. I., Alcalá, R., Cortright, R. D. & Dumesic, J. A. Reaction kinetics measurements and analysis of reaction pathways for conversions of acetic acid, ethanol, and ethyl acetate over silica-supported Pt. *Applied Catalysis: A General 222*, 369-392 (2001).

15   Durndell, L. J. *et al.* Selectivity control in Pt-catalyzed cinnamaldehyde hydrogenation. *Scientific reports* **5**, 9425 (2015).

16   Zhao, B.-H. *et al.* Selective Hydrogenation of Cinnamaldehyde over Pt and Pd Supported on Multiwalled Carbon Nanotubes in a CO2-Expanded Alcoholic Medium. *Industrial & Engineering Chemistry Research* **51**, 11112-11121 (2012).

17   Ammal, S. C. & Heyden, A. Origin of the unique activity of Pt/TiO2 catalysts for the water–gas shift reaction. *Journal of Catalysis* **306**, 78-90 (2013).

18   Contreras-Mora, J. *et al.* Characterization and Evaluation of Carbon-Supported Noble Metals for the Hydrodeoxygenation of Acetic Acid. *Organic Process Research & Development 22*, 1628-1635 (2018).

19   He, Z. & Wang, X. Required catalytic properties for alkane production from carboxylic acids: Hydrodeoxygenation of acetic acid. *Journal of Energy Chemistry 22*, 883-894 (2013).

20   Zhang, K., Zhang, H., Ying, W., Fang, D. & Zhang, H. Effect of Sn Addition in Gas Phase Hydrogenation of Acetic Acid on Alumina Supported PtSn Catalysts. *Catalysis Letters* **144**, 691-701 (2014).

21   Lugo-José, Y. K., Monnier, J. R. & Williams, T. C. Gas-Phase, catalytic hydrodeoxygenation of propanoic acid, over supported group VIII noble metals: Metal and support effects. *Applied Catalysis A: General 469*, 410-418 (2014).

22   da Silva, A. B., Jordão, E., Mendes, M. J. & Fouilloux, P. Effect of metal-support interaction during selective hydrogneaton of cinnamaldehyde to cinnamyl alcohol on platinum based bimetallic catalysts. *Applied Catalysis A: General 148*, 253-264 (1997).

23   Merlo, A. B., Vetere, V., Ruggera, J. F. & Casella, M. L. Bimetallic PtSn catalyst for the selective hydrogenation of furfural to furfuryl alcohol in liquid-phase. *Catalyst Communications* **10**, 1665-1669 (2009).

24   Davis, J. L. & Barteau, M. A. Decarbonylation and Decomposition Pathways of Alcohols on Pd (111). *Surface Science 187*, 387-406 (1987).

25   Bowker, M. *et al.* The decarbonylation of acetaldehyde on Pd crystals and on supported catalysts. *Applied Catalysis A: General 391*, 394-399 (2011).

26   M. A. A. Aziz, A. A. Jalil, S. Triwahyono & Ahmad., A. CO 2 methanation over heterogeneous catalysts: recent progress and future prospects. *Green Chemistry* **17**, 2647-2663 (2015).

27   Wang Wei & Jinlong, G. Methanation of carbon dioxide: an overview. *Frontiers of Chemical Science and Engineering* (2010).

28   Marsh, H. & Taylor, D. W. Carbon gasification in the Boudouard reaction. *Fuel 54*, 218-220 (1975).

29   Flaherty, D. W., Yu, W.-Y., Pozun, Z. D., Henkelman, G. & Mullins, C. B. Mechanism for the water–gas shift reaction on monofunctional platinum and cause of catalyst deactivation. *Journal of Catalysis 282*, 278-288 (2011).

30   Argyle, M. D. & Bartholomew, C. H. Heterogeneous Catalyst Deactivation and Regeneration:A Review. *Catalysts* **5**, 145-269 (2015).

31   Trens, P. *et al.* Poisoning of Pt/C catalysts by CO and its consequences over the kinetics of hydrogen chemisorption. *Applied Catalysis B: Environmental* **92**, 280-284 (2009).

CHAPTER 4

Carboxylic Acid Hydrodeoxygenation over Supported Ru Catalysts

4.1.   Introduction

The use of catalysts has provided pathways for increasing chemical efficiency in different facets of the industrial sector; these efficiencies can pertain to both the economic and environmental impact of a chemical process[1]. There is always a curiosity for ways to push the boundaries of the chemical industry in terms of finding new and more efficient production routes. A growing concern for the environment has created an external motivation for alternative pathways in chemical production through renewable resource-derived industrial feedstocks. Biomass typically consists of heavily oxygenated compounds; its upgrading would require precise removal of targeted oxygen atoms towards desired chemical production[2,3]. Though there has been a proliferation in research of the reduction chemistries for upgrading biomass over the past decade, majority of successful industrial implementation has been in the production of fatty alcohols from bio-based fats and oils for personal care, soaps, detergents and lubricants[4]. Sugar-producing biomass can also have the potential for industrial application as an alternative route to commonly produced petrochemicals, specifically the reduction of the carboxylic acid functional groups as an alternative to hydrocarbon oxidation for specialty chemicals.

Hydrodeoxygenation (HDO) of carboxylic acids can serve as the necessary pathway for facilitating efficient biomass upgrading, however a lot is still unknown about highly active yet selective catalysts for HDO chemistry[5]. Non-precious metals have exhibited high selectivity for HDO; however, there are issues with such catalysts such as slow kinetics as well as irreversible catalyst deactivation. Noble metals have amongst the highest activity for carboxylic acid reduction, but

monometallic noble metals are unselective towards HDO products. Majority of product yield during carboxylic acid HDO over monometallic noble metals are as a result of C-C cleavage via decarbonylation (DCN), decarboxylation (DCX) and hydrogenolysis[6]. Succinic acid, one of the most viable bio-derived feedstocks for chemical production, has shown to be largely unselective to HDO chemistry to produce 1,4-butanediol over monometallic Pt, Ru and Pd; this showed the practical issues with monometallic noble metals however succinic acid is not the ideal candidate for deeper insight into catalytic properties that promote an unfavorable HDO selectivity[7].

Propionic acid can be used as a model system for HDO activity over noble metals because it has a shorter chain as well as the carboxylic functional group, it can be expected to undergo all the important chemistries one would typically expect using succinic acid. Most of the studies on carboxylic acids have been done using acetic acid[8-12], the caveat in using a two-carbon chain is it would be problematic to decouple DCN, hydrogenolysis and methanation chemistries, which would all produce methane. Lugo-José, Monnier and Williams have put out a study on gas phase propionic acid HDO over different noble metals[13]; none of the catalysts explored exhibited significant selectivity towards HDO products (propanol/propanal). Silica supported Ru and Pt had the highest activities than the other catalysts explored, but Ru had a higher product diversity than Pd indicating a wider range of chemistries being facilitated on the catalyst surface[7,14]. It has been shown that bimetallic catalysts have the ability to greatly improve HDO selectivity through the addition of an oxophilic promoter to noble metals[15-18]. However, a lot is still unknown about why monometallic catalysts have such poor selectivity in terms of the kinetic and thermodynamic properties of each pathway present over the catalytic surface and how the pathways interact with one another. Some of the main anticipated pathways for propionic acid include[13,19,20]:

Hydrodeoxygenation 1: $C_2H_5COOH + H_2 \rightarrow C_2H_5CHO + H_2O$

Hydrodeoxygenation 2: $C_2H_5COOH + 2H_2 \rightarrow C_2H_5CH_2OH + H_2O$

Decarbonylation + Hydrogenation: $C_2H_5COOH + H_2 \rightarrow C_2H_6 + CO + H_2O$

Decarboxylation: $C_2H_5COOH \rightarrow C_2H_6 + CO_2$
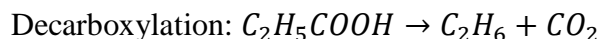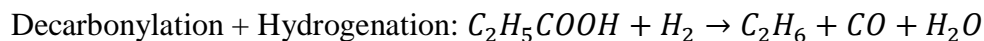
This work aims to provide a deeper insight on propionic acid HDO over silica supported Ru catalysts by exploring the myriad of chemistries that can take place over the catalyst. Carefully selected experiments using propionic acid as well as other reactants would allow for a more expansive reaction network to be proposed for computational modelling. A model can then be used to predict regimes of operation for high selectivity towards HDO products.

4.2.   Materials and Methods

4.2.1. Reagents

Air (Airgas, zero grade); amorphous silica (481.2 m^2/g, 48-90 μm mesh size, Aldrich, 99.8%); ruthenium III chloride hexahydrate (Acros, 99.9%); CO (Praxair, 99.99%); CO/He (Airgas: 0.991% CO, 0.996% Ar, 98% He); ethane Airgas: 0.994% C_2H_4, 1. % Ar, 98% He); ethylene (Airgas: 1% C_2H_4, 1% Ar, 98% He); He (Airgas, 99.999%); H_2 (Airgas, 99.999%); N_2 (Airgas, 99.999%%); O_2/Ar/He (1% O_2, 1% Ar , 98% He); propane (Airgas: 1% propane, 1% Ar, 98% He); 1-propanol (Acros Organics, 99+%); propanal (Acros Organics, 99+%) and propionic acid (Acros Organics, 99%) were employed for catalyst synthesis, catalyst characterization, and reactor operation. Each was used as supplied from commercial vendors. Water (Type II, 18.0 MΩcm^{-1} resistivity) was prepared in house (Spectrapure).

4.2.2. Catalyst Preparation

Ru/SiO$_2$ catalysts were prepared by incipient wetness impregnation of an aqueous ruthenium III chloride hexahydrate solution onto amorphous silica (1.8 grams of chloroplatinic acid solution per gram of silica). Concentrations of ruthenium III chloride hexahydrate were varied as necessary to achieve desired mass loadings of platinum. Catalysts were then dried overnight in static air at 393K. Subsequently, samples were loaded into a quartz flow cell and reduced at 673K under H$_2$ flow for 4 hours (100 ml min^{-1} H$_2$, 3 K min^{-1} ramp rate). Prior to exposure to ambient air, samples were passivated at 298K by purging the cell volume with He for 30 minutes and then exposing the cell to 1% O$_2$ in 1% Ar 98% He for 30 minutes.

4.2.3. Catalyst Characterization

Catalyst surface area and porosity were assessed with N$_2$ physisorption at 77K using a commercial instrument (Micromeritics ASAP 2020). Surface areas were determined using BET analysis; micro/mesoporosity were assessed using t-plot analysis; pore volumes were computed as the cumulative volume of N$_2$ condensed at a relative pressure (P/P$_0$) = 0.995; and average pore diameters were estimated from BJH analysis of the desorption branch of the isotherm. Prior to N2 dosing, samples were dried by evacuating to 500 $\square$m Hg at 298K and then heated to 623 K (240 min hold, 10 K min^{-1} ramp).

We used CO chemisorption to interrogate the Ru surface area available for reaction (Micromeritics ASAP 2020). Prior to CO dosing, samples were dried by evacuating to 5 µm Hg at 298K and subsequently heating to 373 K (30 min hold, 10 K min^{-1} ramp). Samples were then exposed to flowing oxygen and the cell temperature was increased to 673K (10 K min^{-1}, 30 min hold). The cell was then evacuated to 5 µm Hg at 673K, held under vacuum for 15 minutes, cooled under

vacuum to 373K, and then exposed to H_2 flow.The cell was then heated under continuous H2 flow to 673K (10K min^{-1}, 4 h hold). Finally, the cell was evacuated to 5 µm Hg at 673K to remove chemisorbed hydrogen (30 min) and cooled to 308K under vacuum. A CO uptake isotherm was then collected at 308K, the sample cell was evacuated to remove physisorbed CO, and a second CO uptake isotherm was collected at 308K. Irreversible CO uptake was calculated as the difference in CO uptake between the two isotherms. Ru particle size was estimated assuming that Ru has a shape factor of 6, an atomic cross sectional area of 0.614 nm^2 and a density of 12.30 g cm^{-3}. The average diameter of the nanoparticle as well as the dispersion of the metal can be calculated using Eq (1-3):

4.2.4. Catalyst Activity Testing

The reactor system used for all catalytic activity tests is illustrated in Figure 2.2. Gases introduced to the system at controlled flowrates using digital mass flow controllers (Brooks). Reactors always operated under gas phase conditions, but many of our feeds were introduced to the system as liquids using a syringe pump (Cole Parmer). Specifically liquids were fed through a PEEK capillary (130 µm, IDEX) into a home-built, temperature-controlled vaporizer, where they were combined with pre-heated gas feeds. To increase surface area for gas-liquid contact, the vaporizer was packed with quartz granules (850-2000 □m, Aldrich). To ensure complete vaporization, partial pressures of condensable species were maintained below 15% of their vapor pressure at a given reaction condition. After leaving the vaporizer, the process stream flowed through a 6-port valve, which was used to direct flow either to the reactor or to the bypass. During startup, the reactor was bypassed until we observed steady state feed concentrations via Gas Chromatography. Once the reactor feed stream reached steady state, flow was diverted to the reactor.

The packed bed reactor operated in an upflow configuration. It was constructed from ½" stainless steel tubing (McMaster). The catalyst bed was placed between two quartz wool plugs in the center of the tube, and the void volume upstream of the reactor was packed with quartz granules. The reactor temperature was monitored at the external wall using a type-K thermocouple, and the external wall temperature was regulated using a PID controller (LOVE 16A 3010). A second type-K thermocouple was placed inline and used to monitor reactor temperature immediately downstream of the catalyst bed. Data reported in this manuscript reflect the inline temperature measurement. The reactor effluent was transferred, via heat-traced stainless steel tubing, to a pair of online gas-chromatographs (HP 5890) for quantitative resolution of the product mixture. The first GC was equipped with dual inlets leading, respectively, to an HP-PONA column paired with a flame-ionization detector (FID) and a Restek ShinCarbon ST Micropacked column paired with a thermal conductivity detector (TCD). In general, propionic acid, propanal, propanol, propane, ethylene, and ethane were resolved and quantified using the PONA/FID system, while methane, CO, and CO_2 were resolved and quantified using the ShinCarbon/TCD system. The second GC was configured with a single inlet and a Restek ShinCarbon ST Micropacked column leading to a Methanizer/FID detector. This system was used for quantifying CO, CO_2, and methane concentrations that were below TCD detection limits. Species were qualitatively identified using standards prepared from commercial samples. Where necessary, unknown species were identified by injection of gas samples into an offline GC-MS (Agilent 7890 + 5975C MSD). Carbon balances for all conditions reported here closed to 95% or greater.

Reactions were run over various catalysts, temperatures, reactant partial pressures, and contact times, and species production rates were quantified at 15-minute intervals. Unless otherwise noted, reported rates reflect steady state operation. Typically, after startup, reactors were allowed to reach

steady state species production rates under a well-defined, "reference" condition. This typically took less than 1 hour. After reaching steady state, production rates for all species were quantified. Subsequently, a single perturbation in temperature, partial pressure, or contact time was introduced, and the system was allowed to evolve to a new steady state, where effluent flowrates of all species were again quantified. Metal catalysts employed for oxygenate processing are generally susceptible to various modes of deactivation, which can obscure kinetic trends. Accordingly, after quantifying the impact of each perturbation on species flowrates, the system was returned to the reference condition and allowed to reach steady state. This provided a rigorous benchmark for assessing catalyst deactivation. Under most of our operating conditions, deactivation was relatively mild. Differences in zero time production rates and steady state production rates measured at the reference condition throughout the experiment showed less than 10% loss in activity; accordingly, steady state rates were not corrected for deactivation. There is one exception: we have observed that high pressures of propanal induce severe deactivation of Pt, which is consistent with prior reports. In general, high propanal pressures were encountered when feeding propanal or 1-propanol into reactors (the latter readily dehydrogenates over Ru to form propanal). In systems with pronounced deactivation, it is difficult to define meaningful reaction rates from steady state measurements as the available catalytic surface area is generally changing as a function of time on stream. In these systems, initial production rates were estimated by extrapolating the deactivation profile to zero-time-on-stream. During typical startup and between experiments (e.g., changing the feed molecule), the catalyst bed was reduced under flowing H_2 at 673K (10 K min^{-1}, 4h), which was sufficient to restore the initial activity of the catalyst after most experiments.

Species production rates are reported here as site time yields. These are defined in equation 4.1:

$$STY_j = \frac{F_j}{N_{Pt}}$$

Equation 4.1

Where Fj is the total molar flowrate of species j in the reactor effluent and N_{Pt} is the total molar quantity of surface Ru atoms in the catalyst bed as estimated by CO chemisorption. Feed conversion was defined on a carbon basis and computed based on product flowrates (Eq. 4.2)

$$X_i = \frac{\sum_{j \neq i} F_j \cdot C_{n,j}}{F_{i,0} \cdot C_{n,i}}$$

Equation 4.2

Where F_j is the molar flowrate of reaction products, j, in the reactor effluent, $F_{i,0}$ is the inlet flowrate of the reacting species, i, and C_n is the number of carbon atoms in a given molecule. Selectivity to a specific reaction product, k, is defined in terms of molar flowrates of all reaction products, j Eq. 4.3:

$$S_k = \frac{F_k}{\sum_j F_j}$$

Equation 4.3

4.3. Results

4.3.1. Propionic acid

On approaching the propionic acid HDO experiments, we mapped the expected equations as a schematic in Figure 4.1; this figure shows the anticipated pathways propionic acid is expected to

undergo- hydrodeoxygenation to form propanol, hydrodeoxygenation to form propanal, and decarbonylation to form carbon monoxide and ethane.
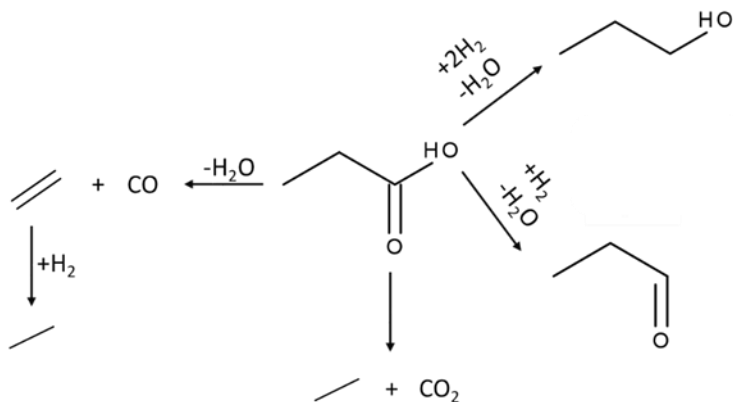
Figure 4.1: Anticipated reaction pathways for propionic acid HDO over Ru.

We first observe how the yield of the anticipated pathways are affected by changes in contact time. This allows us to compare the yield of each of the reaction pathways as well we extract product rates of the pathways. This was done by keeping the partial pressures of propionic acid and hydrogen as well as temperature constant, while manipulating the time in which reactant molecules spend interacting with a catalyst surface. The contact time is varied by adjusting the residence time flow rates, and also changing the amount of available active sites on a catalyst bed. In a typical reaction, the yield increases linearly then eventually forms a plateau; the linear part of a *yield vs contact time* represents the rate of the reaction. The yield of the pathways are plotted separately for clear depiction of pathway trends without figures being overcrowded with data. The effect of contact time on the yield of HDO 1 product propanal is illustrated in Figure 4.2. Propanal yield showed a sharp decrease from 0 - 10 s contact time, then approached a steady yield value of around 7E-05. The yield of the HDO 2 product propanol, as seen in Figure 4.3, showed no discernable trend; in fact, the yield appears to be scattered. Assuming the scatter is around a central point, the average of all the values is a yield of 5.89E-5. Both HDO pathways show odd trends, HDO 2

exhibiting a scattered steady state as well as HDO 1 displaying a decrease in yield. The first steady state suspicion was explored by investigating the proximity to equilibrium of each pathway and is illustrated in Figure 4.2. It can be seen that the reaction quotients of the anticipated HDO pathways are orders of magnitude away from the theoretical equilibrium. A slope being non linear is simply indicative of rates slowing down, but a negative slope holds its own weight which will be investigated further.
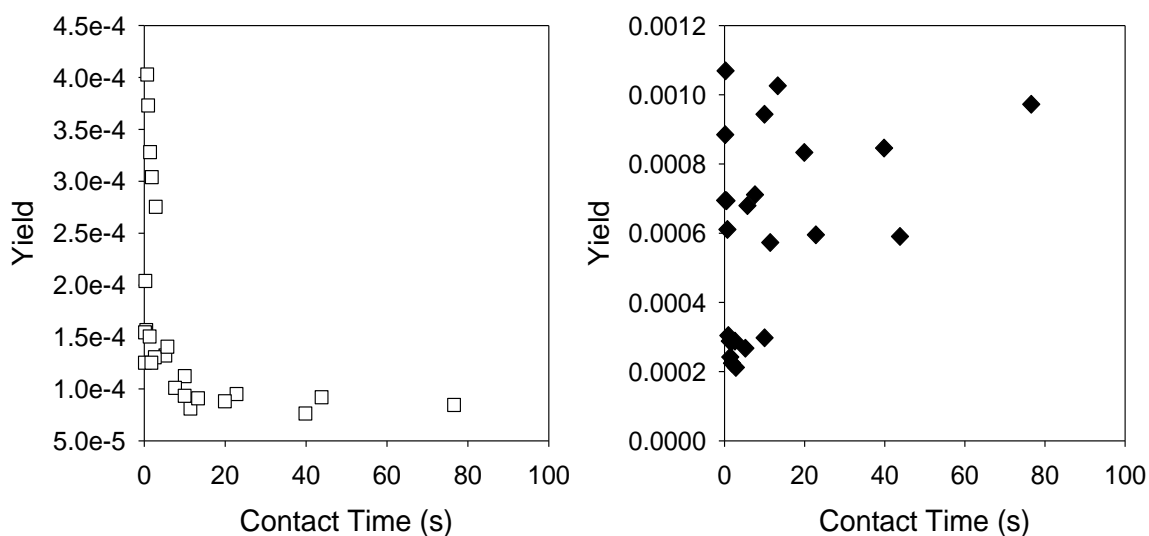
Figure 4.2: Effect of contact time on the yield of HDO 1 (left) and HDO 2 (right) products at propionic acid and hydrogen partial pressures of 5 and 755 torr respectively at 465K over Ru.
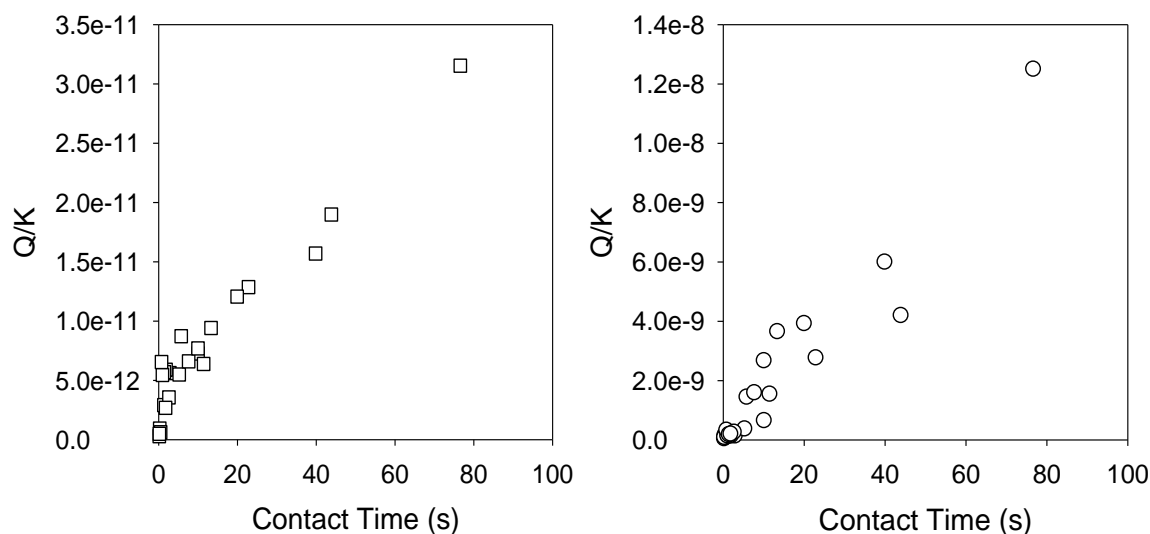
Figure 4.3: Proximity to equilibrium of the pathways HDO 1 (left) and HDO 2 (right) at propionic acid and hydrogen partial pressures of 5 and 755 torr respectively at 465K over Ru.

The trend in yield of DCN products- ethane and carbon monoxide- across different contact times is shown in Figure 4.4. At very low contact times, carbon monoxide and ethane have the same yield, however the yield of ethane eventually becomes more than double that of carbon monoxide; while the steepness of the slopes of both species appear to be decreasing, the rate of carbon monoxide formation slows down much faster than ethane over the contact times tested. Carbon monoxide even appears to be approaching a stable yield value of around 6.73E-3, while ethane shows no clear signs of attaining an observed steady value. The yield of decarboxylation products ethane and carbon dioxide are illustrated in Figure 4.5. Carbon dioxide had the lowest yield of all observed products during propionic acid HDO. Carbon dioxide and ethane did not have equal yield amounts at any contact times tested. In both anticipated pathways that produces ethane, it was formed in equimolar ratios with either carbon monoxide or carbon dioxide, and while ethane and carbon monoxide did have equal yields at low contact times, none of ethane's expected counterparts matched its yield at high contact times. None of the DCN and DCX product yields

linearly scale with contact time over the experimental range, the yields indicate a drop in rates; this is most evident in carbon monoxide, which shows a clear plateau. Both reactions were tested for their proximity to equilibrium across the contact times tested, as illustrated in Figure 4.5. It is shown that DCN and DCX pathways are significantly far from the theoretical equilibrium to be displaying a reduction in rates over the contact time range; this hints towards another occurance taking place on the catalyst surface.
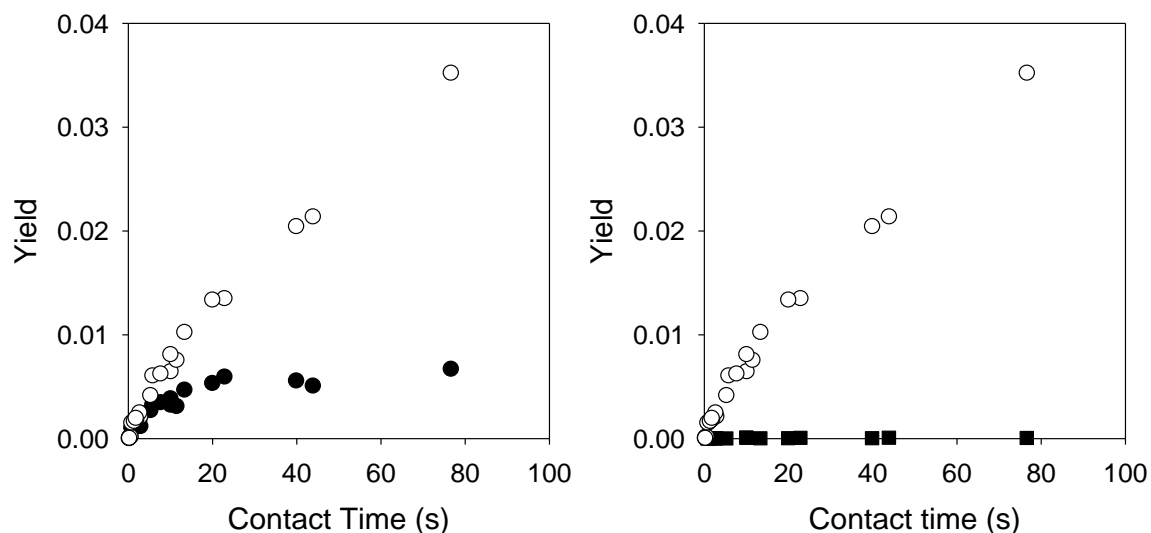
Figure 4.4: Effect of contact time on the yield of DCN (left) and DCX (right) products ethane (○), carbon dioxide (■) and carbon monoxide (●) at propionic acid and hydrogen partial pressures of 5 and 755 torr respectively at 465K over Ru.
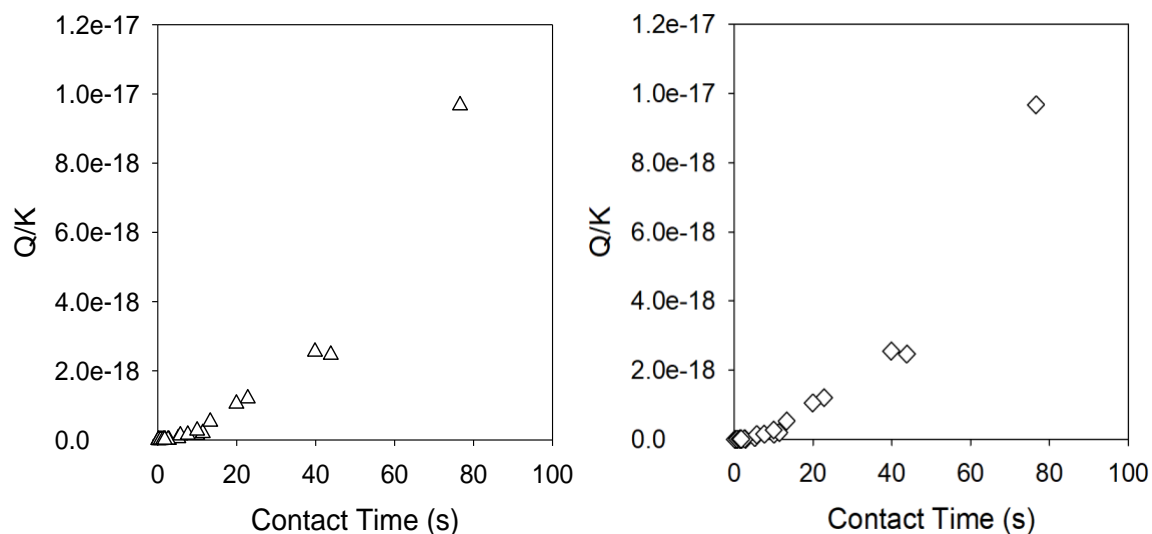
Figure 4.5: Proximity to equilibrium of the pathways DCN (left) and DCX (right) occurring during propionic acid HDO experiments at propionic acid and hydrogen partial pressures of 5 and 755 torr respectively at 465K over Ru.

There were two products observed which were not in the reaction schematic of anticipated reactions (Figure 4.1): propane and methane. The effect of contact time on the yield of these species are illustrated in Figures 4.6 and 4.7. Propane shows a steady increase in yield with contact time with only slight changes in the steepness of the slope. Methane, however, had the most linear data set in the contact time range of all observed species.
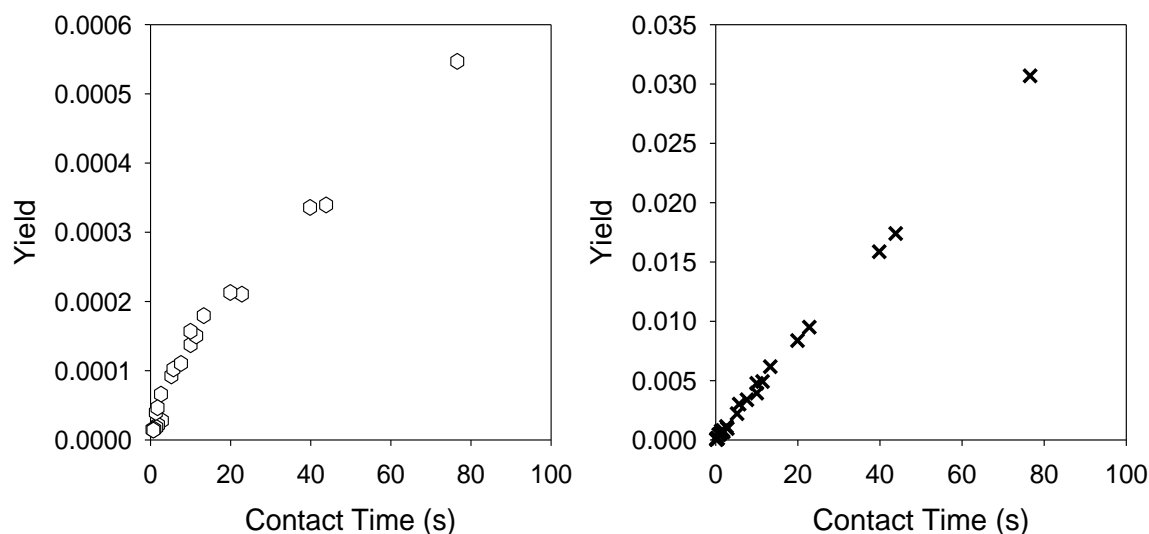
Figure 4.6: Effect of contact time on the yield propane (left) and methane (right) at propionic acid and hydrogen partial pressures of 5 and 755 torr respectively at 465K over Ru.

The rates of formation of carbon monoxide, ethane, carbon dioxide, methane and propane were extracted from the figures which showed the contact time effects on the yield. The yield of propanol and propanal formation left little opportunity for extracting a gradient at low contact times; in those instances, the rates were attained from taking the average of the actual production rates out the reactor at low contact times. Taking an average may be applicable to propanol since all the points were essentially scattered, however applying this to the propanal product rates does not have the highest accuracy because of its decrease in yield. The rates of the anticipated products can be seen in Table 4.1. Propanol had the highest production rate of 0.002s. Carbon monoxide and ethane did not have equal production rates (0.0009 and 0.0006 s^{-1} respectively), this was an unexpected observation because the DCN pathway produces stoichiometric amounts of both products. The production rates makes up a second observation of ethane and carbon monoxide behaving differently, the first being ethane yields were far above those of carbon monoxide at higher contact times. Propanal had a production rate of 0.0006 s^{-1}, it is being produced at the same

rate as carbon monoxide; however, this is not a fair comparison because of the difference in rate quantification. Carbon dioxide had the lowest production rate of the anticipated species, this isn't unexpected since it also had the lowest yields of all the observed species. The production rate of carbon dioxide was two orders of magnitude lower than that of ethane; this explains why their yields were different even though the DCX pathway produces them in stoichiometric amounts.

Table 4.1: Production rates of anticipated species at propionic acid and hydrogen partial pressures of 5 and 755 torr respectively at 465K over Ru.

Species	Production rate (s^{-1})
Ethane	0.0009
Carbon Monoxide	0.0006
Propanol	0.002
Propanal	0.0006
Carbon Dioxide	0.000006

The production rates of the unanticipated products are shown in Table 4.2. The production rate of propane was equal to that of carbon dioxide- 0.000006 s^{-1}. Methane had a sizable production rate for an unanticipated product, 0.0004 s^{-1}, it is also worth pointing out that the sum of carbon monoxide and methane production rates, may equal the rate of ethane production; methanation may be taking away from carbon monoxide's rates.

Table 4.2: Production rates of unanticipated species at propionic acid and hydrogen partial pressures of 5 and 755 torr respectively at 465K over Ru.

Species	Production rate (s^{-1})
Propane	0.000006
Methane	0.0004

From analyzing the yield data, we see that there are pathways that should be included in the schematic of propionic acid HDO over Ru catalyst; also, we observe that the rates are behaving non-linearly with contact time even though the reactions are far from the theoretical equilibrium.

We can use the molar selectivity to investigate the different pathways as well as observing the rate of conversion to tease out inhibition trends.

The trends in molar selectivity with conversion can be used to decouple primary from non-primary pathways. It can be envisioned that towards zero conversion, the partial pressures of the products on the catalyst would be too small to provide any driving force that would facilitate secondary or tertiary reactions. With this in mind, one can imagine that primary products would appear to have nonzero y-intercepts towards the zero conversion limit, while non-primary products would intercept the y-axis at zero; applying this in the reverse direction, a non-primary product would show an increase in selectivity with conversion, which indicates a species, is being formed by a non-primary pathway. The selectivity of a species can also decrease at higher conversions, this means that it is being consumed by a non-primary pathways. A species with a constant selectivity across different conversions is characteristic of a stable species that is neither consumed nor produced from a non-primary pathway. There is also no constraint that prevents primary products from being additionally formed from a non-primary pathway.

The molar selectivity of each of each species were observed across a conversion range, while keeping the reactant partial pressures as well as temperature constant. The effect of conversion on the molar selectivity of HDO 1 and HDO 2 products, propanal and propanol respectively, are illustrated in Figures 4.7 and 4.8. Propanal and propanol appear to have non-zero y-intercept as the fractional conversion approaches zero; this is indicative of both species being formed through primary pathways. The molar selectivity of both species show sharp decreases at short contact times, and eventually reaches a steady value. The decrease in molar selectivity points out that the species are being consumed by secondary pathways. Propanol had the higher molar selectivity

decrease of the two species since its initial selectivity was 72% at the lowest conversion, while propanal's highest recorded selectivity was 13%. It is also worth mentioning that propanol had the highest selectivity at the lowest recorded conversion of all the species. In the range of 0.1 to 7.4 % conversion, the molar selectivity of propanal and propanol decreased to 0.11% and 1.3% respectively.
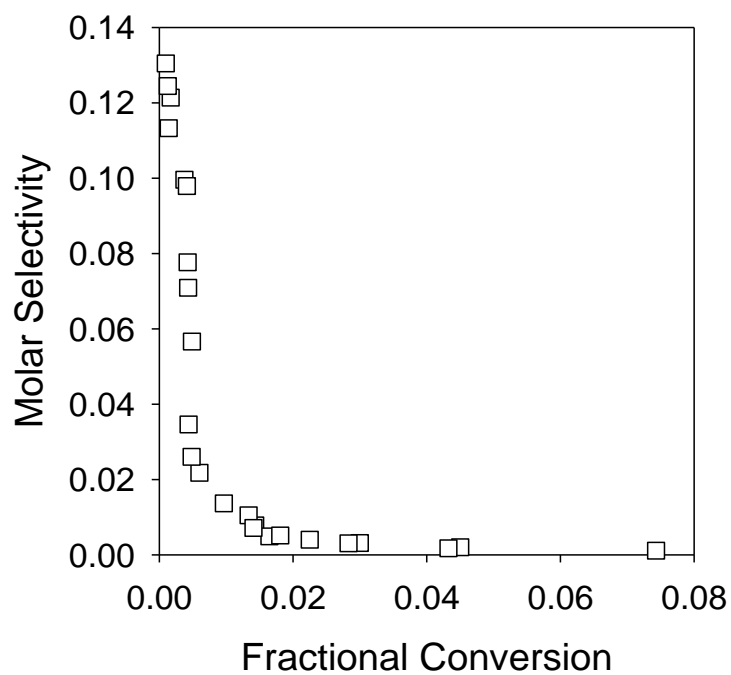
Figure 4.7: Effect of fractional conversion on the selectivity of HDO 1 product propanal at propionic acid and hydrogen partial pressures of 5 and 755 torr respectively at 465K over Ru.
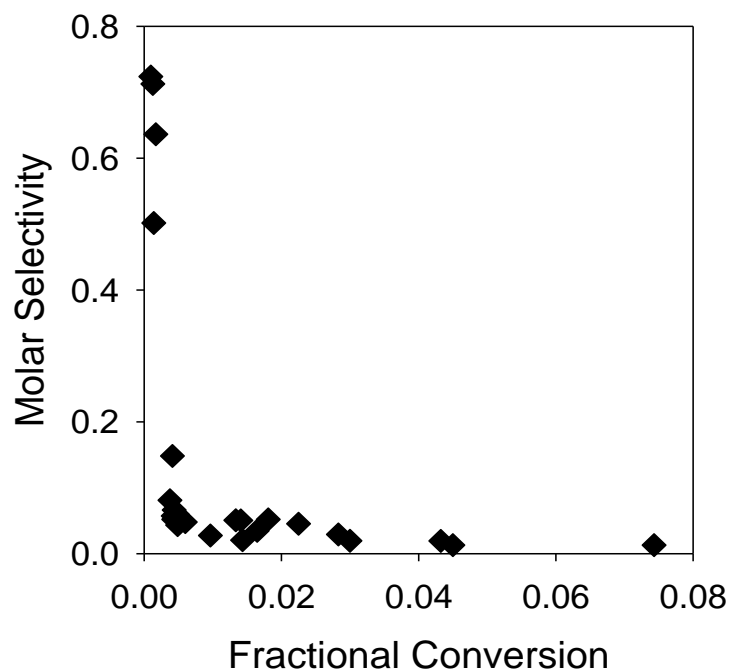
Figure 4.8: Effect of fractional conversion on the molar selectivity of HDO 2 product propanol at propionic acid and hydrogen partial pressures of 5 and 755 torr respectively at 465K over Ru.

The effect of conversion on DCN products, carbon monoxide and ethane, is illustrated in Figure 4.9. Though it may not be explicitly observed, the molar selectivities of carbon monoxide and ethane appear to be approaching either a zero or near-zero y-intercept towards the zero conversion limit. At low conversions, the molar selectivity of both products sharply increases; the products are formed in equal amounts at low conversions. Carbon monoxide and ethane clearly exhibit behavior of products being formed from non-primary pathways. The selectivity to ethane eventually appears to be approaching a steady value of around 47%. Unlike ethane, after its initial sharp increase, carbon monoxide's molar selectivity continuously decreases; it decreased from 32% to 9%- its highest recorded value to the value at the highest conversion in the range. This suggests that carbon monoxide is being produced though non-primary reactions, and then being also being consumed by further non-primary reactions. At the highest recorded conversion, ethane

also had the highest selectivity of all the species observed. Some details are worth mentioning. Carbon monoxide and ethane are observed in a 1:1 molar ratio at low conversions, suggesting that these species were initially coevolved.
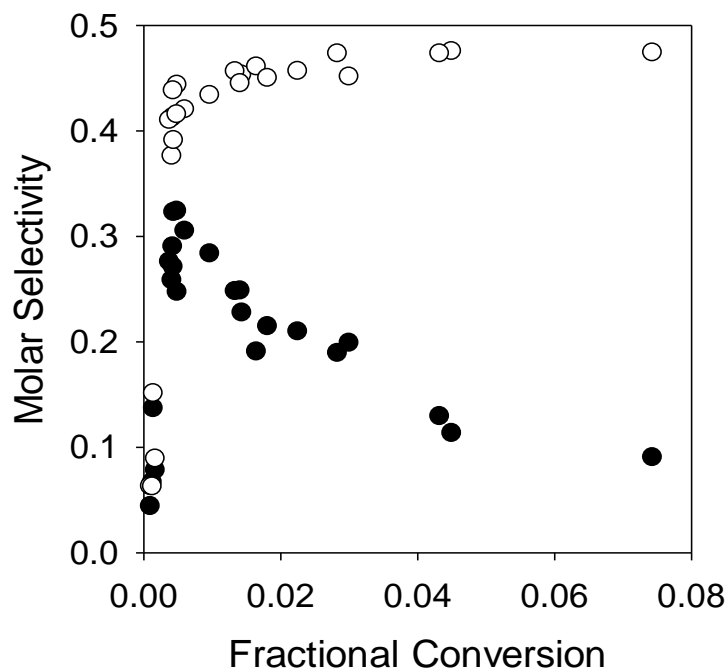
Figure 4.9: Effect of fractional conversion on the molar selectivity of DCN products ethane (○) and carbon monoxide (●) at propionic acid and hydrogen partial pressures of 5 and 755 torr respectively at 465K over Ru.

The molar selectivity of DCX products across the conversions tested is shown in Figure 4.10. The observations in selectivity to ethane was already well described from Figure 4.9. In terms of DCX products being anticipated to be formed in stoichiometric quantities, ethane selectivity was much higher than that of carbon dioxide for all conversions tested. In addition, while ethane showed an increase in selectivity over the conversion range tested, the molar selectivity of carbon dioxide showed a deceasing trend over the conversion range- this might not be clear to see since difference in selectivity between ethane and carbon dioxide affected the scaling of the figure. Carbon dioxide

also intercepts the y-axis at a non-zero value towards to zero fractional conversion limit. Observations point to carbon dioxide being a primary product consumed by a secondary pathway.

Figure 4.10: Effect of fractional conversion on the molar selectivity of DCX products carbon dioxide (■) and ethane (○) at propionic acid and hydrogen partial pressures of 5 and 755 torr respectively at 465K over Ru.

The effect of fractional conversion on the molar selectivity of unanticipated products propane and methane are illustrated in Figures 4.11 and 4.12. Both products appear to intercept the y-axis at zero towards the zero conversion limit, indicating non primary products. Propane showed an initial increase in molar selectivity at short conversions, this changed as the selectivity eventually began to decrease; this observation was similar to that of carbon monoxide in Figure 4.9. Therefore, we can also say that propane is being formed as a non-primary product and also being consumed by another pathway. Methane showed a constant increase in molar selectivity with conversion; in fact, methane eventually achieved the second highest selectivity at the highest conversion tested. One might also say that methane can be forecasted to have the highest molar selectivity of the species

at higher conversions outside of the experimental data points collected. Not only is methane

formed from a non primary pathway, but its rates are the most consistent of all the pathways.
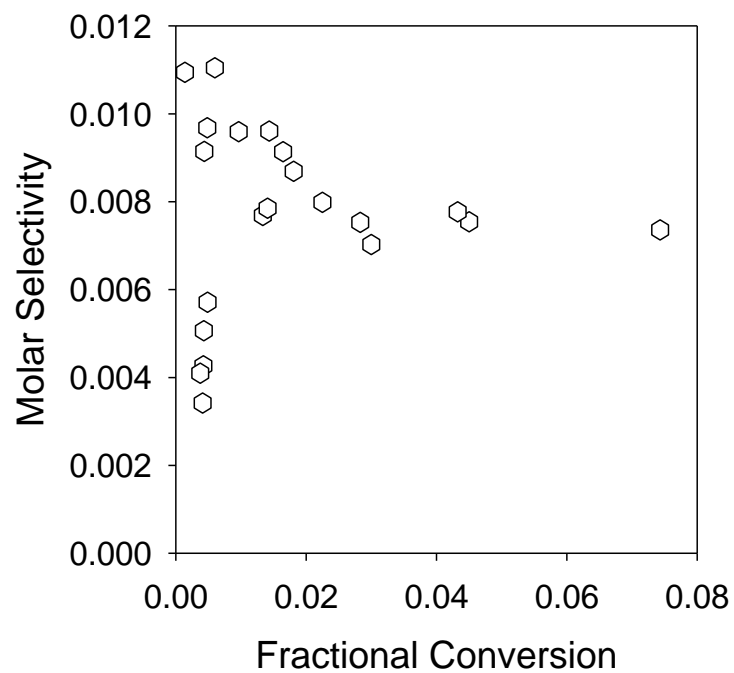
Figure 4.11: Effect of fractional conversion on the molar selectivity of propane at propionic acid and hydrogen partial pressures of 5 and 755 torr respectively at 465K over Ru.
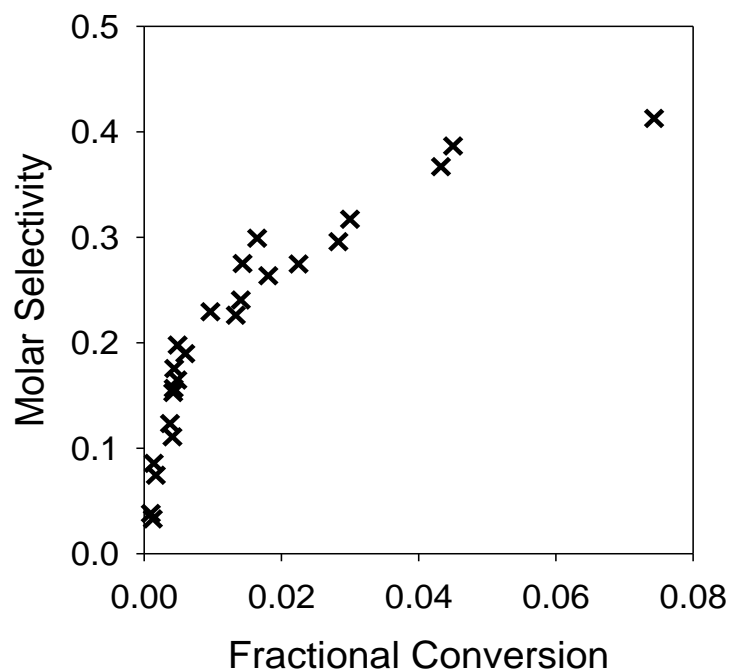
Figure 4.12: Effect of fractional conversion on the molar selectivity of methane at propionic acid and hydrogen partial pressures of 5 and 755 torr respectively at 465K over Ru.

After exploring primary products during propionic acid HDO, as well as whether species are being produced or consumed by non-primary pathways, we revisited the rate problem; i.e. the non-linear yield trends. In addition to the effect of fractional conversion on the molar selectivities of each of the observed products, its effect on the rate of conversion was also observed and is shown in Figure 4.13. The rate of conversion showed a sharp initial decrease over the range less than 1%, then begins to approach a steady value of around 0.9 ks^{-1}. The rate of conversion decreased by 88% over the conversion range tested for propionic acid HDO over Ru, this explain why the yield slopes of most of the species changed with contact time; the catalyst is losing its activity. Mapping out an accurate schematic of reaction pathways would require repeating selectivity experiments using the primary products as reactants in the packed bed reactor. The rate inhibition can also be observed using other the reactants as a means to track its source.
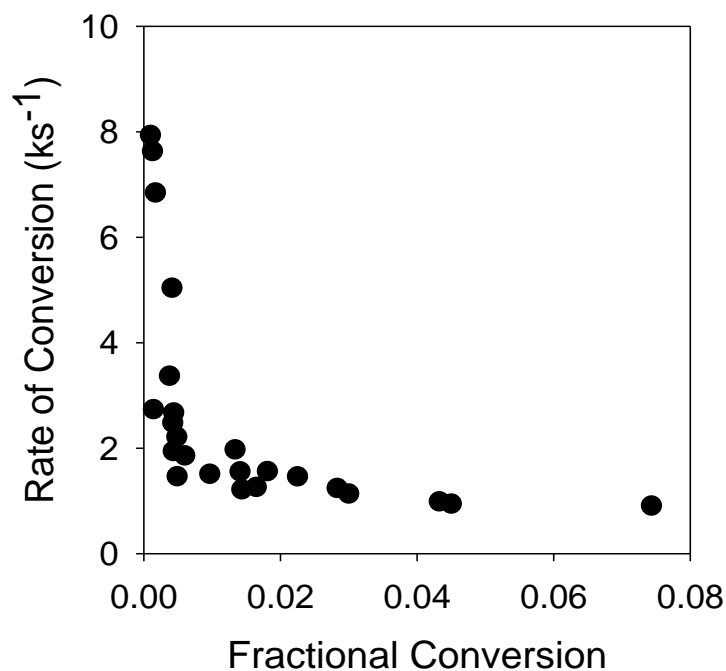
Figure 4.13: The rate of conversion of propionic acid at different fractional conversions during propionic acid HDO at propionic acid and hydrogen partial pressures of 5 and 755 torr respectively at 465K over Ru.

4.3.2. Propanal

A literature survey first established the expected pathways that propanal is expected to undergo over Ru supported catalysts in a hydrogen rich environment[21,22]. Hydrogenation chemistry over Ru is well established and known to be relatively favorable; specifically, hydrogenation of aldehydes to form alcohols is a quite facile reaction. Aldehydes are also well known to undergo C-C cleave reactions via DCN to form Carbon monoxide and a hydrocarbon. Taking into consideration the expected chemistries, we can predict the products that would result from these anticipated pathways. Such pathways would produce propanol, ethane and carbon monoxide, these equations are as follows:

Hydrogenation: $C_2H_5CHO + H_2 \rightarrow C_2H_5CH_2OH$

106

Decarbonylation: $C_2H_5CHO \rightarrow C_2H_6 + CO$
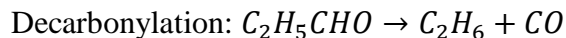
By using the predicted equations, we can visualize a primary reaction network as seen in Figure 4.14.
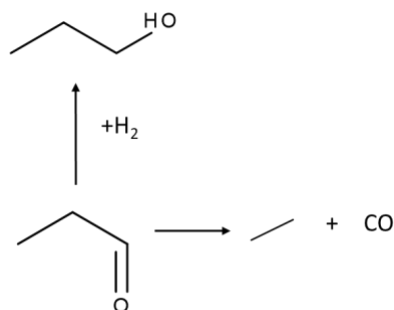
Figure 4.14: Anticipated primary reaction pathways for propanal over Ru.

The effect of conversion on the molar selectivities of all observed species using propanal is investigated similar to what was done using propionic acid as a reactant. Hydrogenation of propanal to form propanol was the most dominant pathway (>80%) at the experimental reaction conditions. The trend in propanol molar selectivity as a function of fractional conversion can be seen in Figure 4.15. Propanol exhibited a stable molar selectivity over the conversion tested in the packed bed reactor. The anticipated DCN products, carbon monoxide and ethane, were observed in near stoichiometric quantities. The molar selectivities of both products are stable over the conversion range tested, as seen in Figure 4.16. Propanol, carbon dioxide and ethane all have non-zero y-intercepts towards the zero conversion limit as seen in their respective figures. This confirms the species being formed from primary pathways as anticipated in Figure 4.14. Propane, carbon monoxide and ethane also show now artifacts of being consumed or formed by non-primary pathways.
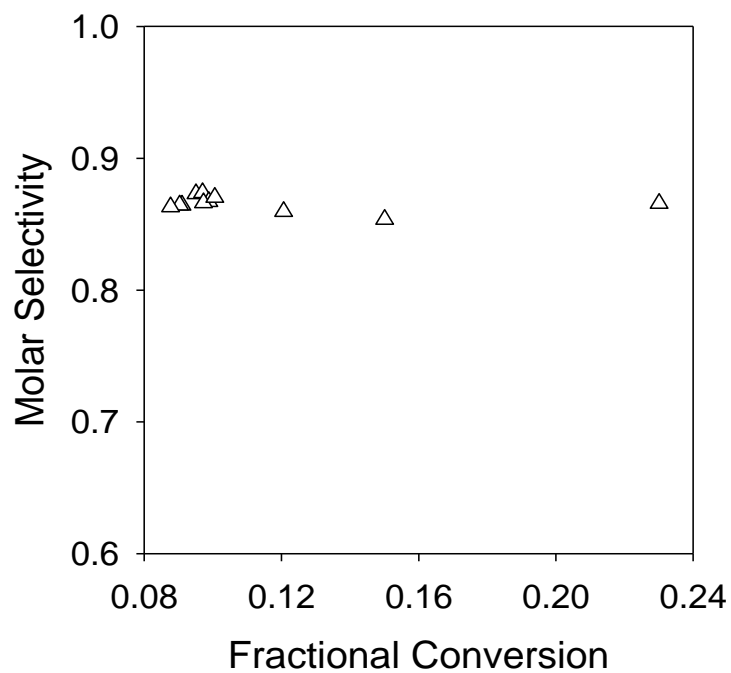
Figure 4.15: Effect of fractional conversion on the molar selectivity of the Hydrogenation product propanol at propanal and hydrogen partial pressures of 5 and 755 torr respectively at 381K over Ru.
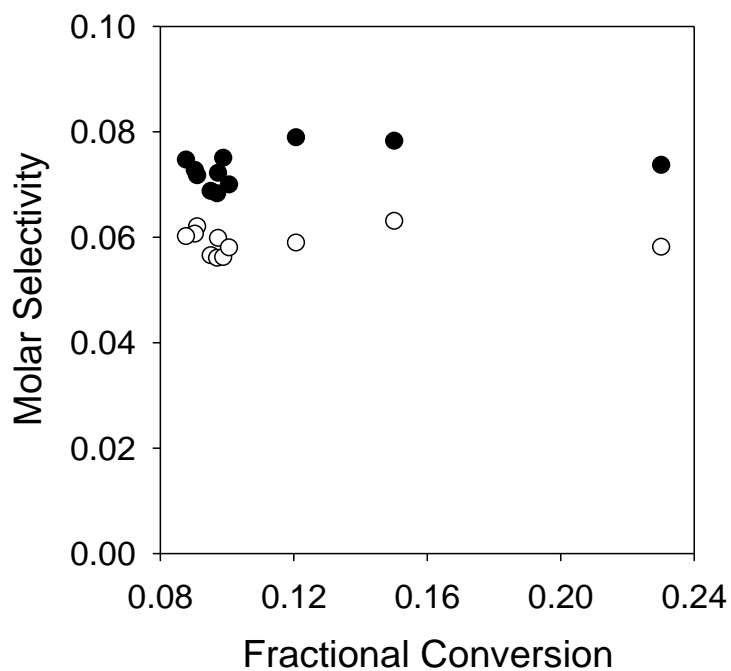
Figure 4.16: Effect of fractional conversion on the molar selectivity of DCN products ethane (○) and carbon monoxide (●) at propanal and hydrogen partial pressures of 5 and 755 torr respectively at 381K over Ru.

Propane was an unanticipated product that was observed during propanal experiments, it has the lowest molar selectivity of all observed products over the conversion range tested. The effect of conversion on propane selectivity is shown in Figure 4.17. Propane shows a slight increase in selectivity with fractional conversion, however since the molar selectivity is less than 0.5% over all data points because of the low quantities formed, arguments can also be made about points being scatter around a central value. The increase in selectivity hints towards being formed by a non-primary pathway; none of the observed primary products showed signs of being consumed by a secondary pathway, however, the selectivity was so small that any consumption of such small amounts would not cause a big enough change to observe.
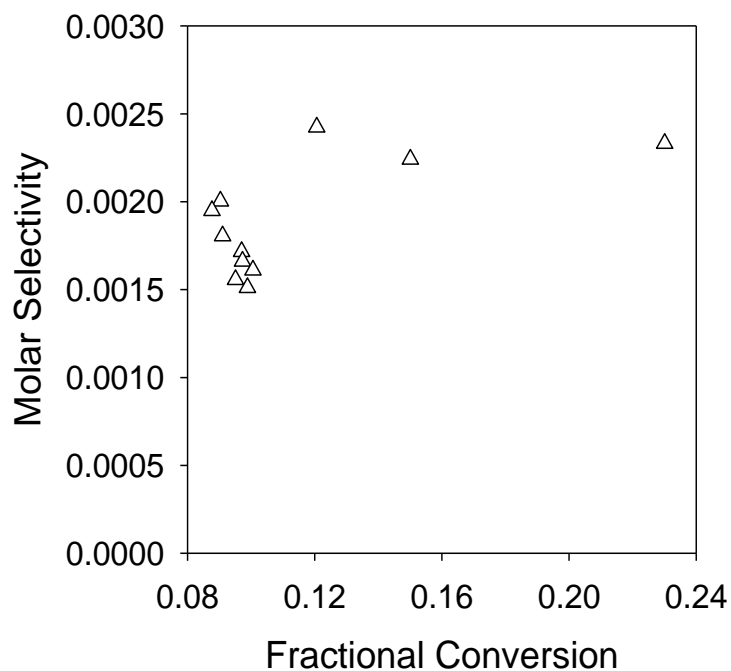
Figure 4.17: Effect of fractional conversion on the molar selectivity of the unanticipated product propane at propanal and hydrogen partial pressures of 5 and 755 torr respectively at 381K over Ru.

The rate of conversion was observed over the range of fractional conversions, this is illustrated in Figure 4.18. As fractional conversion increased, the rate of conversion greatly decreased- it showed a more than 80% decrease over the conversion range tested during propanal HDO. This is quite similar to the Figure 4.13, where the rate of conversion during propionic acid HDO also showed a large drop as conversion was increased.
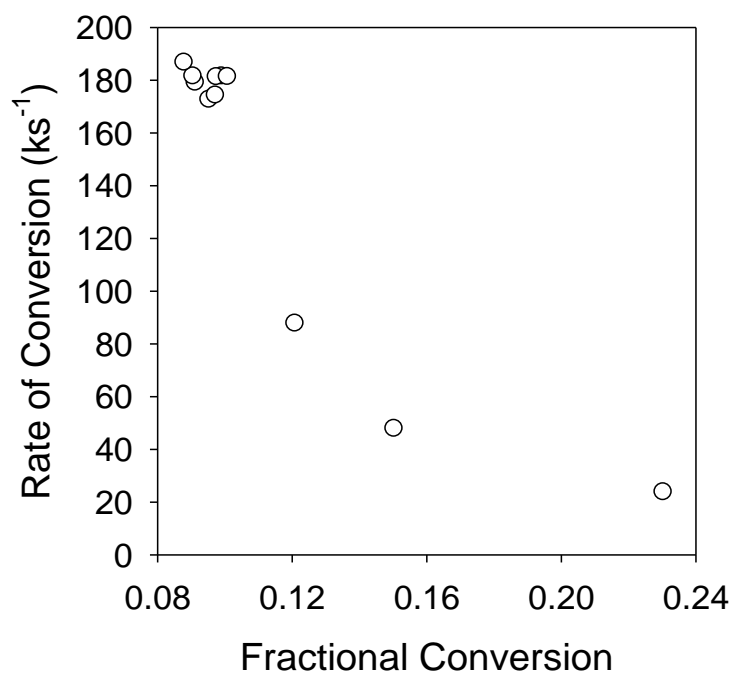
Figure 4.18: The rate of conversion of propanal at different fractional conversions during propanal HDO at propanal and hydrogen partial pressures of 5 and 755 torr respectively at 381K over Ru

4.3.3. Propanol

Alcohol chemistry over Ru catalysts are widely reported throughout the literature[12,23]. As propanol was mentioned during anticipating propanal experiments, one can expect propanol to undergo dehydrogenation to form propanal. Dehydration of propanol to form propylene is a well known reaction, in a hydrogen rich environment, propylene is expected to immediately undergo

hydrogenation to form propane; this two-step dehydration/hydrogenation reaction can be envisioned as one hydrogenolysis reaction. The equations for the mentioned anticipated reactions are as follows:

Hydrogenolysis: $C_2H_5CH_2OH + H_2 \rightarrow C_3H_8 + H_2O$

Dehydrogenation: $C_2H_5CH_2OH \rightarrow C_2H_5CHO + H_2$
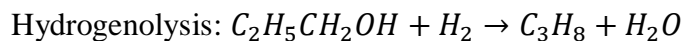
Using the equations of the anticipated reactions, we can construct a schematic to represent the expected reaction network, this is shown in Figure 4.19.
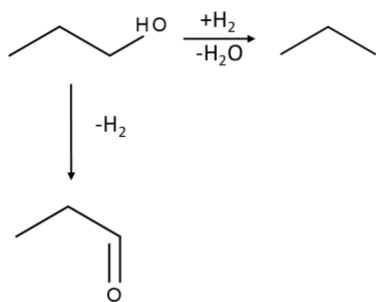
Figure 4.19: Anticipated primary reaction pathways for propanol over Ru.

The effect of fractional conversion on the molar selectivity of propanal is displayed in Figure 4.20. Propanal's selectivity is stable over the fractional conversion range, it also appears to have a non-zero y-intercept towards zero conversion. Propanol hydrogenolysis to form propane, as illustrated in Figure 4.21, has the lowest selectivity of all the observed products over all experimental conversions. The selectivity to propane is stable over the conversions range during propanol experiments, this selectivity also appears to have a non-zero y-intercept as the conversion approaches the zero conversion limit. This confirms that propane and propanal are primary products that appear to be stable over the experimental conditions during propanol HDO.
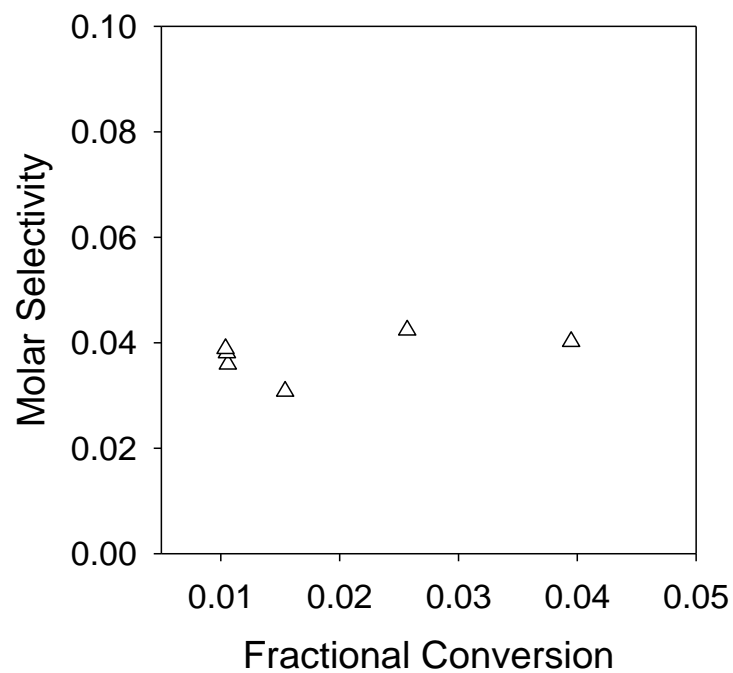
Figure 4.20: Effect of fractional conversion on the molar selectivity of the dehydrogenation product propanal at propanol and hydrogen partial pressures of 5 and 755 torr respectively at 420K over Ru.
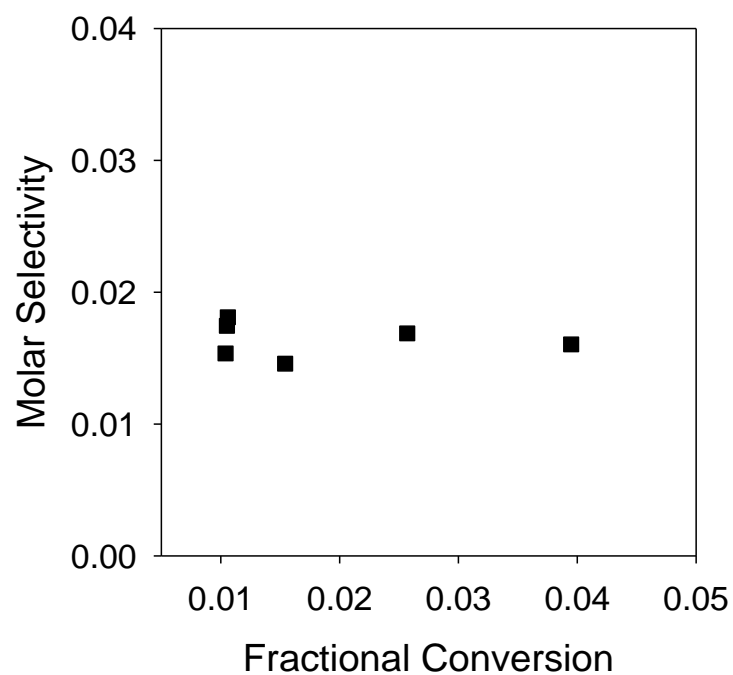
Figure 4.21: Effect of fractional conversion on the molar selectivity of the Hydrogenolysis product propane at propanol and hydrogen partial pressures of 5 and 755 torr respectively at 420K over Ru.

The unanticipated products observed during propanol experiments over Ru include: ethane, carbon monoxide and methane. The molar selectivities of these products at difference fractional conversions are illustrated in Figure 4.22. All three products appear to have a non-zero y-intercept towards zero conversion, methane may intercept the y-axis at zero conversion if experiments could have achieved lower conversions, but laboratory practicality limit. Ethane had the highest selectivity of all observed products for all fractional conversions tested; this attribute may change because of the species trends. Both ethane and carbon monoxide appears to be decreasing as the conversion is increased; the carbon monoxide decrease is much more noticeable than that of ethane. Carbon monoxide and ethane are likely being consumed by two different pathways, each occurring at different rates. Methane shows a steady increase in molar selectivity with fractional conversion, it can be forecasted to eventually be the most selective product at higher conversions; as methane is the only product selectivity that is increasing with conversion, multiple terminal pathways may be ending at this product.
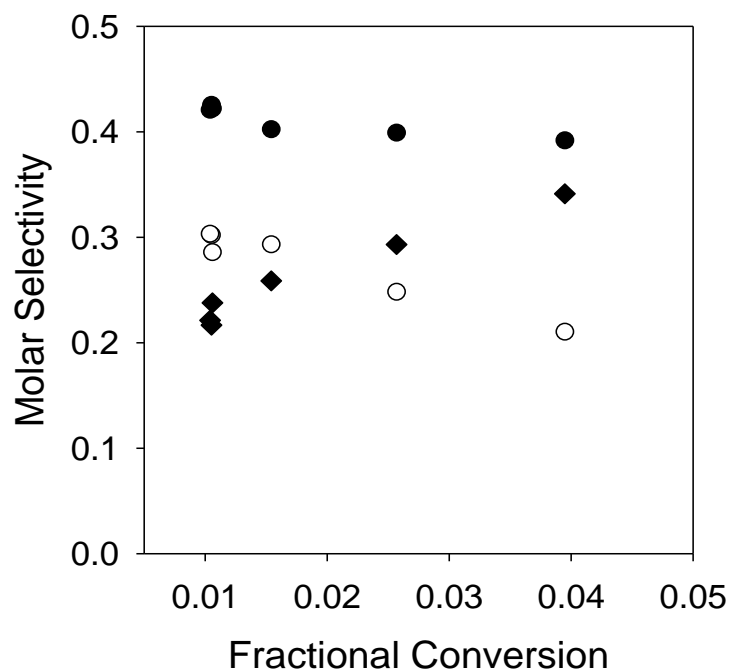
Figure 4.22: Effect of fractional conversion on the molar selectivity of the unanticipated products ethane (○), carbon monoxide (●), and methane (♦) at propanol and hydrogen partial pressures of 5 and 755 torr respectively at 420K over Ru.

There are a few issues with the molar selectivity trends during propanol HDO. The first is that there has been no reported decarbonylation of alcohols in the literature. Accordingly, we hypothesize that propanal formed by propanol dehydrogenation undergoes rapid decarbonylation, giving it the appearance of a primary product in the range of experimentally tractable contact times. Subsequently, we probe this hypothesis by considering the relative site time yields (product formation rates per unit active site) observed during HDO of propanol and propanal. At 401K, propanal decarbonylation had a STY of 0.21 min-1, while dehydrogenation of propanol at that same temperature had a STY of 0.026 min-1. Propanal decarbonylation occurred an order of magnitude faster than propanol dehydrogenation at similar temperature; we present this as evidence of carbon monoxide and ethane's *apparent* primary pathway characteristics in Figure 4.22.

The rate of conversion over the range of fractional conversions recorded during propanol HDO over Ru is illustrated in Figure 4.23. There is a constant decrease in rate of conversion as the fraction conversion for propanol HDO is increased; there was more than 50% loss in activity within the range of conversions recorded. This observation is similar for propionic acid and propanal experiments, the rate inhibition is present in all reactant instances thus far.
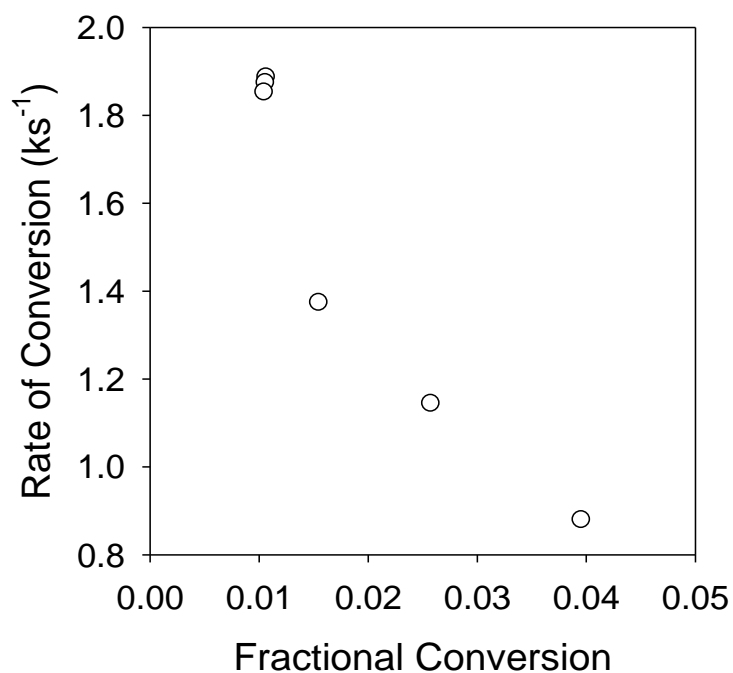
Figure 4.23: The rate of conversion of propanol at different fractional conversions during propanol HDO at propanol and hydrogen partial pressures of 5 and 755 torr respectively at 420K over Ru

4.3.4. Propane

There has been evidence of non DCN C-C cleavage over Ru catalyst[24,25]; this can be envisioned to essentially crack various hydrocarbons. Applying this chemistry to propane, we can anticipate the following equation:

Hydrogenolysis: $C_3H_8 + H_2 \rightarrow C_2H_6 + CH_4$
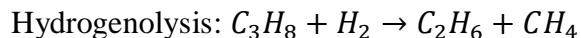
The effect of fractional conversion on the molar selectivity of methane and ethane are illustrated in Figure 4.24. Ethane and methane are approaching the y-axes at a non-zero intercept towards the zero conversion limit. At lowest conversion, both products appear to have equal molar selectivity, but this changes as the fractional conversion is increased; the selectivity to ethane decreases while that of methane increases. No additional products are observed during propane experiments. Both products are formed from primary pathways, however a secondary pathway is consuming ethane while a primary pathway is forming methane; this is likely because ethane is undergoing hydrogenolysis to form methane.
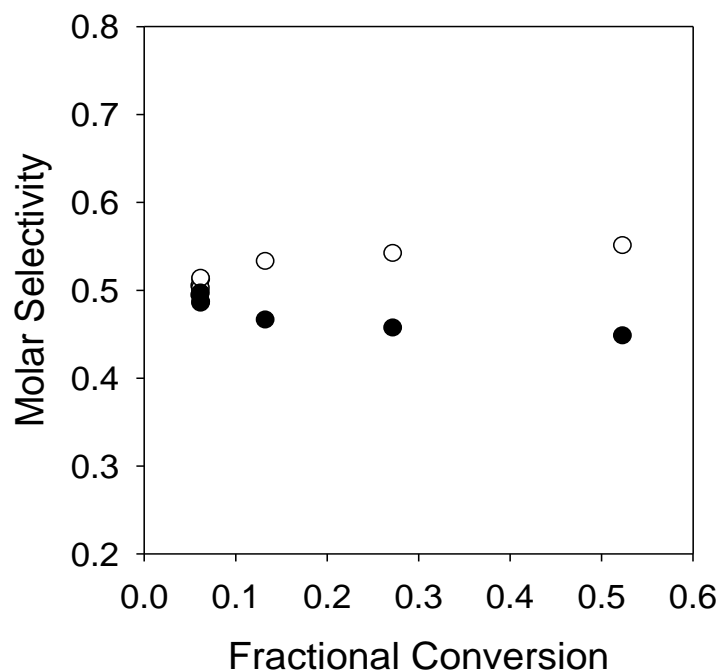
Figure 4.24: Effect of fractional conversion on the molar selectivity of the hydrogenolysis products methane (○) and ethane (●) at propane and hydrogen partial pressures of 3.9 and 381 torr respectively at 760 torr with a balance He at 436K over Ru.

The rate of conversion was observed for the different fractional conversions tested during propane hydrogenolysis experiments, this is shown in Figure 4.25. The rate of conversion is stable across the fractional conversion range tested using propane. This is the only instance where the rate of conversion was stable across the fractional conversion range; the main characteristic that sets propane experiments apart from the others is the presence of the DCN pathway over the surface.
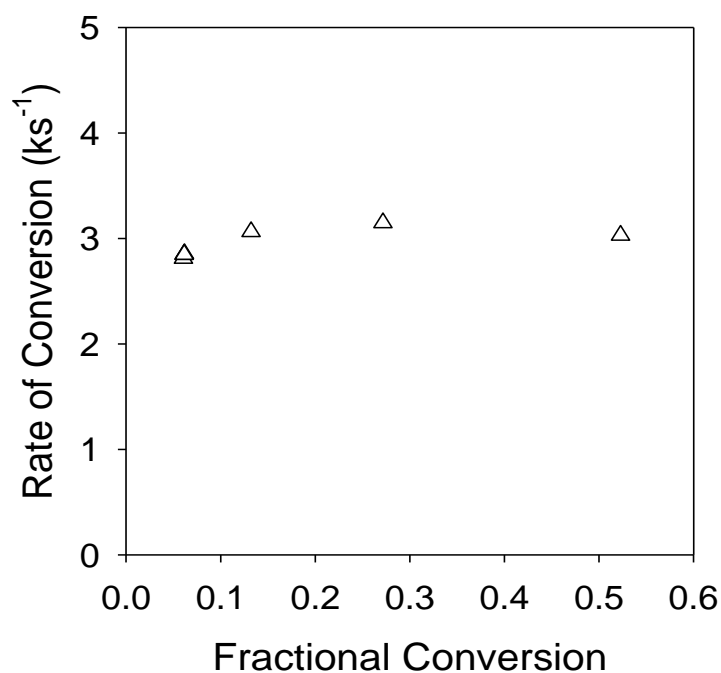
Figure 4.25: The rate of conversion of propanol at different fractional conversions during propane hydrogenolysis at propane and hydrogen partial pressures of 3.9 and 381 torr respectively at 760 torr with a balance He at 436K over Ru.

4.3.5. Carbon Monoxide

Carbon monoxide showed evidence in the literature of being able to undergo the following reactions[26-28]:

Methanation: $CO + 3H_2 \rightarrow CH_4 + H_2O$

Boudouard Reaction: $CO + CO \rightarrow CO_2 + C$
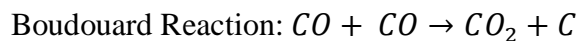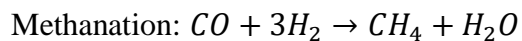
Water-Gas Shift: $CO + H_2O \rightarrow CO_2 + H_2$

Since the study is investigating propionic acid HDO, the conditions for the carbon monoxide reactions is carried out around the range of those during propionic acid (similar temperature and hydrogen partial pressure). Carbon monoxide well undergoes methanation at 465K, but does not show as much activity for water-gas shift and Boudouard reactions at this condition; this observation also holds at higher temperatures up to 600K. Carbon dioxide is now the third source of methane, as propane and ethane were both observed to undergo reactions that produce methane.

4.4.   Discussion

Majority of the products of the anticipated reactions had the lowest yields at high contact times; ethane and methane had the highest yields at high contact times, the latter being an unanticipated product. In both anticipated pathways that produced ethane, it was formed in equimolar ratios with either carbon monoxide or carbon dioxide, however ethane appeared to be in a league of its own at high contact times. Carbon dioxide in addition to the HDO 1 pathway to form propanal both should evidence of achieving a steady state yield around 20 s, an important difference however, is that propanal decreased to a steady value while carbon increased to its stable yield. Propanol showed no discernable trend, other than its scatter, it can be assumed to be stable over the range of contact time conditions. It was seen that the reaction quotients of the anticipated pathways are orders of magnitude away from the theoretical equilibrium (Figures 4.3 and 4.5).

While in an ideal setting, a decrease in rates is typically observed approaching equilibrium, here we have an instance of some sort of rate inhibition occurring on the catalyst surface that gives off an appearance as if pathways beginning to be in an equilibrium regime. The observation of

118

unanticipated products also hints towards pathways that were not originally accounted for in Figure 4. We used selectivity and rate of conversion trends to investigate the reaction pathways over Ru as well as the surface phenomena causing the yields to plateau prematurely.

4.4.1. Propionic Acid Pathways

During Propionic acid HDO over Ru, three species exhibit characteristics of primary products. Specifically: carbon dioxide, propanol and propanal all show non-zero y-intercepts. Carbon dioxide selectivity is roughly constant as a function of conversion, suggesting it is a stable primary product that is neither formed or consumed by secondary reactions; ethane, methane and propane all show increasing selectivity as a function of conversion, which suggests they are formed by secondary and/or tertiary reactions; and propanol and propanal decrease in selectivity as a function of conversion, suggesting they are both consumed by sequential reactions. Carbon monoxide shows an initial increase in product selectivity until 0.5% conversion, after which its selectivity decreases with further conversion. This suggests carbon monoxide is being produced though non-primary reactions, and then being consumed by tertiary reactions. The decrease in propanal selectivity mirrors the increase in ethane/ carbon monoxide selectivity, which suggests aldehyde decarbonylation is a significant source of carbon monoxide and ethane in this system. The decrease in selectivity of carbon monoxide from 0.5% conversion onwards mirrors the increase in methane selectivity, while the decrease in propanol selectivity mirrors the increase in propane selectivity. In order to further resolve contributions from primary, secondary and tertiary reactions, we analyze product distributions formed from each of the other species when they were used as reactants in a hydrogen rich environment over Ru

4.4.2. Propanal Pathways

Figures 4.15-4.17 reveal that three products show a non-zero y-intercept, indicating that carbon monoxide, ethane, and propanol are all primary products of propanal conversion. Propane is the only product to exhibit secondary product behavior in Figure 17. Primary formation of carbon monoxide, ethane and propanol are consistent with the expectations for this system. Specifically that propanal can undergo either hydrogenation (to form propanol) or decarbonylation (to form carbon monoxide and ethane); decarbonylation is especially evident from the 1:1 molar ratios of ethane and carbon monoxide selectivity.

At 401K, propanal hydrogenation had a STY of 1.29 min^{-1}, while propanol formation during propionic acid HDO had a STY of 0.006 min^{-1}. Propanal hydrogenation to form propanol is a fast and thermodynamically favorable reaction, this explains why propanol extrapolated to a non-zero y intercept in Figure 4.8. From the evidence presented in this section, the major primary product formed during propionic acid HDO is propanal.

4.4.3. Propanol Pathways

Figures 4.20 –4.22 revealed that four products show a non-zero y-intercept, indicating that carbon monoxide, ethane, propanal, and propane are all *apparent* primary products of 1-propanol conversion. Methane is the only product to exhibit secondary product behavior. Primary formation of propanal and propane are consistent with the expectations for this system, specifically that propanol can undergo either dehydrogenation (to form propanal) or hydrogenolysis (to form propane). However, we know of no direct pathway for decarbonylation of 1-propanol to yield carbon monoxide and ethane, whereas decarbonylation of propanal is reportedly facile[17,22,29,30].

The rates of DCN from propanal are significantly faster than over propanol, this is evidence of propanal DCN being so fast that it appears as a primary product from propanol.

An important observation from Figure 4.22 is that carbon monoxide and ethane, although both decarbonylation products, deviate from being stoichiometrically equivalent with increasing conversion. Although both products show a decrease in selectivity as conversion is increased; the extent to which ethane selectivity decreases is quite different from carbon monoxide's which exhibits a much faster decrease in selectivity. Methane is the only product observed that is being formed from a non-primary pathway using propanol as the reactant; both ethane and carbon monoxide may be sources of methane.

4.4.4. Propane Pathways

Hydrogenolysis of propane occurred over Ru catalyst to form ethane and methane. From Figure 4.25, it can be observed that at low conversions, equimolar amounts of ethane and methane was formed, after which ethane selectivity decreases with increasing conversion; this observation is mirrored by methane's selectivity increasing with conversion. The most plausible reason for the observations is that the hydrogenolysis of ethane is likely taking place; this confirms that ethane can contribute to methane rates.

4.4.5. Carbon Monoxide Pathways

We probed the extent of carbon monoxide methanation, water-gas shift, and the Boudouard reaction under characteristic operating conditions; this meant low carbon monoxide partial pressures in a hydrogen rich environment. Methanation was tested over a range of conditions that

include partial pressures of 1-60 torr and temperatures of 450-500K. In general, we observe that Ru readily catalyzes methanation under our reaction conditions such that this pathway should be considered as a primary source of methane in this system.

Carbon dioxide was observed as a product during propionic acid HDO when carbon monoxide product partial pressures were in the range of 0.003 - 0.11 torr, this range was troublesome to attain as 0.5 torr was the lowest achievable partial pressure given the materials available. The Boudouard reaction showed no observable activity at a carbon monoxide partial pressure of 0.5 torr in the temperature range of 450-500K; however carbon dioxide formation rates were seen above 600K. In testing water-gas shift reaction, the closest reaction feed composition to operating conditions during propionic acid HDO consisted of 0.1% CO, 0.1% H_2O, 79.9% H_2 and 19.9% He at 760 torr; there was no observable carbon dioxide production using this feed composition from 450-500. These observations suggest that the extent of WGS and Boudouard chemistry are minimal under our reaction conditions, and that direct decarboxylation of propionic acid is likely the only source of carbon dioxide in this system.

4.4.6. Pathway Summary

Through a pathway analysis of propionic acid HDO over supported Ru catalysts, we observe a large change in the initial network proposed in Figure 4.1. The only primary pathway occurring over the experimental conditions is HDO to form propanal. The carbon monoxide, ethane and propanol are all formed from secondary pathways through propanal: DCN and hydrogenation reactions. Methane showed to be formed through carbon monoxide methanation as well as hydrogenolysis of propane and ethane. The pathways involved during propionic acid HDO over Ru is illustrated in Figure 4.26:
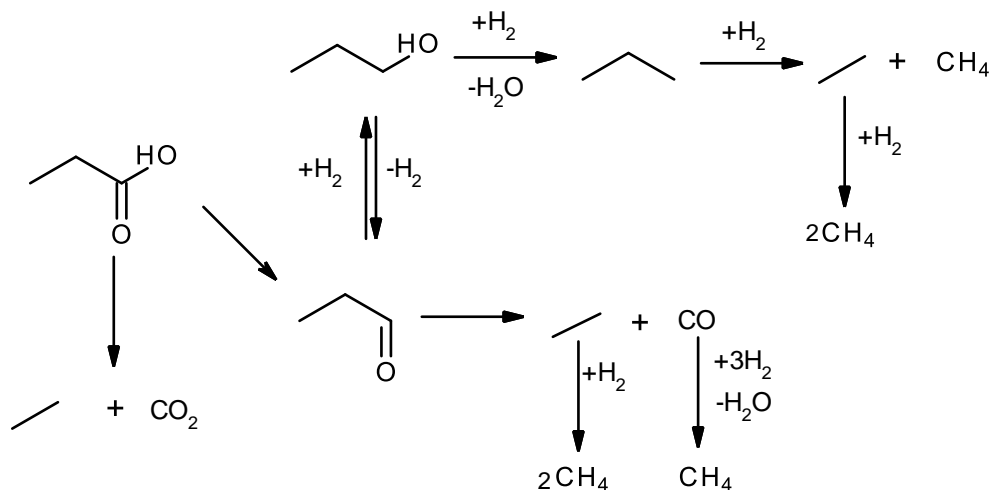
Figure 4.26: Reaction schematic after taking into account results from selectivity experiments.

4.4.7. Rate Inhibition

We observed in Figure 4.13 that the rate of conversion showed a large decrease over the fractional conversions tested. Noble metal catalysts have been showed to be susceptible to carbon monoxide poisoning[31]. In the reaction network occurring during propionic acid HDO over Ru, propanal decarbonylation is one of the most dominant and facile reactions, this can directly contribute to carbon monoxide being formed on the catalyst surface. Figure 4.27 shows how the carbon monoxide partial pressure on the surface increases with fractional conversion; as it is being formed, inhibiting the active sites.
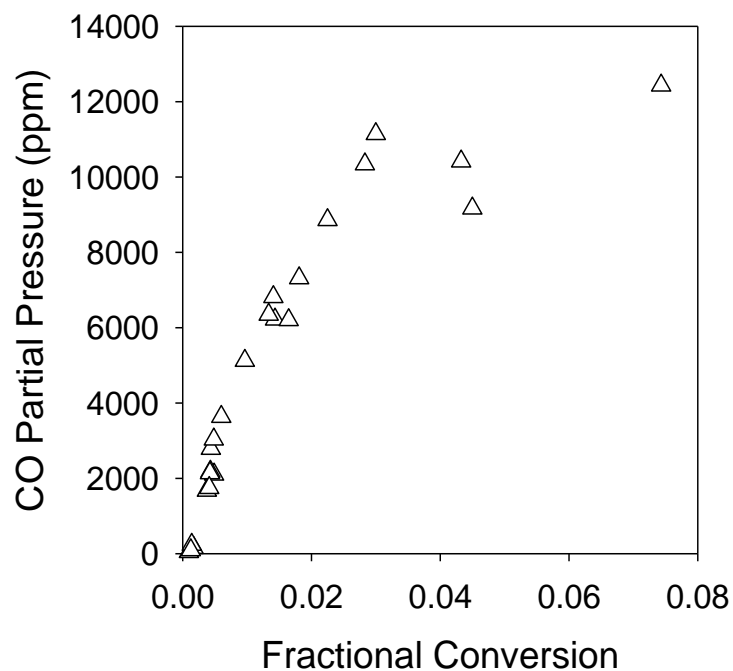
Figure 4.27: Formation of carbon monoxide in relation to the fractional conversion of propionic acid over Ru.

We can also directly observe how the rate of propionic acid HDO changes with the partial pressure of carbon monoxide over the catalyst; this is illustrated in Figure 4.28. Propionic acid HDO increases can be seen to be inversely proportional to carbon monoxide partial pressure up to a point at which it is observed to achieve a steady rate. An important overall consideration to tie this hypothesis together is comparing the rate of conversions of the presented species (Figures 4.13, 4.18, 4.23 and 4.25). There was only one instance where the rate of conversion did not decrease at higher fractional conversion- during experiments using propane as a reactant; coincidently, this is also the only instance where carbon monoxide was not present during the reaction since it was not a product.
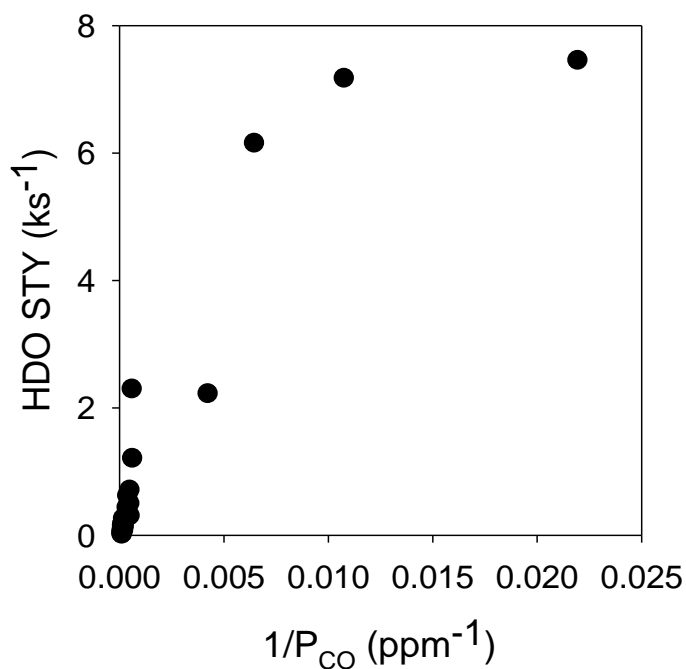
Figure 4.28: The relationship between rate of propionic acid HDO and partial pressure of CO over Ru.

4.4.8. Modelling Propionic Acid HDO over Ru

There were certain characteristics of the system that a computational model had to successfully capture. The model has to represent all the equations present during propionic acid HDO as well as capture the inhibition effects of carbon monoxide. In order to account for the carbon monoxide poisoning, the coverages of the species had to be incorporated so that species' build up can be taken into consideration. Therefore, a semi-empirical approach was taken by making use of Langmuir-Hinshelwood surface kinetics. The list of equations used in the MATLAB model is seen below. It was assumed that the rate of the reactions were in first order dependence on the coverage of the reactants; these coverages were assumed to be in equilibrium with the gas phase species. Because the rate of the reaction was constantly changing across the reactor bed, it was not possible to assume a differential reactor, therefore we had to integrate the species over the active sites

present in the reactor at different experiment al conditions. This allowed us to capture the trends in propionic acid HDO over Ru and also extrapolate to results over a large range of temperatures, pressures and residence times. This means that even though there were practical limitations to achieving extremely low conversions, the model would allow us to observe these conditions that were originally hard to reach during reactor experiments.

1. $C_2H_5COOH + H_2 \rightarrow C_2H_5CHO + H_2O$
2. $C_2H_5COOH \rightarrow C_2H_6 + CO_2$
3. $C_2H_5CHO + H_2 \leftrightarrow C_3H_7OH$
4. $C_2H_5CHO \rightarrow C_2H_6 + CO$
5. $C_3H_7OH + H_2 \rightarrow C_3H_8 + H_2O$
6. $CO + H_2O \leftrightarrow CO_2 + H_2$
7. $CO + 3H_2 \rightarrow CH_4 + H_2O$
8. $C_3H_8 + H_2 \rightarrow C_2H_6 + CH_4$
9. $C_2H_6 + H_2 \rightarrow 2CH_4$

List of Equations used in MATLAB model.

The main governing equations of the model are as follows:

$$k_i = k_m \cdot e^{\frac{-E_A}{R\Delta T}}$$

$$K_j = K_m \cdot e^{\frac{-DH}{R\Delta T}}$$

$$\theta_* = \frac{1}{1 + \sum K_j \cdot p_j}$$

$$\theta_j = K_j \cdot p_j \cdot \theta_*$$

$$r_i = k_i \cdot \prod \theta_j$$

Where DH is the binding enthalpy, E_A is the activation energy, θ_j is the species coverage, k_m is the mean rate constant, K_m is the mean binding constant, K_j is the binding constant, k_i is the rate constant and r_i is the rate of the reaction. The mean rate constants and mean binding constants are use in order to regress the model parameters with experimental values. The parameters that undergo regression in order to fit the data include the activation energies, mean rate constants, and the mean binding constants and enthalpies for the non-terminal species. The trends were successfully captured by the model as seen in Figure 4.29:
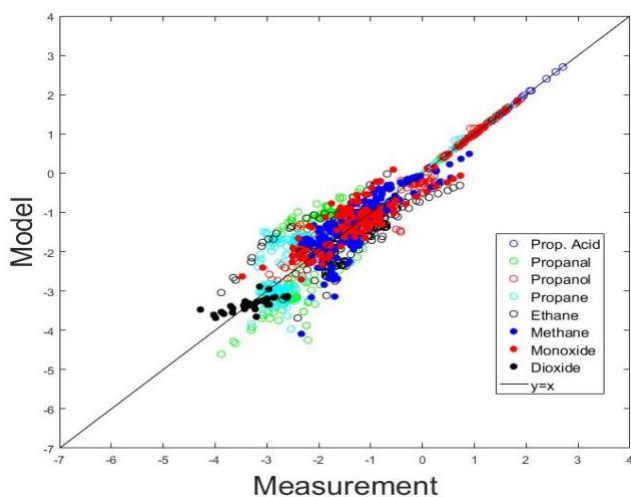
Figure 4.29: Parity plot of the natural logarithm of experimental rates versus theoretical rates for all species involved in reactions proposed for Ru.

Figure 4.30 illustrates predicted trends in selectivity of the desired carboxylic acid HDO products (propanol and propanal specifically) over Ru catalysts. High HDO activity was seen at lower temperatures than what was carried out in the laboratory experiments; at 400K, there is 100% selectivity to HDO products around the residence time range of 10^{-4} sec to 10^{-1} sec. Over Ru catalyst, low residence times favor HDO selectivity; at least less than 10^{-3} sec. The biggest reason for the impractical nature of Ru catalysts is that high HDO selectivity was only observed at short residence times, where conversions are near zero. This means that a single pass conversion for

high HDO yields is quite unfeasible, in fact, monometallic Ru would only be able to deliver good HDO yields at low pass per conversion and high recycle ratios. In terms of the actual values of the parameters regressed, they hold no accurate meaning because the system was overparameterized; using macroscopic equations provided too many parameters as the model could have found multiple minimums during regressions.
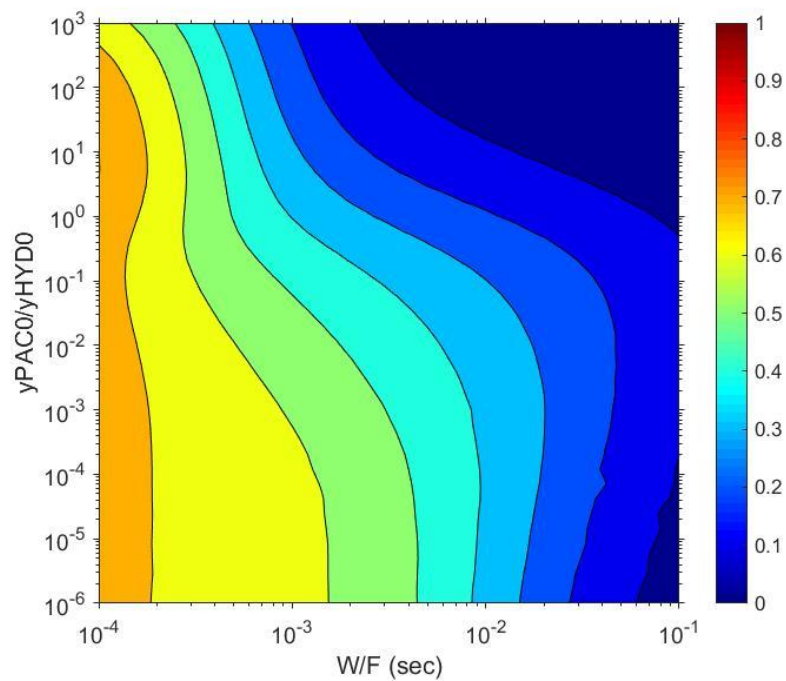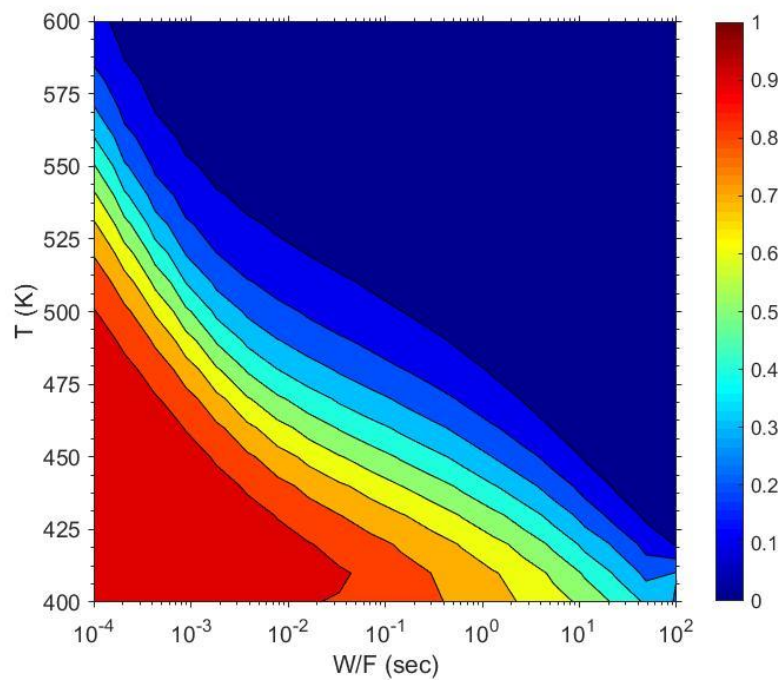
Figure 4.30: (Top) Effect of temperature and propionic acid residence time on the selectivity of HDO products at a ratio of propionic acid to hydrogen partial pressure of 10^{-2} over Ru. **(Bottom)** Effect of the ratio of propionic acid to hydrogen partial pressure and propionic acid residence time on the selectivity of HDO products at 4503K over Ru.

4.5. Conclusion

The major setbacks to monometallic Ru catalysts for propionic acid HDO are its selectivity and product inhibition issues. There are a number of undesired pathways that are more selective than HDO chemistry. DCN and Methanation are the dominant pathways at high conversions, the former being a secondary pathway and the latter formed through multiple tertiary pathways. Carbon monoxide is also poisoning the Ru active sites as it is being produced; this proves unfortunate since it is a product of one of the most dominant pathways during catalytic activity. By using the computational capabilities of MATLAB, the regime that would deliver high HDO yields is at low pass conversions with high recycle ratios; this evidently shows that monometallic Ru catalysts are unfeasible for practical use in reactions requiring high HDO yields. Investigations should be done into the addition of an oxophilic promoter, as it has been reported to tune the catalytic selectivity towards more oxygenated products[7,15,18,32]. A semi-empirical approach may not be enough to provide useful parameters because of the tendency to overparameterize the system using macroscopic equations; a more microkinetic approach should be considered.

## 4.6.	References

1	Moulijn, J. A., van Leeuwen, P. W. N. M. & van Santen, R. A. in *Studies in Surface Science and Catalysis* Vol. 79 Ch. Chapter 2, 23-67 (1993).

2	Wu, L., Moteki, T., Gokhale, A. A., Flaherty, D. W. & Toste, F. D. Production of Fuels and Chemicals from Biomass: Condensation Reactions and Beyond. *Chem* **1**, 32-58 (2016).

3	Simonetti, D. A. & Dumesic, J. A. Catalytic Production of Liquid Fuels from Biomass-Derived Oxygenated Hydrocarbons: Catalytic Coupling at Multiple Length Scales. *Catalysis Reviews 51*, 441-484 (2009).

4	Wang, S., Guo, Z., Cai, Q. & Guo, L. Vol. 45 138-143 (Biomass and Bioenergy 2012).

5	Pritchard, J., Filonenko, G. A., Van Putten, R., Hensen, E. J. M. & Pidko, E. A. Heterogeneous and homogeneous catalysis for the hydrogenation of carboxylic acid derivatives: history, advances and future directions *Chemical Society Reviews* **44**, 3808 (2015).

6	Tomishige, K., Nakagawa, Y. & Tamura, M. Selective hydrogenolysis and hydrogenation using metal catalysts directly modified with metal oxide species *Green Chemistry* **19**, 2876 (2017).

7	Vardon, D. R. *et al.* Ru/Sn/Ac for the squeous phase reduction of succinic acidk to 1,4-butanediol under continuous process conditions. **7** (2017).

8	Rachmady, W. & Vannice, M. A. Acetic Acid Hydrogenation over Supported Platinum Catalysts. *Journal of Catalysis 192*, 322-334 (2000).

9	He, Z. & Wang, X. Required catalytic properties for alkane production from carboxylic acids: Hydrodeoxygenation of acetic acid. *Journal of Energy Chemistry 22*, 883-894 (2013).

10	Contreras-Mora, J. *et al.* Characterization and Evaluation of Carbon-Supported Noble Metals for the Hydrodeoxygenation of Acetic Acid. *Organic Process Research & Development 22*, 1628-1635 (2018).

11	Shangguan, J., Olarte, M. V. & Chin, Y.-H. Mechanistic insights on CAO and CAC bond activation and hydrogen insertion during acetic acid hydrogenation catalyzed by ruthenium clusters in aqueous medium. *Journal of Catalysis 340*, 107-121 (2016).

12	Gursahani, K. I., Alcalá, R., Cortright, R. D. & Dumesic, J. A. Reaction kinetics measurements and analysis of reaction pathways for conversions of acetic acid, ethanol,

and ethyl acetate over silica-supported Pt. *Applied Catalysis: A General 222*, 369-392 (2001).

13   Lugo-José, Y. K., Monnier, J. R. & Williams, T. C. Gas-Phase, catalytic hydrodeoxygenation of propanoic acid, over supported group VIII noble metals: Metal and support effects. *Applied Catalysis A: General 469*, 410-418 (2014).

14   Chen, L. *et al.* Aqueous-phase hydrodeoxygenation of carboxylic acids to alcohols or alkanes over supported Ru catalysts. *Journal of Molecular Catalysis A: Chemical 351*, 217-227 (2011).

15   He, D.-H., Wakasa, N. & Fuchikami, T. Hydrogenation of Carboxylic Acids Using Bimetallic Catalysts Consisting of Group 8 to 10, and Group 6 or 7 Metals. *Tetrahedron Letters 36*, 1059-1062 (1995).

16   Keels , J. M. *et al.* Aqueous-Phase Hydrogenation of Succinic Acid Using Bimetallic Ir–Re/C Catalysts Prepared by Strong Electrostatic Adsorption. *ACS Catalysis* **8**, 6486-6494 (2018).

17   da Silva, A. B., Jordão, E., Mendes, M. J. & Fouilloux, P. Effect of metal-support interaction during selective hydrogneaton of cinnamaldehyde to cinnamyl alcohol on platinum based bimetallic catalysts. *Applied Catalysis A: General 148*, 253-264 (1997).

18   Englisch, M., Ranade, V. S. & Lercher, J. A. Hydrogenation of crotonaldehyde over Pt based bimetallic catalysts. *Journal of Molecular Catalysis A: Chemical* **121**, 69-80 (1997).

19   Lugo-José, Y. K., Monnier, J. R., Heyden, A. & Williams, C. T. Hydrodeoxygenation of propanoic acid over silica-supported palladium: effect of metal particle size. *Catalysis Science & Technology 4*, 3909-3916 (2014).

20   Behtash, S. *et al.* Solvation Effects in the Hydrodeoxygenation of Propanoic Acid over a Model Pd(211) Catalyst. *The Journal of Physical Chemistry* **120**, 2724-2736 (2016).

21   Bowker, M. *et al.* The decarbonylation of acetaldehyde on Pd crystals and on supported catalysts. *Applied Catalysis A: General 391*, 394-399 (2011).

22   Durndell, L. J. *et al.* Selectivity control in Pt-catalyzed cinnamaldehyde hydrogenation. *Scientific reports* **5**, 9425 (2015).

23   Merlo, A. B., Vetere, V., Ruggera, J. F. & Casella, M. L. Bimetallic PtSn catalyst for the selective hydrogenation of furfural to furfuryl alcohol in liquid-phase. *Catalyst Communications* **10**, 1665-1669 (2009).

24   Bond, G. C., Rajaram, R. R. & Burch, R. Hydrogenolysis of Propane, n-Butane, and Isobutane over Variously Pretreated Ru/TI02. Catalysts. *Journal of Physical Chemistry* **90**, 4877-4881 (1986).

25   Guilleux, M. F., Dalmon, J. A. & Martin, G. A. Mechanism and structure sensitivity of propane hydrogenolysis over Ni/SiO2 catalysts. *Journal of Catalysis 62*, 235-242 (1980).

26   M. A. A. Aziz, A. A. Jalil, S. Triwahyono & Ahmad., A. CO 2 methanation over heterogeneous catalysts: recent progress and future prospects. *Green Chemistry* **17**, 2647-2663 (2015).

27   Marsh, H. & Taylor, D. W. Carbon gasification in the Boudouard reaction. *Fuel 54*, 218-220 (1975).

28   Utaka, T., Okanishi, T., Takeguchi, T., Kikuchi, R. & Eguchi, K. Water gas shift reaction of reformed fuel over supported Ru catalysts. *Applied Catalysis A: General 245*, 343-351 (2003).

29   Zhao, B.-H. *et al.* Selective Hydrogenation of Cinnamaldehyde over Pt and Pd Supported on Multiwalled Carbon Nanotubes in a CO2-Expanded Alcoholic Medium. *Industrial & Engineering Chemistry Research* **51**, 11112-11121 (2012).

30   Merlo, A. B., Machado, B. F., Vetere, V., Faria, J. L. & Casella, M. L. PtSn/SiO2 catalysts prepared by surface controlled reactions for the selective hydrogenation of cinnamaldehyde. *Applied Catalysis A: General* **383**, 43-49 (2010).

31   Argyle, M. D. & Bartholomew, C. H. Heterogeneous Catalyst Deactivation and Regeneration: A Review. *Catalysts* **5**, 145-269 (2015).

32   Garrick, T. R. *et al.* The Effect of the Surface Composition of Ru-Pt Bimetallic Catalysts for Methanol Oxidation. *Electrochimica Acta* **195**, 106-111 (2016).

CHAPTER 5

Carboxylic Acid Hydrodeoxygenation over Supported PtSn Catalysts

5.1 Introduction

The energy densities for fuels such as crude oil and natural gas are among the largest, only surpassed by uranium, such densities have made them very attractive because of the low cost of extracting valuable derivatives to be used in various sectors in society like transportation, industrial, electricity and residential[1]. Biomass is an attractive renewable resource because its energy density is not largely far off from crude oil[2]. While biomass can be converted to a fuel through processes like gasification and pyrolysis, a market can also exist for replacing platform chemicals in industry using bio-derived species[3-6]. Chemical components of biomass are heavily oxygenated. Producing polyoxygenated hydrocarbons from biomass thus requires that one remove oxygen from a heavily oxygenated starting material as opposed to, in the case of alkane functionalization, adding oxygen to an oxygen deficient starting material. The former is generally more kinetically and thermodynamically feasible than the latter. However, the extensive oxygen content in biomass and its derivative products means there are multiple reactive functional groups in a single molecule, and activating a specific chemical moiety is a significant selectivity challenge[7,8]. Because of the relative cost of biomass compared to fossil reserves, economically converting biomass into useful chemical commodities requires precise control over upgrading chemistries.

Maleic anhydride (MA) is an important industrial platform chemical. Presently, it is synthesized by n-butane oxidation, and it is used in in the synthesis of 1,4-butanedieol (BDO), γ-butyrolactone (GBL) and tetrahydrofuran (THF)[9]. The hydrolyzed (open ring) structure of maleic anhydride is maleic acid (MAc). Succinic acid (SAc) is functionally similar to MAc; the only difference

between the two is that the C_2-C_3 in SAc is fully hydrogenated, whereas the C_2-C_3 bond in MAc is unsaturated (i.e., an alkene). The three species are interconvertible through hydration/dehydration (MA/MAc) and hydrogenation/dehydrogenation (MAc/SAc) (Fig. 1.3). Presently, MA is converted into BDO, GBL and THF using the Davy process. Because of their chemical similarity (and the fact that the Davy process is reductive in nature), there is potential for succinic acid to be used as the chemical feedstock. Thus, bio-based succinic acid paves the way for renewable BDO, GBL, THF and various derivative polymers and solvents. In order for SAc to compete with MA as an HDO feedstock in the production of BDO, THF and GBL, one must be able to control its HDO selectivity in order to deliver target molecules in good yield while preventing side reactions that lead to formation of low value products. Hydrodeoxygenation (HDO) of carboxylic acids is an important reaction that can be fine-tuned in order to target specific oxygen molecules on carbonyl compounds to yield desired compounds such as alcohols, aldehydes and hydrocarbons[10-14].

Supported noble metals, such Pt, Ru, Pd, Rh and Ni are active catalysts for carboxylic acid hydrodeoxygenation; however, such catalysts have high activity for many other reactions as well. Specifically, HDO studies reported in the literature over these metals highlight that, although the metals are active, they are not generally selective due to their tendency to also enable multiple, undesired reactions such as decarbonylation, methanation and hydrogenolysis, which are kinetically facile over many noble metals and thus prevalent at high SAc conversions[15-18]. This limits the practicality of these systems. From a reaction engineering perspective, SAc HDO can be considered as a series reaction network in which the initial steps—conversion of a carboxylic acid into an aldehyde, ester, and alcohols are difficult and yield desirable products—while latter steps— conversion of aldehydes and alcohols into carbon oxides and light hydrocarbon fragments—are

facile but yield undesirable products. Producing these "intermediate" oxygenates selectively requires control over intrinsic catalyst performance as well as reactor operating conditions. Pairing noble metals with oxophilic promoter metals has shown to modify both catalyst activity and selectivity. Vardon et.al examined SAc HDO over various noble metals and the effect of Sn on catalytic performance[19]; a ratio of 1:1 between the promoter and noble metal showed to have the best selectivity towards oxygenated products. There exist practical problems with studying carboxylic acid HDO at a fundamental level using SAc such as stainless steel leaching during liquid phase reactions, and then gas phase reactions being problematic because SAc is not easily amenable to the gas phase.

Propionic acid (PAc) can be seen as a useful model species for HDO because it is a short enough molecule to gain useful knowledge on HDO without being too long, in that longer-chained molecules would present a large number of products that may complicate data. There has been work done on PAc HDO using monometallic as well as bimetallic catalysts that also reflects selectivity issues as well as the positive effects of promoter metals[8,17,20-25]. Platinum supported catalysts have demonstrated to have high selectivity for propionic acid HDO pathways from theoretical calculations, however experimental data in the literature fail to even observe HDO products because of the selectivity to the decarbonylation products, carbon monoxide and ethane[17].

This study aims to use propionic acid as a gateway to further insight about carboxylic acid HDO over Pt and Pt-Sn catalysts. The limitations of monometallic Pt will be identified as well how these limitations are mitigated with the addition of the promoter metal, Sn. Rates will be observed in relation to the amount of tin added to the catalyst. The effect of reaction conditions will be also used to hypothesize ways of being able to tune the selectivity between the groups of oxygenated

products. The apparent activation energy as well as PAc- and H_2-dependent reaction orders will also be procured for bimetallic Pt-Sn HDO.

5.2 Materials and Methods

5.2.1. Reagents

Air (Airgas, zero grade); alumina (206 m^2/g, 48-90 μm mesh size, Strem Chemicals, 97+%%); hexachloroplatinate(IV) hydrate (Acros, 99.9%); Tin(II) chloride dihydrate (Acros Organics, 98+%) ; hydrochloric acid (Fisher Scientific, Trace Metal Grade); sodium hydroxide (Sigma-Aldrich, ≥98%); nitric acid (Fisher Scientific, TraceMetal Grade); CO (Praxair, 99.99%); CO/He (Airgas: 0.991% CO, 0.996% Ar, 98% He); ethane Airgas: 0.994% C_2H_4, 1. % Ar, 98% He); ethylene (Airgas: 1% C_2H_4, 1% Ar, 98% He); He (Airgas, 99.999%); H_2 (Airgas, 99.999%); N_2 (Airgas, 99.999%%); O_2/Ar/He (1% O_2, 1% Ar , 98% He); propane (Airgas: 1% propane, 1% Ar, 98% He); 1-propanol (Acros Organics, 99+%); propanal (Acros Organics, 99+%) and propionic acid (Acros Organics, 99%) were employed for catalyst synthesis, catalyst characterization, and reactor operation. Each was used as supplied from commercial vendors. Water (Type II, 18.0 MΩcm^{-1} resistivity) was prepared in house (Spectrapure).

5.2.2. Catalyst Preparation

The bimetallic study involved preparing catalysts via strong electrostatic adsorption to take advantage of the accuracy involved with the procedure. Bimetallic catalysts were prepared sequentially. Pt was the first metal to be adsorbed, a precursor solution of the Pt salt with a concentration of 200 μg/mL and pH of 1. The volume of precursor satisfied a surface loading of 1000 m^2/L for a given mass of alumina support. The support-precursor mixture was allowed to

mix for an hour on an orbital rotator set to 80 rpm. Catalysts were then dried overnight in static air at 373K. Subsequently, samples were loaded into a quartz flow cell, calcined in air (100 ml min^{-1} Air, 3 K min^{-1} ramp rate) at 623 K for 3 hours, then reduced at 673K under H_2 flow for 4 hours (100 ml min^{-1} H_2, 3 K min^{-1} ramp rate), and cooled to 298K under H_2. Prior to exposure to ambient air, samples were passivated at 298K by purging the cell volume with He for 30 minutes and then exposing the cell to 1% O_2 in 1% Ar 98% He for 30 minutes.

The addition of Sn required the Pt catalysts to be calcined in air an additional time (100 ml min^{-1} Air, 3 K min^{-1} ramp rate, 623 K for 3 hours) in order to prevent leeching of the Pt into solution. The Sn precursor solution was made at a concentration of 300 µg/mL. Since the pH has a strong influence on the amount of metal adsorbed on the support, the desired wt% of Sn was leveraged by altering the pH of the precursor solution. The SEA procedure and post treatment steps for the Sn followed same as what was carried out when adsorbing the Pt metal.

5.2.3. Catalyst Characterization

Catalyst surface area and porosity were assessed with N_2 physisorption at 77K using a commercial instrument (Micromeritics ASAP 2020). Surface areas were determined using BET analysis; micro/mesoporosity were assessed using t-plot analysis; pore volumes were computed as the cumulative volume of N_2 condensed at a relative pressure $(P/P_0) = 0.995$; and average pore diameters were estimated from BJH analysis of the desorption branch of the isotherm. Prior to N2 dosing, samples were dried by evacuating to 500 µm Hg at 298K and then heated to 623 K (240 min hold, 10 K min^{-1} ramp).

We used CO, O_2 and H_2 (titrants) chemisorption to interrogate the metal sites available for reaction (Micromeritics ASAP 2020). Prior to titrant dosing, samples were dried by evacuating to 5 µm Hg at 298K and subsequently heating to 373 K (30 min hold, 10 K min^{-1} ramp). Samples were then exposed to flowing oxygen and the cell temperature was increased to 673K (10 K min^{-1}, 30 min hold). The cell was then evacuated to 5 µm Hg at 673K, held under vacuum for 15 minutes, cooled under vacuum to 373K, and then exposed to H_2 flow. The cell was then heated under continuous H2 flow to 673K (10K min^{-1}, 4 h hold). Finally, the cell was evacuated to 5 µm Hg at 673K to remove chemisorbed hydrogen (30 min) and cooled to 308K under vacuum. Each titrant uptake isotherm was then collected at 308K, the sample cell was evacuated to remove any physisorbed titrant, and a second titrant uptake isotherm was collected at 308K. Irreversible titrant uptake was calculated as the difference in the titrant uptakes between the two isotherms. Pt particle size was estimated assuming that Pt has a shape factor of 6, an atomic cross sectional area of 0.08 nm^2 and a density of 21.450 g cm^{-3}. The average diameter of the nanoparticle as well as the dispersion of the metal can be calculated using Equations 2.1-2.3.

The metal weight percents on the catalyst surface were quantified using Inductively Coupled Plasma Mass Spectrometry (Perkin Elmer Elan 6100). Samples first had to be digested in aqua regia before ICP-MS analysis The aqua regia solution consisted of a mixture of 7 mL hydrochloric acid and 3 mL nitric acid. Digestion was carried out in a round bottom flask kept in a mineral oil bath at 373K and stirred constantly, a reflux system kept at 288 K was incorporated to prevent the escape of any gases; digestions were allowed to occur for 12 hours. After digestion, the solution was diluted to 25 ml using DI water, then further diluted in 1% nitric acid for ICP-MS using a Perkin Elmer Elan 6100 instrument. The metal responses were compared to a curve made from calibrations using high purity commercial standards.

5.2.4. Catalyst Activity Testing

Gases were introduced to the system at controlled flowrates using digital mass flow controllers (Brooks). Reactors always operated under gas phase conditions, but many of our feeds were introduced to the system as liquids using a syringe pump (Cole Parmer). Specifically liquids were fed through a PEEK capillary (130 μm, IDEX) into a home-built, temperature-controlled vaporizer, where they were combined with pre-heated gas feeds. To increase surface area for gas-liquid contact, the vaporizer was packed with quartz granules (850-2000 □m, Aldrich). To ensure complete vaporization, partial pressures of condensable species were maintained below 15% of their vapor pressure at a given reaction condition. After leaving the vaporizer, the process stream flowed through a 6-port valve, which was used to direct flow either to the reactor or to the bypass. During startup, the reactor was bypassed until we observed steady state feed concentrations via Gas Chromatography. Once the reactor feed stream reached steady state, flow was diverted to the reactor.

The packed bed reactor operated in an upflow configuration. It was constructed from ½" stainless steel tubing (McMaster). The catalyst bed was placed between two quartz wool plugs in the center of the tube, and the void volume upstream of the reactor was packed with quartz granules. The reactor temperature was monitored at the external wall using a type-K thermocouple, and the external wall temperature was regulated using a PID controller (LOVE 16A 3010). A second type-K thermocouple was placed inline and used to monitor reactor temperature immediately downstream of the catalyst bed. Data reported in this manuscript reflect the inline temperature measurement. The reactor effluent was transferred, via heat-traced stainless steel tubing, to a pair of online gas-chromatographs (HP 5890) for quantitative resolution of the product mixture. The

first GC was equipped with dual inlets leading, respectively, to an HP-PONA column paired with a flame-ionization detector (FID) and a Restek ShinCarbon ST Micropacked column paired with a thermal conductivity detector (TCD). In general, propionic acid, propanal, propanol, propane, ethylene, and ethane were resolved and quantified using the PONA/FID system, while methane, CO, and CO_2 were resolved and quantified using the ShinCarbon/TCD system. The second GC was configured with a single inlet and a Restek ShinCarbon ST Micropacked column leading to a Methanizer/FID detector. This system was used for quantifying CO, CO_2, and methane concentrations that were below TCD detection limits.

Reactions were run over various catalysts, temperatures, reactant partial pressures, and contact times, and species production rates were quantified at 15-minute intervals. Unless otherwise noted, reported rates reflect steady state operation. Typically, after startup, reactors were allowed to reach steady state species production rates under a well-defined, "reference" condition. This typically took less than 1 hour. After reaching steady state, production rates for all species were quantified. Subsequently, a single perturbation in temperature, partial pressure, or contact time was introduced, and the system was allowed to evolve to a new steady state, where effluent flowrates of all species were again quantified. Metal catalysts employed for oxygenate processing are generally susceptible to various modes of deactivation, which can obscure kinetic trends. Accordingly, after quantifying the impact of each perturbation on species flowrates, the system was returned to the reference condition and allowed to reach steady state. This provided a rigorous benchmark for assessing catalyst deactivation. Under most of our operating conditions, deactivation was relatively mild. Differences in zero time production rates and steady state production rates measured at the reference condition throughout majority of the experiment showed less than 10% loss in activity; accordingly, steady state rates were not corrected for

deactivation. In experiments with pronounced deactivation, it is difficult to define meaningful reaction rates from steady state measurements as the available catalytic surface area is generally changing as a function of time on stream. In these systems, initial production rates were estimated by extrapolating the deactivation profile to zero-time-on-stream. During typical startup and between experiments (e.g., changing the feed molecule), the catalyst bed was reduced under flowing H_2 at 673K (10 K min^{-1}, 4h), which was sufficient to restore the initial activity of the catalyst after most experiments. Species production rates are reported here as site time yields. These are defined in equation 5.1:

$$STY_j = \frac{F_j}{N_{Pt}}$$
Equation 5.1

Where Fj is the total molar flowrate of species j in the reactor effluent and N_{Pt} is the total molar quantity of surface Pt atoms in the catalyst bed as estimated by CO chemisorption. Feed conversion was defined on a carbon basis and computed based on product flowrates (Equation 5.2)

$$X_i = \frac{\sum_{j \neq i} F_j \cdot C_{n,j}}{F_{i,0} \cdot C_{n,i}}$$
Equation 5.2

Where F_j is the molar flowrate of reaction products, j, in the reactor effluent, $F_{i,0}$ is the inlet flowrate of the reacting species, i, and C_n is the number of carbon atoms in a given molecule. Selectivity to a specific reaction product, k, is defined in terms of molar flowrates of all reaction products, j Equation 5.3:

$$S_k = \frac{F_k}{\sum_j F_j}$$
Equation 5.3

5.3 Results

5.3.1. Catalyst Characterizations

The weight percents of Pt and Sn in the synthesized bimetallic catalysts as well as the amount of Pt recovered can be seen in Table 5.1. Catalysts had a range of various Sn uptakes that was affected by the pH of the solution used in the SEA procedure. Majority of the Pt was recovered (>90% recovered) after bimetallic synthesis apart from the catalyst made at a pH of -0.05; in this instance, only 49% of original Pt adsorbed was recovered.

The results of the chemical adsorption experiments using CO, O_2 and H_2 can be seen in Table 5.2. In terms of the CO adsorption, all the site densities decreased from the base value upon Sn addition. Catalysts with Sn weight percent 0.09, 3.04, 1.46 and 1.24 caused the largest decrease (>20%) in adsorbed CO among the catalysts prepared. On average, the decrease in H_2 adsorbed was greater for each of the bimetallic catalysts prepared. Standout H_2 values that decreased occurred for catalysts with 0.09 and 3.04 Sn weight percent loadings, which showed a 60% and 80% drop respectively.

Chemical adsorption using O_2 showed different results from the other titrant gases. Majority of the bimetallic catalysts were either unchanged or showed increase in O_2 adsorbed. Bimetallic catalysts with 3.04 and 0.51 Sn weight percent loadings exhibited among the highest increases in O_2 adsorbed, they showed 60% and 25% respectively. The catalysts with 0.09 Sn weight percent loading stood out as the only catalyst with a clear decrease in the amount of O_2 adsorbed, a 45% decrease.

Table 5.1: Metal loadings of Pt/Al_2O_3 and $Pt-Sn/Al_2O_3$ catalysts. $Pt-Sn/Al_2O_3$ catalysts are named for the initial pH of synthesis solution and the percent of Pt recovered from the base catalyst is also provided.

Catalyst	Base Catalyst	Pt weight (%)	Sn weight (%)	Pt Recovered (%)
Pt/Al_2O_3 1	-	3.39		-
Pt/Al_2O_3 2	-	3.38		-
Pt/Al_2O_3 3	-	2.34		-
Pt/Al_2O_3 4	-	2.76		-
-0.05	Pt/Al_2O_3 1	1.67	0.09	49
1.02	Pt/Al_2O_3 4	2.49	3.04	90
2.05	Pt/Al_2O_3 2	3.36	1.46	100
3.00	Pt/Al_2O_3 4	3.04	1.24	110
4.00	Pt/Al_2O_3 4	2.73	0.12	99
5.14	Pt/Al_2O_3 3	2.47	0.03	106
6.02	Pt/Al_2O_3 3	2.30	0.43	99
6.93	Pt/Al_2O_3 4	2.55	0.39	93
8.33	Pt/Al_2O_3 4	2.65	0.16	96
12.00	Pt/Al_2O_3 3	2.37	0.51	102

Table 5.2: Chemical adsorptions of CO, H$_2$, and O$_2$ on Pt/Al$_2$O$_3$ base catalysts and Pt-Sn/Al$_2$O$_3$ bimetallic catalysts. Metal dispersion was calculated using CO adsorption data.

Catalyst	Base Catalyst	CO Adsorption (μmol/g$_{cat}$)	H$_2$ Adsorption (μmol/g$_{cat}$)	O$_2$ Adsorption (μmol/g$_{cat}$)	Metal Dispersion (%)
Pt/Al$_2$O$_3$ 1	-	149.8 ± 0.3	51.0 ± 0.2	70.6 ± 0.5	86.2
Pt/Al$_2$O$_3$ 2	-	128.4 ± 0.2	51.6 ± 0.2	75.7 ± 0.5	74.1
Pt/Al$_2$O$_3$ 3	-	96.0 ± 0.3	34.8 ± 0.2	55.1 ± 0.5	80.0
Pt/Al$_2$O$_3$ 4	-	107.4 ± 0.2	42.4 ± 0.3	59.3 ± 0.4	76.0
-0.05	Pt/Al$_2$O$_3$ 1	66.3 ± 0.2	20.4 ± 0.1	39.1 ± 0.2	77.4
1.02	Pt/Al$_2$O$_3$ 4	53.1 ± 0.4	8.0 ± 0.3	94.6 ± 0.7	41.6
2.05	Pt/Al$_2$O$_3$ 2	101.9 ± 0.3	44.5 ± 0.2	72.2 ± 0.6	59.2
3.00	Pt/Al$_2$O$_3$ 4	83.0 ± 0.4	29.0 ± 0.3	67.2 ± 0.4	53.3
4.00	Pt/Al$_2$O$_3$ 4	98.1 ± 0.4	36.6 ± 0.2	60.1 ± 0.5	70.1
5.14	Pt/Al$_2$O$_3$ 3	90.1 ± 0.2	35.1 ± 0.3	51.3 ± 0.4	71.2
6.02	Pt/Al$_2$O$_3$ 3	83.5 ± 0.4	29.1 ± 0.1	57.2 ± 0.5	70.8
6.93	Pt/Al$_2$O$_3$ 4	94.4 ± 0.7	33.0 ± 0.3	54.9 ± 0.5	72.2
8.33	Pt/Al$_2$O$_3$ 4	95.4 ± 0.3	36.7 ± 0.2	56.7 ± 0.5	70.2
12.00	Pt/Al$_2$O$_3$ 3	79.8 ± 0.2	27.5 ± 0.2	68.9 ± 0.5	65.7

5.3.2. Reactor Experiments

The effect of Sn on the selectivity of propionic acid HDO in the packed bed reactor was first observed as seen in Table 5.3. The ratio of Pt/Sn was used to identify the catalysts in Table 5.3

because some bimetallics had different weight loadings of Pt on the base catalyst used in their preparations; using a ratio allows for a normalization of the amount of Sn added on the catalyst with the amount of Pt that was originally adsorbed. It is also important to mention that each of the data presented comparing different catalysts were recorded at similar conversions (1.5-2.8 %). In terms of HDO products (Propanol and propanal), catalysts with the Pt/Sn ratios 2.30 and 0.82 had the selectivity towards HDO products, 60.45 and 99.4% respectively; these catalysts also had the lowest selectivity towards CO, CO_2, methane, ethane and propane. It is also fair to say that the remaining Pt/Sn ratio catalysts had similar selectivity values as the catalyst with no Sn.

Table 5.3: Comparisons in the selectivity of different catalysts during propionic acid HDO at propionic acid and hydrogen partial pressures of 5 and 755 torr respectively at 468K

$\dfrac{\text{wt\% Pt}}{\text{wt\% Sn}}$	Selectivity						
	CO	CO 2	Methane	Ethane	Propane	Propanal	Propanol
18.56	0.22	0	0	0.27	0.11	0.097	0.308
5.35	0.17	0.0068	0.020	0.25	0.17	0.052	0.332
4.65	0.18	0.0063	0.019	0.23	0.15	0.085	0.330
2.30	0.13	0	0.019	0.18	0.07	0.087	0.514
0.82	0.00	0	0	0.01	0	0.457	0.537
No Sn	0.16	0	0.04	0.23	0.22	0.05	0.30

The effect of the Sn weight loading on rates of HDO and DCN was then explored in Table 5.4. Since there is no established method for establishing site densities on PtSn bimetallic catalysts, rates were normalized using each of the titrant gases used in the chemical adsorption characterization experiments as well as the moles of Pt on the catalyst, which was found using the ICP-MS weight loadings and mass of catalyst used in the experiment. The rate of HDO when normalized by the moles of Pt remained unchanged for all weight loadings of Sn. For the other

HDO rates, all catalysts apart from the 3.04 wt% Sn had relatively the same values regardless of the site titrant used. The HDO rate of the 3.04 wt% Sn increased for the sites normalized by CO and H_2 adsorbed during chemical adsorption, while it decreased when normalized by O_2. The DCN rates were slightly more sensitive to Sn addition than HDO rates, the two highest weight loadings of Sn showed a decrease in DCN rates for all methods of normalization; the 3.04 wt% Sn (highest) had the lowest rate of DCN of all the catalysts.

Table 5.4: Comparisons in the site time yield rates of HDO and DCN for different catalysts during propionic acid HDO normalized by moles of Pt as well as different titrant gases. This was carried out at propionic acid and hydrogen partial pressures of 5 and 755 torr respectively at 468K

wt% Sn	Rate of HDO (ks^{-1})				Rate of DCN (ks^{-1})			
	Moles of Pt	CO	H_2	O_2	Moles of Pt	CO	H_2	O_2
0	1.08	1.43	1.83	1.30	0.51	0.68	0.87	0.62
0.09	0.92	1.19	1.97	1.01	0.47	0.61	1.01	0.52
0.43	0.91	1.28	1.85	0.94	0.45	0.64	0.92	0.47
0.51	1.04	1.57	2.25	0.91	0.48	0.73	1.04	0.42
1.46	0.85	1.45	1.62	1.01	0.24	0.42	0.47	0.29
3.04	1.10	2.65	8.78	0.74	0.01	0.02	0.05	0.00

After observing the trends associated with different quantities of Sn on a catalyst surface, it was then time to start comparing the bimetallic PtSn catalysts with monometallic Pt catalysts. The 3.04 wt% Sn was chosen as the bimetallic catalysts for further investigation since it showed the most promising results in terms of HDO selectivity and rates. The first distinction can be seen in Figure 5.1, which shows how the selectivity towards HDO products increases with time for PtSn as opposed to Pt, where there was a slow deactivation with time. The masses of catalysts used in Figure 5.1 were similar to avoid misinterpreting transient behavior.
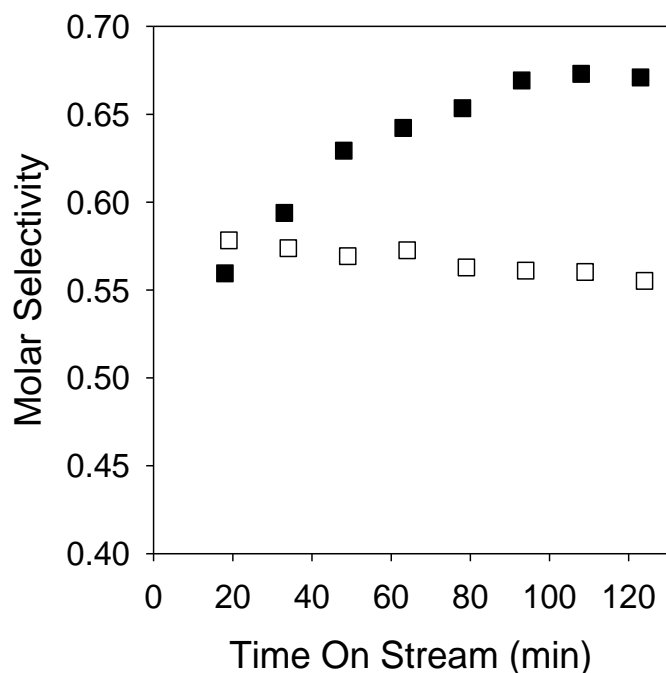
Figure 5.1: Time on stream trends for HDO selectivity for Pt (□) and PtSn (■) at propionic acid and hydrogen partial pressures of 5 and 755 torr respectively at 468K over Pt.

The rates of HDO over Pt and PtSn catalysts were compared in Table 5.5, using various normalization methods. For PtSn, the rates were approximately the same –with some scatter- for all conversions regardless when normalized by moles of Pt, as well as CO and H_2 adsorbed. The PtSn rates showed a decreasing trend in rates normalized by O_2 adsorbed with increasing conversion. The HDO rates over Pt showed a general decreasing trend at higher conversions for all normalized values. The PtSn rates were higher than those for Pt when normalized by moles of Pt, CO_2 adsorbed and H_2 adsorbed, but the rates normalized by O_2 adsorbed seemed to be quite similar between both catalysts- especially at conversions below 10%.

Table 5.5: Comparisons in the site time yield rates of HDO at different conversions over Pt and PtSn catalysts during propionic acid HDO normalized by moles of Pt as well as different titrant gases. This was carried out at propionic acid and hydrogen partial pressures of 5 and 755 torr respectively at 468K

Fractional Conversion	PtSn HDO (ks^{-1})				Pt HDO (ks^{-1})			
	Moles of Pt	CO	H2	O2	Moles of Pt	CO	H2	O2
0.03	1.23	2.96	9.80	0.83	0.61	1.30	1.66	1.18
0.03	1.27	3.07	10.16	0.86	0.43	0.91	1.16	0.83
0.04	1.13	2.71	8.98	0.76	0.45	0.95	1.21	0.86
0.05	1.05	2.52	8.35	0.70	0.38	0.80	1.02	0.73
0.09	0.91	2.20	7.29	0.61	0.47	0.97	1.24	0.88
0.18	1.64	3.95	13.08	1.10	0.24	0.50	0.64	0.46
0.21	0.97	2.35	7.77	0.65	0.20	0.43	0.54	0.39

The effect of conversion on molar selectivity during propionic acid HDO over Pt and PtSn can be observed in Figures 5.2 and 5.3 respectively. The products formed during propionic acid HDO over Pt (Figure 5.2) are carbon monoxide, methane, ethane, propanol and propanal. Carbon dioxide was observed in very small quantites (<2%) The molar selectivities are not constant for all species over the conversion range tested. Towards zero conversion, carbon monoxide, ethane, propane, propanol and propanol appear to be intercepting the y-axis within similar non-zero selectivity ranges (15-30 %), but methane shows a clear extrapolation to a zero y intercept towards zero conversion. Molar selectivities are much more distinct towards higher conversions; propanol has the highest selectivity followed by ethane, propane, carbon monoxide, methane and propanal in decreasing order.

During Propionic acid HDO over PtSn (Figure 5.3), there were less major product formations: propanol, propanal and propyl propanoate. There were trace amounts of carbon monoxide, carbon dioxide, ethane and propane formed (<1%), while no methane was observed. Towards

zero conversion, there was almost an equimolar amount of propanol and propanal formed, while there was no observable propyl propanoate in the low conversion range (<10%). At the higher conversions, propanol was the most selective product- maintaining above 80% selectivity for conversions above 15%. At the highest conversion tested over PtSn, propyl propanoate was slightly more selective than propanal.

The trends in molar selectivity over Pt and PtSn catalysts across the conversions tested can be deeper highlighted. For both Pt and PtSn, propanol and propanal selectivity follow the same trends; propanol increases sharply in the low conversion range then stabilizes, while propanal decreases just as quickly over low conversions then becomes steady. The propane and ethane formed over Pt seems to be stable over the conversion range tested. Carbon monoxide formation over Pt shows to be initially in equimolar amounts with ethane at low conversions, however its selectivity then steadily decreases with higher conversions. Propionic acid HDO over Pt also shows a steady increase in the selectivity towards methane as the conversion is increased; it is worth mentioning that this steady increase may push methane to surpass other products' molar selectivities. The propyl propanoate formed over PtSn catalysts steadily increases with conversion.
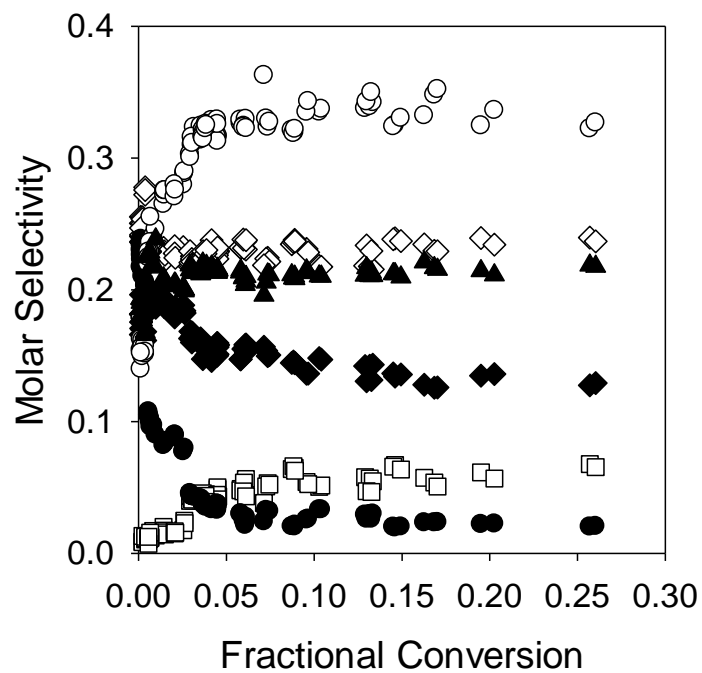
Figure 5.2: Effect of fractional conversion on the molar selectivities of methane (□), propanol (○), carbon monoxide (♦), ethane (◊), propane (▲) and propanal (●) at propionic acid and hydrogen partial pressures of 5 and 755 torr respectively at 468K over Pt.
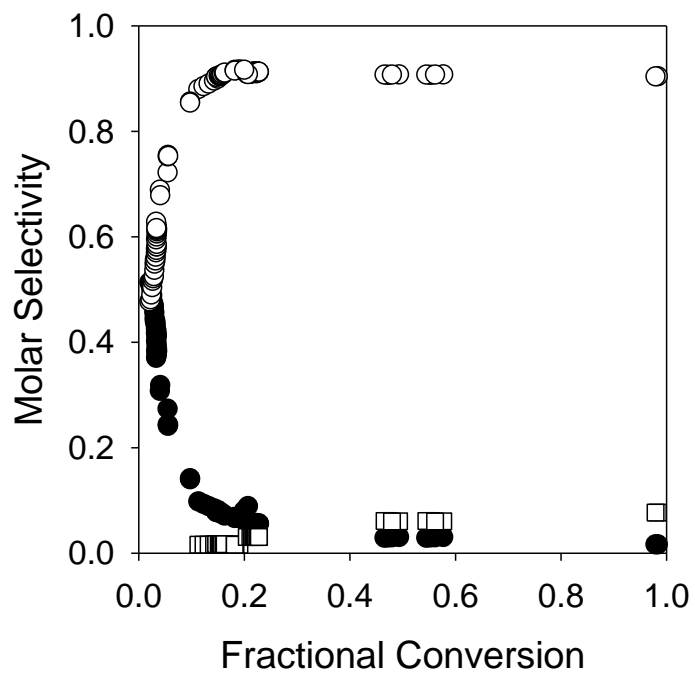
Figure 5.3: Effect of fractional conversion on the molar selectivities of propanol (○), propanal (●) and propyl propanoate (□) at propionic acid and hydrogen partial pressures of 5 and 755 torr respectively at 468K over PtSn.

Since Table 5.5 showed a decrease in HDO rates at higher conversions, the rate of conversion across the conversion ranges tested Pt and PtSn were procured in Figures 5.4 and 5.5 respectively, this allowed for another benchmark of comparison between the catalysts. The rate of conversion over Pt decreased over the conversion range- over 80% loss in activity. PtSn appeared to have an initial decrease at low conversions, but reached a steady rate of conversion at a far higher value than that over Pt. Assuming the PtSn rate of conversion initially decreased (as opposed to coincidental trend in scatter), it can be observed that Pt and PtSn can extrapolate to the similar rate of conversions towards the zero conversion limit.
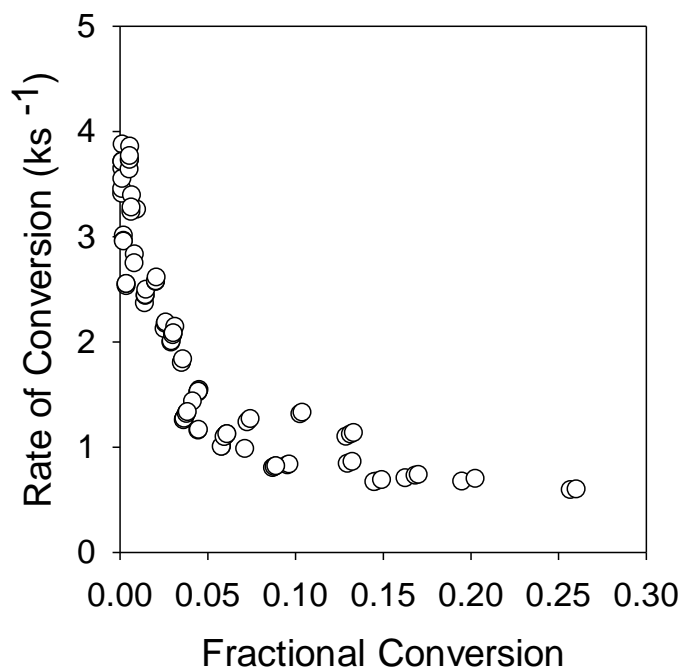
Figure 5.4: The rate of conversion of propionic acid HDO at different fractional conversions over Pt at propionic acid and hydrogen partial pressure of 5 and 755 torr respectively at 468K.
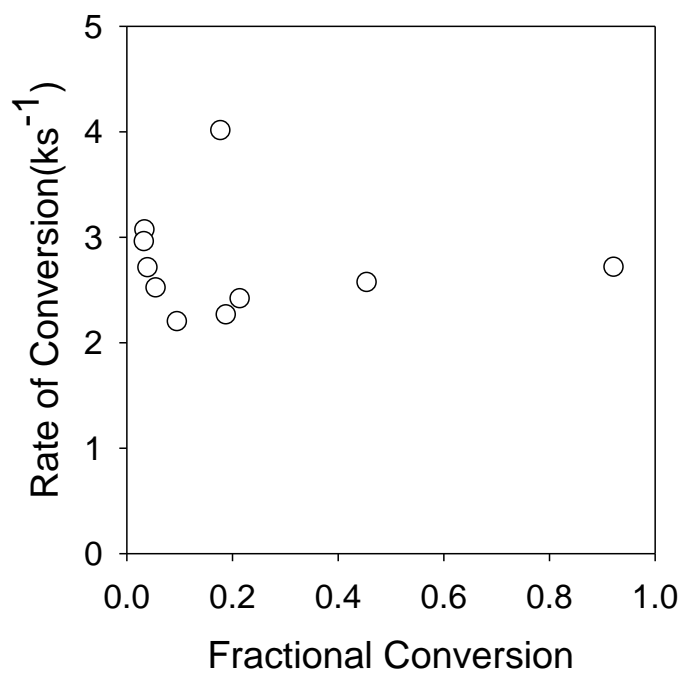
Figure 5.5: The rate of conversion of propionic acid HDO at different fractional conversions over PtSn at propionic acid and hydrogen partial pressure of 5 and 755 torr respectively at 468K.

The fractional conversion across a range of contact times over Pt and PtSn catalysts can be seen in Figure 5.6. The fractional conversions of both catalysts appear to be similar at short contact times, but fractional conversion over PtSn becomes increasingly higher at longer contact times. The fractional conversion appears to be in a linear relationship with contact time for PtSn, while the slope changes across contact times over Pt.
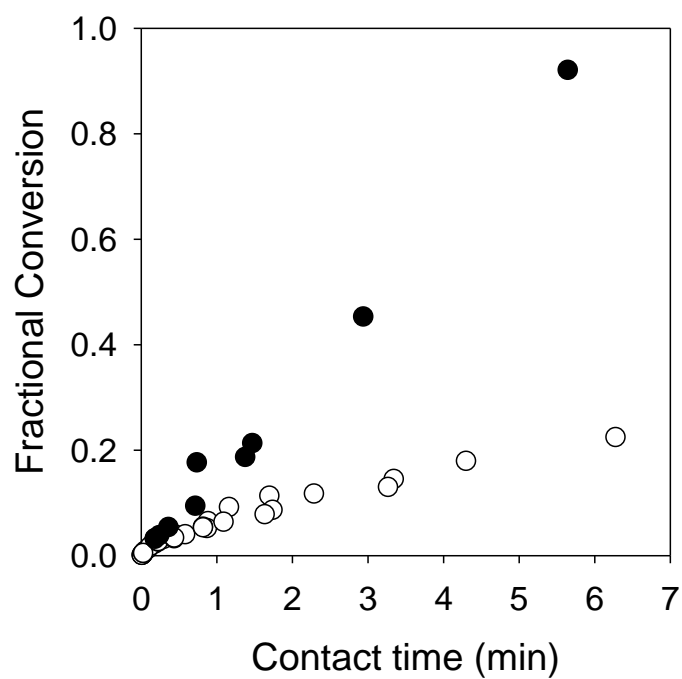
Figure 5.6: The fractional conversion of propionic acid HDO at various contact times over Pt (○) and PtSn (●) at propionic acid and hydrogen partial pressure of 5 and 755 torr respectively at 468K.

The amount of carbon monoxide produced at different fractional conversions during propionic acid HDO over Pt is shown in Figure 5.7. The ppm of carbon monoxide appears to linearly increase with fractional conversion.
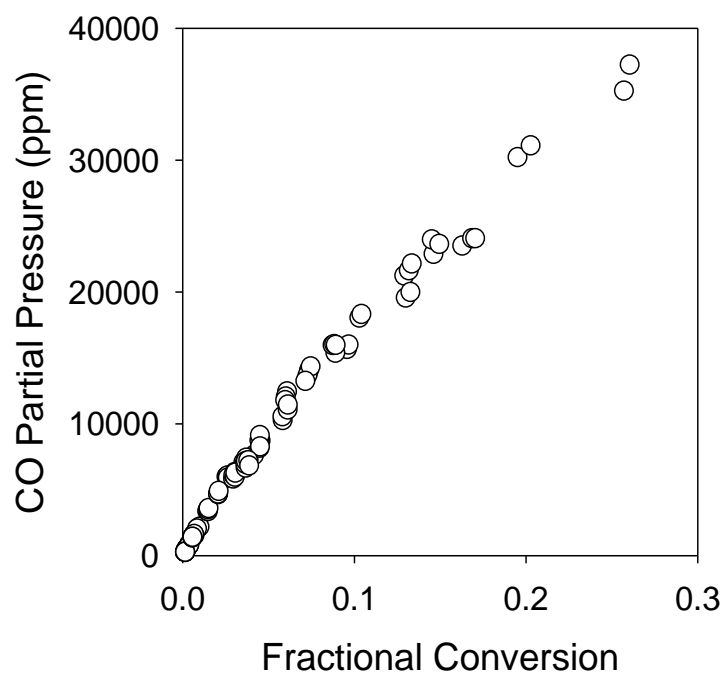
Figure 5.7: Partial pressures of Carbon monoxide produced with increasing conversion over Pt at propionic acid and hydrogen partial pressure of 5 and 755 torr respectively at 468K.

Carbon monoxide was cofed into the reactor during propionic acid HDO over PtSn; CO partial pressures range from 0 to 4 torr. The effect of carbon monoxide on the rate of HDO is shown in Figure 5.8. The HDO rates were unchanged when different partial pressures of carbon monoxide were introduced to the catalyst bed during reactions. The values of the HDO rates in Figure 5.8 is approximately the same as the "steady" rate of conversion in Figure 5.5
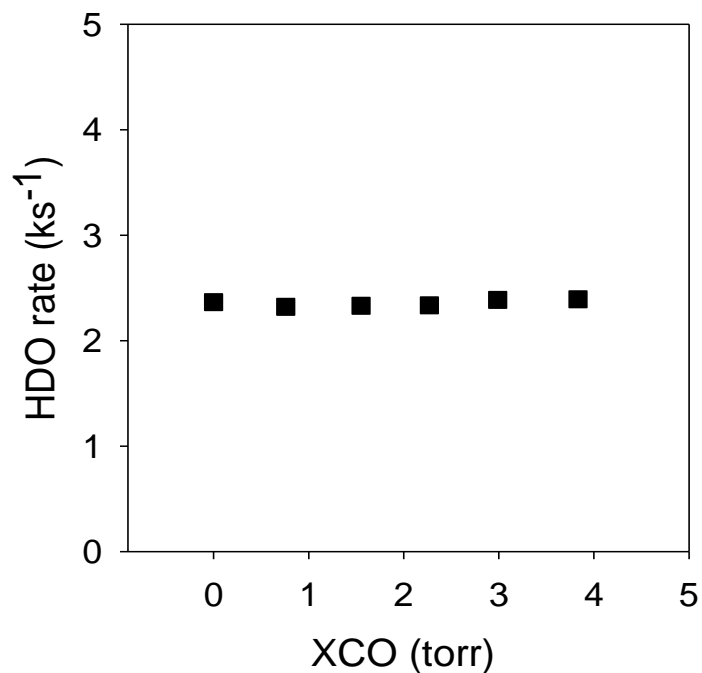
Figure 5.8: The effect of cofed carbon monoxide partial pressures on propionic acid HDO rates over PtSn. The propionic acid and hydrogen partial pressures are 5 and 375 torr respectively with a balance helium at 1atm and 468K.

The effect of temperature on the molar selectivities as well as rates were observed in Figures 5.9 and 5.10. It can be seen in Figure 5.9 that the selectivity towards propanal (at given contact time) becomes more favorable at higher temperatures, and selectivity towards carbon monoxide and ethane also increases. The apparent barrier for propionic acid HDO over PtSn as illustrated in Figure 5.10 is 52 ± 2 kJ mol^{-1} within the range of 469–569 K.
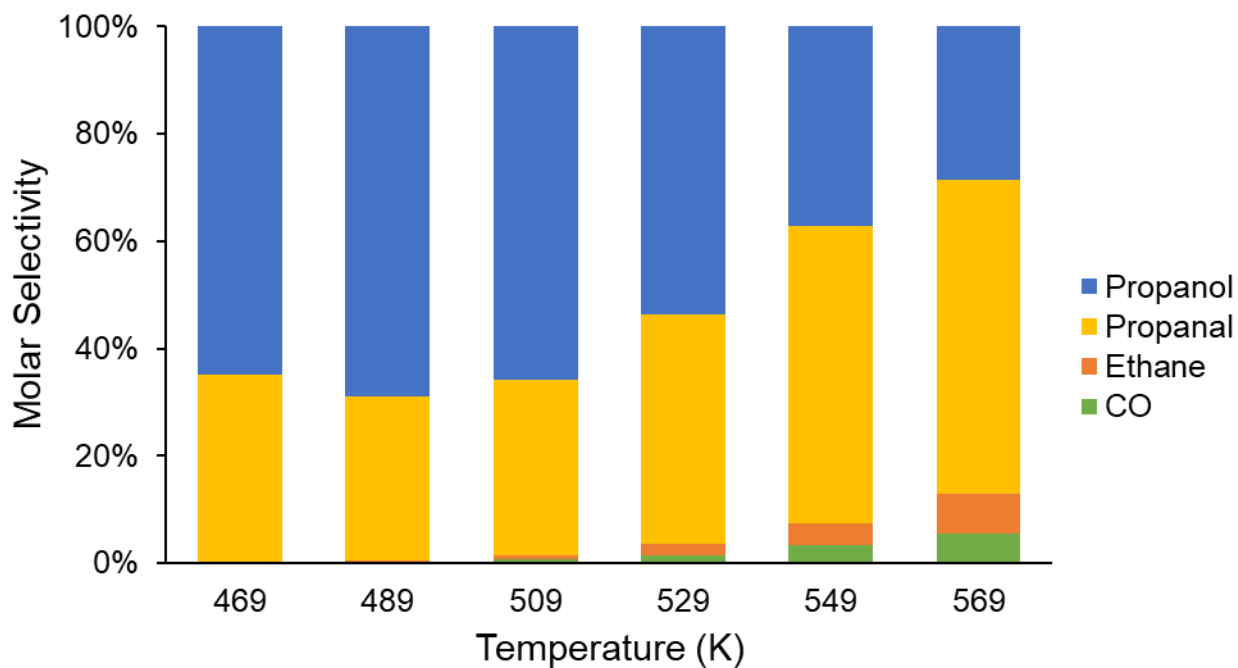
Figure 5.9: Effect of temperature on molar selectivity during propionic acid HDO from 459-469K at a propionic acid and hydrogen partial pressures of 5 and 755 torr respectively over PtSn.
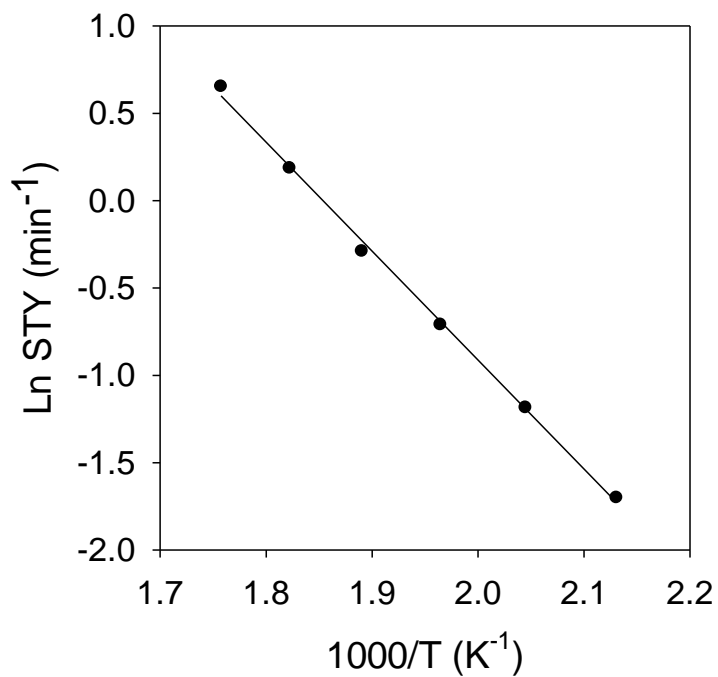
Figure 5.10: Arrhenius plot for propionic acid HDO from 459-469K at a propionic acid and hydrogen partial pressures of 5 and 755 torr respectively over PtSn.

The partial pressure dependence on HDO rates for propionic acid and hydrogen are illustrated in Figure 5.11. HDO rates (Defined as a site time yield, STY) showed a slightly positive 0.15 order dependence on propionic acid pressure and an apparent 0.39 order dependence on hydrogen.
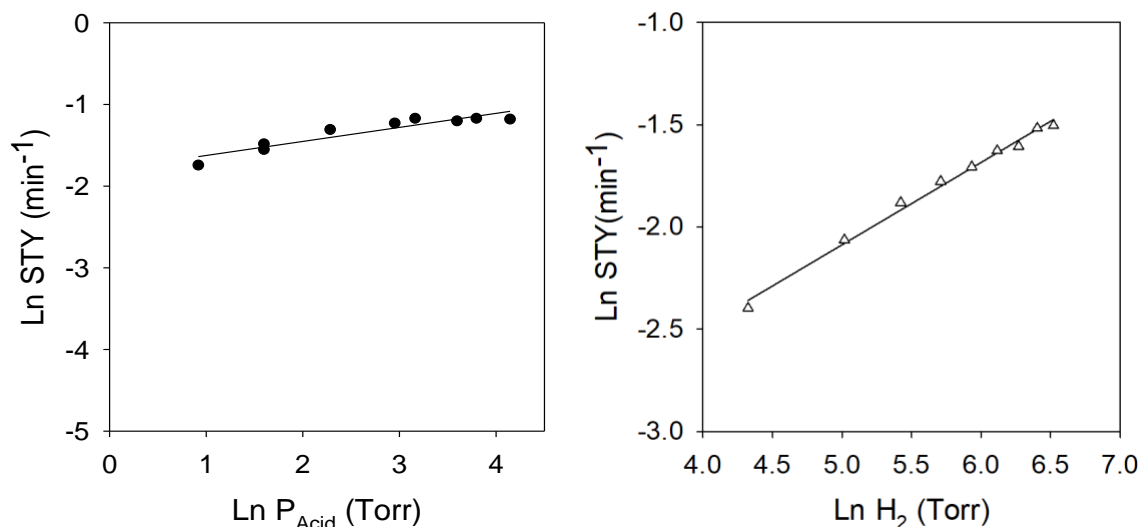
Figure 5.11: Effect of propionic acid (left) and hydrogen (right) partial pressures on the rates of HDO at 468K over PtSn. Propionic acid partial pressures were varied from 2–68 torr and hydrogen partial pressures were kept were varied from 75-755 torr.

The stability and regeneration characteristic of PtSn catalysts were explored by observing the molar flow rates of the main pathways, DCN and HDO over a series of experiments on the same catalyst bed. This consisted of three runs of a similar condition: the first is using the fresh catalyst bed; after the first run, the catalyst is reduced under H_2 flow at 673 K for four hours before beginning the second run; after the second run, the catalyst is calcined in air at 273 K for 3 hours and then reduced under H_2 flow at 673 K for four hours before beginning the third run. The second and third runs can be thought of as various regeneration procedures for Pt catalysts. The results of these experiments are illustrated in Figures 5.12 and 5.13. The HDO molar flowrate of the fresh catalyst took around 20 hours to reach a steady state value; the other runs reached a steady state in by 30 mins. The HDO steady state values for all three runs were fairly close, 0.6-0.7 μmol min⁻¹.

The DCN molar flow rates for the fresh catalyst took the same time to reach steady state as the HDO molar flow rates, except DCN flow rates decreased to a steady state value while HDO increased to its steady state value. After reduction as well as calcination and reduction, the DCN molar flow rates immediately took to the steady state values of the fresh catalyst instead of starting around its initial rate.
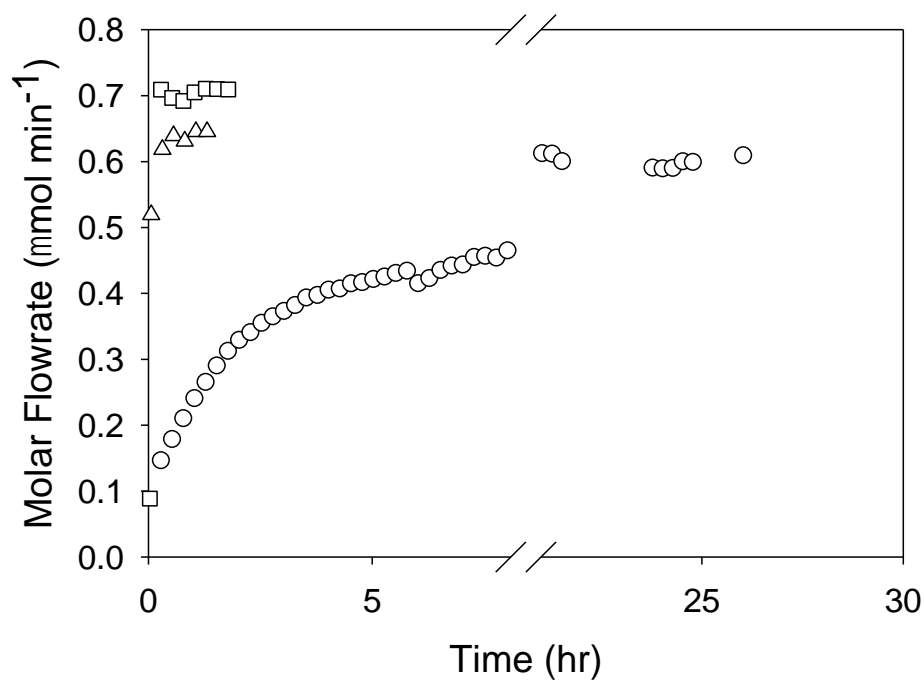
Figure 5.12: Time on stream data for HDO molar flow rates during propionic acid HDO over PtSn at propionic acid and hydrogen partial pressure of 5 and 755 torr respectively at 458K. The runs include fresh catalyst (○), after reduction (△), and after calcination & reduction (□).
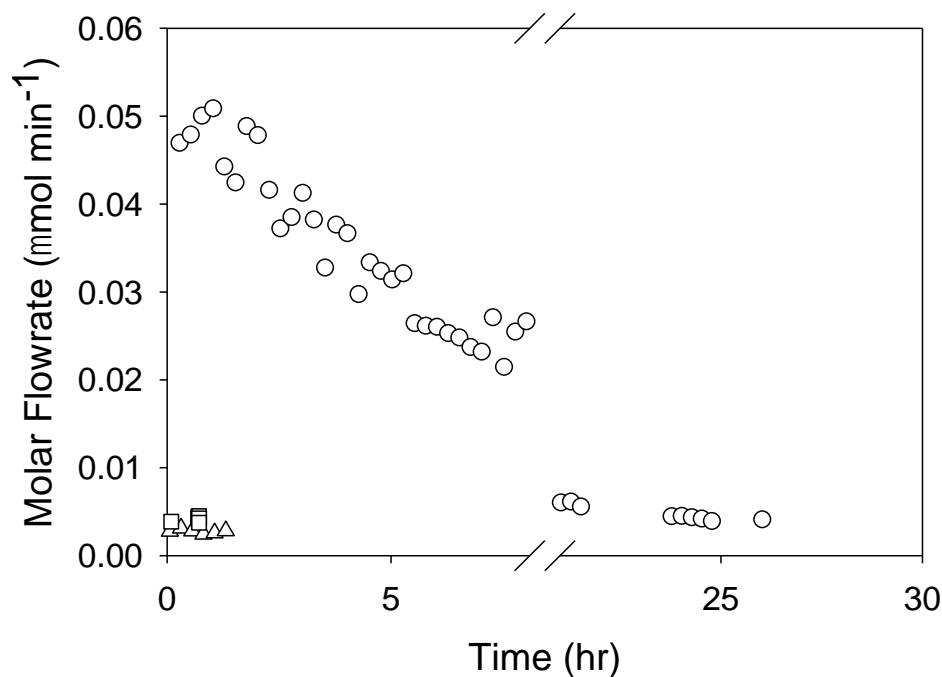
Figure 5.13: Time on stream data for DCN molar flow rates during propionic acid HDO over PtSn at propionic acid and hydrogen partial pressure of 5 and 755 torr respectively at 458K. The runs include fresh catalyst (○), after reduction (△), and after calcination & reduction (□).

5.4   Discussion

5.4.1.   Comparing Monometallic and Bimetallic Catalysts

The results show clear differences in how the addition of the "oxophilic promoter", Sn, changes the catalytic activity alumina supported Pt catalysts. We first identify the main challenges in using monometallic Pt as a catalyst for propionic acid HDO. There are selectivity issues with Pt catalysts, it is difficult to target a specific product over these monometallic catalysts because of the diverse product landscape as seen in Figure 5.2. In addition to the HDO products, propanol and propanal, we also see ethane, carbon monoxide, propane and methane. The pathways involved during propionic acid HDO was discussed in Chapter 3; the major unwanted pathways occurring over Pt/Al$_2$O$_3$ include decarbonylation, hydrogenolysis and methanation. Figure 5.2 can be reworked to better represent the current monometallic Pt catalyst, this is illustrated in Figure 5.14.
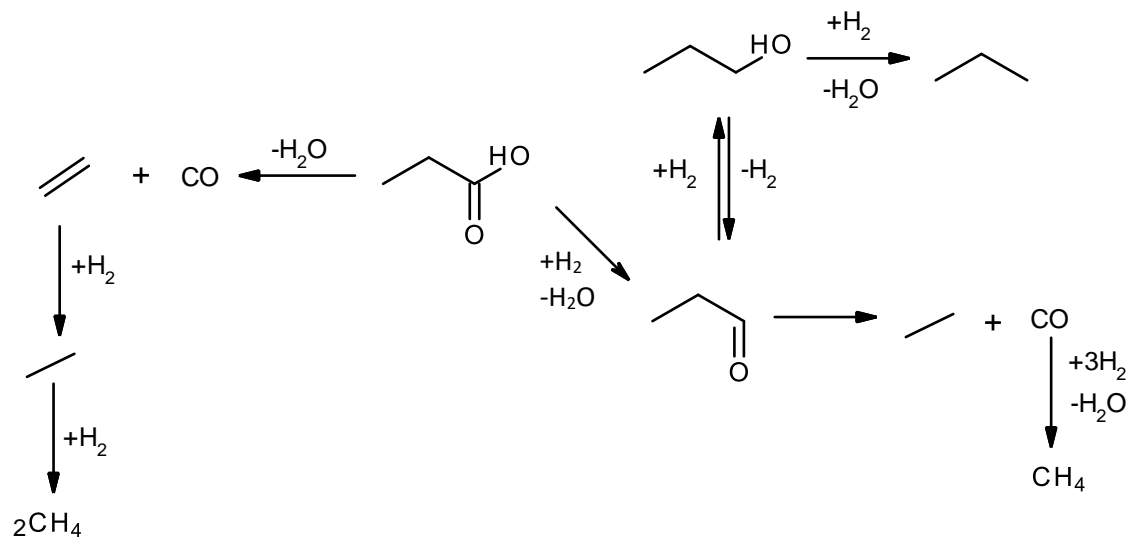
Figure 5.14: Reaction schematic over Pt.

Another problem identified is shown in Figure 5.4, which is the rate of conversion decreasing towards higher fractional conversions. The drop in rate of conversion is attributed to carbon monoxide poisoning of the active Pt sites, Figure 5.7 corroborates this as it shows the partial pressure of carbon monoxide on the surface increasing with fractional conversion. Carbon monoxide poisoning not only reduces the rate of conversion as conversion increases, it also reduces the rate as a function of time; deactivation is observed over time over time on stream as well (Figure 5.1).

Incorporating Sn onto Pt catalysts, we observed how each of the highlighted issues were mitigated and also gained insight onto possible hypothesis for the reason behind this change. We first compare the catalyst stability; similar mass of catalysts ere used in Figure 5.1, and we were able to observe how the selectivity towards HDO products increases with time over bimetallic catalysts unlike the deactivating properties of the monometallic properties that actually saw a decrease in selectivity. After the initial observation in Figure 5.1, this increase in selectivity with time on

161

stream was explored further for PtSn catalysts. Figures 5.12 and 5.13 shows how the selectivity towards the major pathways were affected by time on stream, not only does this corroborate the observations in Fig 5.1, but it also allows for the creation of a hypothesis. The time on stream data for HDO and DCN points out possible movement on the catalyst surface. The fresh catalyst took around 20 hours to reach steady (increase to) HDO and (decrease to) DCN flow rates. The flow rates were observed instead of selectivity because if one pathway had a constant flow rate, while the other increased, then a figure of the selectivities would not highlight the fact that the DCN flow rate is in fact decreasing. A decreasing flow rate is typically a sign of deactivation, which can be rectified by regenerating the catalysts; however, as seen in Figure 5.13, after different regeneration procedures, the DCN molar flowrates never achieved its "original initial flow rate." The same can be said about the HDO flow rates in Figure 5.12; after regenerations, the molar flow rates quickly attained the steady molar flow rate of the fresh catalyst in less than an hour, instead of undergoing the 20 hour transient-like phenomena. These time on stream observations is most likely because of catalyst restructuring, the Sn and/or Pt sites were initially mobile until it found its most comfortable position or orientation; confirmation of this hypothesis would be dependent on microscopy imaging of catalysts before and after reactions.

The bimetallic catalysts had a drastic effect on the product landscape during propionic acid HDO; this can be clearly seen by comparing Figures 5.2 and 5.3. The major products observed when employing PtSn catalysts include propanol, propanal and propyl propanoate; this shift in selectivity towards oxygenate products is well supported in the literature[19,23-27]. The partial pressures of propanol on the surface are high enough for esterification to take place with unreacted propionic acid reactant. The new selectivity landscape can allow Figure 5.14 to be updated for a schematic specifically for the PtSn catalyst; this is represented by Figure 5.15:
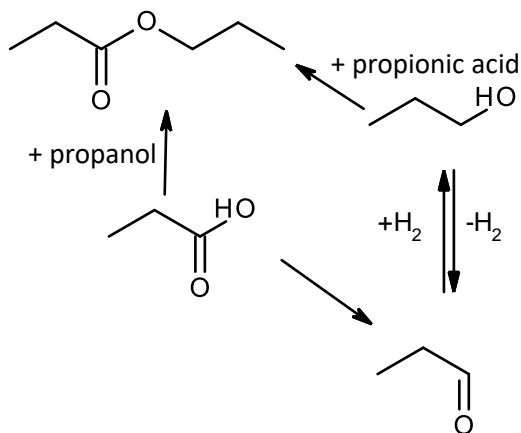
Figure 5.15: Reaction schematic over PtSn.

While the molar selectivity figure for PtSn is using the bimetallic catalyst with the most favorable attributes, Table 5.3 actually shows a the gradual catalytic improvement upon decreasing the ratio of Pt/Sn; it is observed how more Sn relative to Pt, decreases selectivity to DCN and hydrogenolysis products while increasing the selectivity to HDO products. The temperature and pressure effects provided information on how the operating conditions can be used to manipulate the selectivity among the HDO; while propanol showed to have the highest selectivity in Figure 5.3, propanal selectivity can be increased by increasing the temperature or reducing the partial pressure of hydrogen.

Addition of Sn also affected the catalytic stability in terms of the rate of conversion at higher fractional conversions. It was originally seen that the rate of conversion over monometallic catalysts decreased at higher conversions, bimetallic catalysts showed a fairly consistent rate of conversion at conversions more than double than those tested using the monometallic catalysts. The bimetallic catalyst did exhibit a slight initial decrease, while it is likely an initial poisoning of the few Pt sites not interacting with Sn, there is no way to prove that hypothesis in this current study and would need further investigation. The stable rate of conversion over bimetallic catalysts

had a direct effect on the fractional conversion at different contact times (Figure 5.6), as it allowed the fractional conversion to increase linearly with contact time, unlike the monomotellic catalysts where the constantly changing (decreasing) rate of conversion caused a non-linear relationship between its fractional conversion and contact time. An important insight into rate of conversion is that the initial rate of conversion for both catalysts extrapolate to the same value (approximately 4 ks_{-1}), this is important because it shows that the addition of Sn does not affect the overall rate of conversion. In terms of quantifying rates in order to compare Pt and PtSn catalysts, the method of normalizing sites showed to be very important; using moles of Pt, carbon monoxide and hydrogen showed clear differences in the rate of HDO between the two catalysts. The HDO rates over bimetallic catalysts were higher than that of the monometallic catalysts at each fractional conversion; this is an interesting observation because combining with another made previously, Sn appears to only affect the rate the HDO reaction but not the overall rate of conversion. Using oxygen as a titrant to normalize sites showed no effect of adding Sn to Pt catalysts as the normalized HDO rates were around the same for the fractional conversions tested; this will be further investigated in the following section on chemisorption properties.

5.4.2. Investigating Bimetallic Chemisorption Properties

After establishing that PtSn catalysts are intrinsically better than Pt catalysts for HDO chemistry, a hypothesis had to be made on the reason for this favorable outcome; this is done by incorporating observations from the other results. The central standout observation using the bimetallic catalysts is the absence of the DCN pathway, this chemistry introduced carbon monoxide into the product stream which led to the catalysts being poisoned. While without DCN, the catalyst cannot be poisoned, it had to be investigated on whether poisoning was even a possibility; this was proven in Figure 5.8. The bimetallic catalysts showed no sign of poisoning when carbon monoxide partial

pressures were cofed to the system during propionic acid HDO, this resistance to poisoning is likely as a result of chemical adsorption capabilities (or lack of) between Sn and carbon monoxide. The chemical adsorption data from the catalyst characterization experiments corroborates this hypothesis. Tables 5.1 and 5.2 was summarized to highlight the important observations, this is illustrated in Table 5.6. The ratio of Pt/Sn was used as a way to observe how the Sn can affect the changes in chemical adsorption of the different titrant gases; the difference was calculated from the titrant adsorbed after Sn minus the adsorption sans Sn. The ratio of 18.6 can be disregarded because only 49% of the original Pt on the support was recovered, this means that all the adsorption values are inaccurate for this catalysts. Low Pt/Sn ratios show the largest drop in carbon monoxide adsorbed, this is a clear trend that follows along the other bimetallic ratios- apart from the disregarded catalyst; this observation is well reported[19,24]. This reduction in carbon monoxide adsorbed is a direct reflection on the bimetallic catalyst's ability to be resistant to poisoning; carbon monoxide does not bind to catalysts because of the abundance of Sn sites in relative to Pt sites. Hydrogen follows a similar trend to carbon monoxide, although its values are not as pronounced, apart from the distinct difference at the 0.8 Pt/Sn ratio, this was observed by other studies[19,23,28]. While the chemical adsorption data supports the hypothesis for PtSn catalysts being resistance to carbon monoxide poisoning, it also paves way for an addendum to that hypothesis. The oxygen titrant showed the opposite trend to hydrogen and carbon monoxide; more oxygen was adsorbed at low Pt/Sn ratios, indicating the oxophilic properties of Sn. We propose that the reason carbon monoxide adsorption decrease is because the presence of Sn prevents the molecule from binding onto the catalyst surface; this means that there is no irreversible uptake of carbon monoxide by the catalysts, which is why less was adsorbed. It is likely that while both carbon and oxygen atoms on a molecule can bind to Pt, only oxygen can bind to Sn; this prevents the C-C cleavage of

propionic acid which directly results in DCN products. When the ratio of Pt/Sn is high, this means that there are enough Pt sites within proximity to each other to facilitate C-C cleavage. This hypothesis is supported by other reports in the literature[19,29,30]. Oxygen's ability to bind to both metals can also explain why it appeared as if the HDO rates in Table 5.5 were unaffected by the addition of Sn.

Table 5.6: Summary of Sn effects on Chemical Adsorption Properties

Pt/Sn ratio	Δ CO Adsorbed	Δ H_2 Adsorbed	Δ O_2 Adsorbed	Pt Recovered (%)
0.8	-54.3	-34.4	35.3	90
2.3	-26.5	-7.1	-3.5	100
2.5	-13	-5.8	12.1	110
4.6	-16.2	-7.3	13.8	102
5.3	-12.5	-5.7	2.1	99
6.5	-13	-9.4	-4.4	93
16.6	-12	-5.7	-2.6	96
18.6	-83.5	-30.6	-31.5	49
22.8	-9.3	-5.8	0.8	99
82.3	-5.9	0.3	-3.8	106

5.5 Conclusion

Bimetallic catalysts display high potential in being used as feasible methods of increasing noble metal selectivity towards oxygenated products during hydrodeoxygenation reactions. Addition of an oxophilic promoter , Sn, has the ability to improve the selectivity as well as stability of Pt

catalysts. Bimetallic catalysts kept its stability and selectivity up to near 100% conversions, indicating how ready it can be made for upgrading biomass derivatives to value added chemicals. The most fundamental reason for the large change in catalytic performance is the ability of Sn to prevent C-C cleavage of molecules; a prevention of this cleavage reduces the amount of carbon monoxide on the catalyst surface, which has been identified as the poison that causes a reduction in reaction rates. Additional characterization techniques can be used to further support the hypothesis made in this study such as microscopy and spectroscopy. The PtSn catalysts did show evidence of restructuring which should be probed further using transmission electron microscopy of catalysts before and after reactor performance; microscopy also be used in order to observe the proximity of Sn to Pt atoms at different metal ratios. Spectroscopy can also be employed in order to observe bonding orientations of the different types of species on the catalyst surface, this will provide insight on the species' relationship between Pt and Sn atoms on the alumina support.

5.6 References

1   Carmona, M., Feria, J., Golpe, A. & Iglesias, J. Energy consumption in the US reconsidered. Evidence across sources and economic sectors. *Renewable and Sustainable Energy Reviews 77*, 1055-1068 (2017).

2   Curley, R. in *Encyclopedia Britannica*   (2019).

3   LoVoi, A. *Diesel vs. biodiesel vs. vegetable oil*, 2014).

4   Srifa, A., Faungnawakij, K., Itthibenchapong, V. & Assabumrungrat, S. Roles of monometallic catalysts in hydrodeoxygenation of palm oil to green diesel. *Chemical Engineering Journal 278*, 249-258 (2015).

5   Wu, L., Moteki, T., Gokhale, A. A., Flaherty, D. W. & Toste, F. D. Production of Fuels and Chemicals from Biomass: Condensation Reactions and Beyond. *Chem* **1**, 32-58 (2016).

6   Werpy, T. & Petersen, G. Top Value Added Chemicals from Biomass. (204).

7   Gurbuz, E., Bond, J. Q., Dumesic, J. A. & Román-Leshkov, Y. in *The Role of Catalysis for the Sustainable Production of Bio-fuels and Biochemicals*   261-288 (Elsevier, 2013).

8   Alonso, D. M., Wettstein, S. G. & Dumesic, J. A. Bimetallic catalysts for upgrading of biomass to fuels and chemicals. *Chemical Society Reviews* (2012).

9   Harris, N. & Tuck, M. W. Butanediol via maleic anhydride. *Hydrocarbon Processing* **69** (1990).

10   Chen, L. *et al.* Aqueous-phase hydrodeoxygenation of carboxylic acids to alcohols or alkanes over supported Ru catalysts. *Journal of Molecular Catalysis A: Chemical 351*, 217-227 (2011).

11   Wang, S., Guo, Z., Cai, Q. & Guo, L. Vol. 45   138-143 (Biomass and Bioenergy 2012).

12   Pritchard, J., Filonenko, G. A., Van Putten, R., Hensen, E. J. M. & Pidko, E. A. Heterogeneous and homogeneous catalysis for the hydrogenation of carboxylic acid derivatives: history, advances and future directions   *Chemical Society Reviews* **44**, 3808 (2015).

13   Primo, A., Concepción, P. & Corma, A. Synergy between the metal nanoparticles and the support for the hydrogenation of functionalized carboxylic acids to diols on Ru/TiO2. *Chemical Communications 47*, 3613-3615 (2011).

14   He, D.-H., Wakasa, N. & Fuchikami, T. Hydrogenation of Carboxylic Acids Using Bimetallic Catalysts Consisting of Group 8 to 10, and Group 6 or 7 Metals   *Tetrahedron Letters* **36**, 1059-1062 (1995).

15   He, Z. & Wang, X. Required catalytic properties for alkane production from carboxylic acids: Hydrodeoxygenation of acetic acid. *Journal of Energy Chemistry 22*, 883-894 (2013).

16   Contreras-Mora, J. *et al.* Characterization and Evaluation of Carbon-Supported Noble Metals for the Hydrodeoxygenation of Acetic Acid. *Organic Process Research & Development 22*, 1628-1635 (2018).

17   Lugo-José, Y. K., Monnier, J. R. & Williams, T. C. Gas-Phase, catalytic hydrodeoxygenation of propanoic acid, over supported group VIII noble metals: Metal and support effects. *Applied Catalysis A: General 469*, 410-418 (2014).

18   Behtash, S. *et al.* Solvation Effects in the Hydrodeoxygenation of Propanoic Acid over a Model Pd(211) Catalyst. *The Journal of Physical Chemistry* **120**, 2724-2736 (2016).

19   Vardon, D. R. *et al.* Ru/Sn/Ac for the squeous phase reduction of succinic acid to 1,4-butanediol under continuous process conditions. **7** (2017).

20   Lugo-José, Y. K., Monnier, J. R., Heyden, A. & Williams, C. T. Hydrodeoxygenation of propanoic acid over silica-supported palladium: effect of metal particle size. *Catalysis Science & Technology 4*, 3909-3916 (2014).

21   Lu, J., Faheem, M., Behtash, S. & Heyden, A. Theoretical investigation of the decarboxylation and decarbonylation mechanism of propanoic acid over a Ru(0001) model surface. *Journal of Catalysis* **324**, 14-24 (2015).

22   Englisch, M., Ranade, V. S. & Lercher, J. A. Hydrogenation of crotonaldehyde over Pt based bimetallic catalysts. *Journal of Molecular Catalysis A: Chemical* **121**, 69-80 (1997).

23   He, D.-H., Wakasa, N. & Fuchikami, T. Hydrogenation of Carboxylic Acids Using Bimetallic Catalysts Consisting of Group 8 to 10, and Group 6 or 7 Metals. *Tetrahedron Letters 36*, 1059-1062 (1995).

24   da Silva, A. B., Jordão, E., Mendes, M. J. & Fouilloux, P. Effect of metal-support interaction during selective hydrogneaton of cinnamaldehyde to cinnamyl alcohol on platinum based bimetallic catalysts. *Applied Catalysis A: General 148*, 253-264 (1997).

25   Garrick, T. R. *et al.* The Effect of the Surface Composition of Ru-Pt Bimetallic Catalysts for Methanol Oxidation. *Electrochimica Acta* **195**, 106-111 (2016).

26   Merlo, A. B., Vetere, V., Ruggera, J. F. & Casella, M. L. Bimetallic PtSn catalyst for the selective hydrogenation of furfural to furfuryl alcohol in liquid-phase. *Catalyst Communications* **10**, 1665-1669 (2009).

27   Murillo, L. E. & Chen, J. G. Adsorption and reaction of propanal, 2-propanol and 1-propanol on Ni/Pt(111) bimetallic surfaces. *Surface Science 602*, 2412-2420 (2008).

28   Keels , J. M. *et al.* Aqueous-Phase Hydrogenation of Succinic Acid Using Bimetallic Ir–Re/C Catalysts Prepared by Strong Electrostatic Adsorption. *ACS Catalysis* **8**, 6486-6494 (2018).

29   Santori, G. F. *et al.* Hydrogenation of aromatic ketones with Pt- and Sn-modified Pt catalysts. *Applied Catalysis A: General* **269**, 215-223 (2004).

30   Zhang, K., Zhang, H., Ying, W., Fang, D. & Zhang, H. Effect of Sn Addition in Gas Phase Hydrogenation of Acetic Acid on Alumina Supported PtSn Catalysts. *Catalysis Letters* **144**, 691-701 (2014).

CHAPTER 6

Building a Kinetic Model For Propionic Acid HDO over Pt/SiO$_2$

6.1.   Introduction

Catalysts with high activity have the potential to change the landscape of chemical production, bringing to the forefront possibilities of new chemistries that may be cheaper, more sustainable and better for the environment[1,2]. Biomass upgrading for creating platform chemicals is one such example where catalysts can increase the feasibility of incorporating more renewable resources in a sector heavily influenced by fossil fuel derived material. Hydrodeoxygenation (HDO) is the chemical pathway for breaking down heavily oxygenated bio-derived feedstocks into targeted chemicals[3]. Succinic acid one such bio-derived platform chemical that has been shown to undergo HDO to form gamma butyrolactone (GBL), 1,4-butanediol (BDO) and tetrahydrofuran (THF)[4]; BDO is one of the most in demand chemicals used in the plastics industry, an annual demand of over 1 million tons[5]. There are catalytic setbacks associated with carboxylic acid HDO over supported noble metals such as selectivity and stability issues. HDO chemistry is highly unselective over Pt catalysts, molecules that result from C-C cleavage chemistries dominate product yields such as: decarbonylation (DCN), decarboxylation (DCX) and hydrogenolysis[6-12]. In addition to unwanted chemistries, catalysts lose a large portion of activity during reactions because of product inhibition caused by catalyst poisoning. Propionic acid has been used as a probe molecule for investigating carboxylic acid HDO over Pt; ethane and carbon monoxide (C-C cleavage) was seen as the most dominant products while propanal and propanal (C-O cleave) were rarely observed, this lack of selectivity makes it difficult to quantify HDO rates and extract apparent kinetics.

Kinetic modelling of reaction systems is a useful tool in understanding problems as a means towards providing relevant solution. Computational models can provide useful information such as regimes of operation for tuning the selectivity during catalytic operation as well as parameters like activation barriers, binding energies, etc[13-17]. The complexity of models can range from simple linear algebraic equations to multivariable differential equations; it is largely dependent on the type of information required from the system.

In this study, we use propionic acid HDO over silica supported Pt catalysts to build a model that can capture experimental trends while also providing accurate parameters. We iterate though different methods of model development by using reactor trends as well as past studies in the literature. We hope that this will be a resource for further studies on tuning catalytic properties such as how oxophilic promoters affect catalytic activity on a more molecular scale.

6.2. Materials and Methods

6.2.1. Reagents

Air (Airgas, zero grade); amorphous silica (481.2 m^2/g, 48-90 µm mesh size, Aldrich, 99.8%); chloroplatinic acid (Acros, 99.9%); CO (Praxair, 99.99%); CO/He (Airgas: 0.991% CO, 0.996% Ar, 98% He); ethane Airgas: 0.994% C_2H_4, 1. % Ar, 98% He); ethylene (Airgas: 1% C_2H_4, 1% Ar, 98% He); He (Airgas, 99.999%); H_2 (Airgas, 99.999%); N_2 (Airgas, 99.999%%); $O_2/Ar/He$ (1% O_2, 1% Ar , 98% He); propane (Airgas: 1% propane, 1% Ar, 98% He); 1-propanol (Acros Organics, 99+%); propanal (Acros Organics, 99+%) and propionic acid (Acros Organics, 99%) were employed for catalyst synthesis, catalyst characterization, and reactor operation. Each was

used as supplied from commercial vendors. Water (Type II, 18.0 MΩcm^{-1} resistivity) was prepared in house (Spectrapure).

6.2.2. Catalyst Preparation

Pt/SiO$_2$ catalysts were prepared by incipient wetness impregnation of an aqueous chloroplatinic acid solution into amorphous silica (1.8 grams of chloroplatinic acid solution per gram of silica). Concentrations of chloroplatinic acid were varied as necessary to achieve desired mass loadings of platinum. Catalysts were then dried overnight in static air at 393K. Subsequently, samples were loaded into a quartz flow cell, calcined in air (100 ml min^{-1} Air, 3 K min^{-1} ramp rate) at 623 K for 3 hours, then reduced at 673K under H$_2$ flow for 4 hours (100 ml min^{-1} H$_2$, 3 K min^{-1} ramp rate), and cooled to 298K under H$_2$. Prior to exposure to ambient air, samples were passivated at 298K by purging the cell volume with He for 30 minutes and then exposing the cell to 1% O$_2$ in 1% Ar 98% He for 30 minutes.

6.2.3. Catalyst Characterization

The catalytic site densities were determined using chemisorption on an ASAP 2020. Sample cells were evacuated to a set point of 5μmHg while the temperature was being increased from room temperature to 100°C at a rate of 10°Cmin^{-1} .Oxygen was then flowed in the cell while its temperature was increase from 100°C to 350°C at 10°Cmin^{-1}. Oxygen was flowed over the cell at the elevated temperature for 30 minutes. The cell was then evacuated to 5μmHg and held for 15 minutes to eliminate oxygen present and cooled to 100℃ after which hydrogen was introduced. Under hydrogen, the cell was heated to 400°C at 10°Cmin^{-1} and held for 4 hours, and then the hydrogen was evacuated and held at 5μmHg for 30 minutes. After cooling to 35°C under vacuum,

carbon monoxide was then dosed twice as the analysis gas for chemisorption. Site densities were derived from the difference between the adsorption isotherms of both CO dosages.

6.2.4. Catalyst Activity Testing

The liquid reactants were sent for pretreatment from glass syringes (Hamilton) using a syringe pump (Cole Parmer) via capillary PEEK tubing (McMaster) where it was vaporized and swept to a fully reduced packed bed reactor by H_2 or He. Gas Feeds were delivered using digital mass flow controllers (Brooks); the experimental volumetric flow rate was measured using a bubble flow-meter since in some instances, the digital volumetric flow rate on the mass flow controller did not match the actual volumetric flow rate. The temperature of the vaporizer was maintained at conditions in accordance with Antoine Coefficients to ensure that all liquid feeds entered and remained in the gas phase. The vaporizer consisted of stainless steel furnace that was heated using a band heater (McMaster), which encapsulated a 0.25-inch diameter dead volume that was filled with quartz chips. The dead volume served as a medium where the liquid feed came into contact with the reactant/carrier gas, quartz chips served to ensure dispersion and uniform vaporization. The temperature of the vaporizer furnace was measured using type-K thermocouples (Omega) and power was supplied to the band heater using a temperature controller (Omega). Species flowed through a two-position 6 port valve that decided whether reactants would go to the reactor or bypass the reactor straight to the gas chromatograph. Before sending reactants to the reactor system, reactant signals were observed in the bypass to be certain all of the liquid feed was vaporized. Bypass signals coupled with the volumetric flow rate from the bubble meter also serves as a final leak test before sending species to the reactor system.

The reactor system consisted of a 1/2-inch stainless steel tube (McMaster) that was used in an up-flow packed bed reactor. The reactor consisted of quartz chips to achieve full dispersion across the diameter of the tubing to ensure the entire gaseous species came into maximum contact with the catalyst bed. The bed was sandwiched between quartz wool to keep it intact and prevent catalyst loss. The reactor was placed in a stainless steel furnace controlled by a band heater. The temperature of the reactor furnace was measured using type-K thermocouples (Omega) and power was supplied to the band heater using a temperature controller (Omega). The temperature was also measured at the catalyst bed to account for the temperature gradient that exists between the bed and walls of the furnace; this was measured by a type-K thermocouple. Tubing between reactor and the analysis systems was 1/8-inch stainless steel (McMaster) that was heat traced using nichrome wire (McMaster), which was fed power by a variac transformer; the heating of the tubing served the purpose of making sure all chemicals remained in the gas phase for proper analysis. The design for the described reaction setup is shown in Figure 2.2.The chemical species were analyzed by gas chromatography (HP5890) using a HP-PONA column with a flame-ionized detector (FID) and a Restek ShinCarbon ST Micropacked column with a thermal conductivity detector (TCD). For instances where the limitations of the TCD sensitivity affected the precision of data points, the reactor effluent was sent to a methanizer which made using a Restek ShinCarbon ST Micropacked column connected to a microreactor that was filled with a nickel catalyst which ended at a FID. The function of the methanizer was to convert species like carbon monoxide and carbon dioxide into methane for an FID since it is a more sensitive than the TCD.

Reactions were run over many varying conditions such as temperatures, reactant partial pressures, catalyst site densities and contact times. Conversions in each reaction were kept below 5% to ensure differential conditions. Bracketing techniques were employed when making changes in

order to track deactivation; that is, after every change, a reference condition was revisited which helped in correcting data that might have been affected by the deactivation of sites. Data was collected at steady state for majority of conditions, however for reactions that showed significant deactivation of the catalyst bed such as those involving propanal and propanol, initial rate data was extrapolated using the deactivation profile as a function of time on stream. Carbon atom balances were performed at each reaction condition to make sure that all species were accounted for towards atom conservation; data points reported consisted of the average of multiples ones that exhibited a carbon balance of 95% or greater. The reaction bed was regenerated after every reaction by reduction under H_2 at 673K for four hours, however for reactions using propanol as a feed the bed had to first be calcined in air at 623K for 3 hours before reduction due to the formation of oxygenates on the surface. Reference conditions for each feed were established at the beginning of every experiment to ensure than the catalyst bed was fully regenerated after deactivation from previous experiments.

6.3.   Results and Discussion

A reaction schematic of the pathways involved during propionic acid HDO over Pt was developed in chapter 3; this is illustrated below as Figure 6.1. It was also established that because of multiple pathways as well as product inhibition on the catalysts surface, extracting rates had to be done by modelling the reactor. Building a reactor model on a system involving many pathways meant that experiments needed to be done involving not only propionic acid, but also the primary and secondary reactions in the reaction schematic. The positive aspect of the data collection is that information about the secondary and tertiary reactions can be verified and most of the reactions are well reported in the literature; we use this verification as a means of assuring confidence in the

data, as the accuracy of parameterization is largely dependent on the experimental data against which regression takes place.
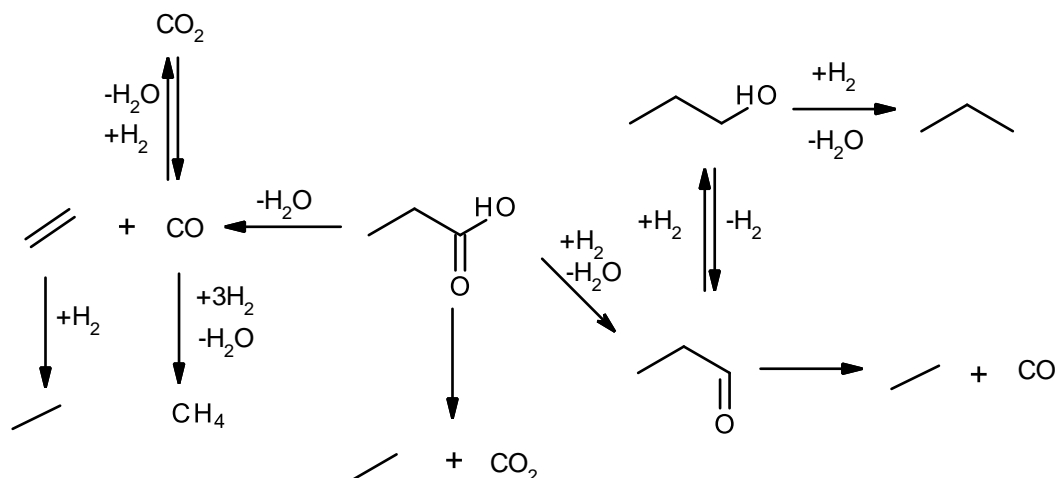
Figure 6.1: Reaction schematic involved during propionic acid HDO over Pt.

6.3.1. Verifying Data Collected

We use parameters such as activation barriers and reaction orders to draw comparison with past studies of similar reaction chemistries.

Carbon Monoxide

Carbon monoxide was used to generate methanation data across a range of conditions. The information from the temperature study used to generate an Arrhenius plot as seen in Figure 6.2. The carbon monoxide and hydrogen dependent reaction orders were derived from Figures 6.3 and 6.4. The apparent activation barrier for methanation that was extracted from the slope of Figure 6.2 for the stated reaction conditions was found to be 93 kJ/mole ±5 kJ/mole; this is quite close to the barrier reported in past studies which was 70-101 kJ/mole[18]. The hydrogen-dependent reaction order from the slope of Figure 6.3 was 0.28, which is common for hydrogenation reaction orders

to be positive. The slope of Figure 6.4 was -0.08, which represents the carbon monoxide dependent reaction order. In an environment with a much lower carbon monoxide partial pressure and excess hydrogen, the conversion to methane would increase.
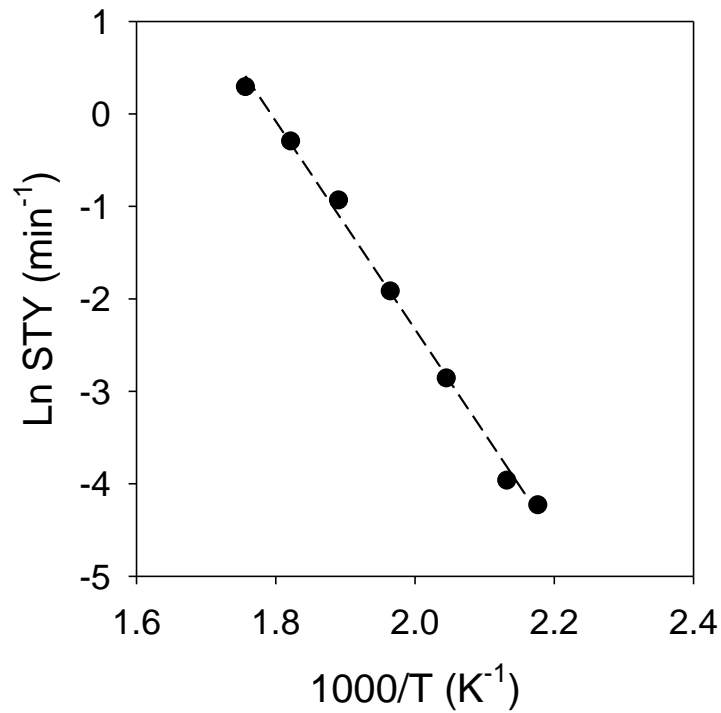
Figure 6.2: Arrhenius Plot for methanation from 460 to 570 K using a feed consisting of 1% Carbon Monoxide, 50% Hydrogen and 49% Helium.
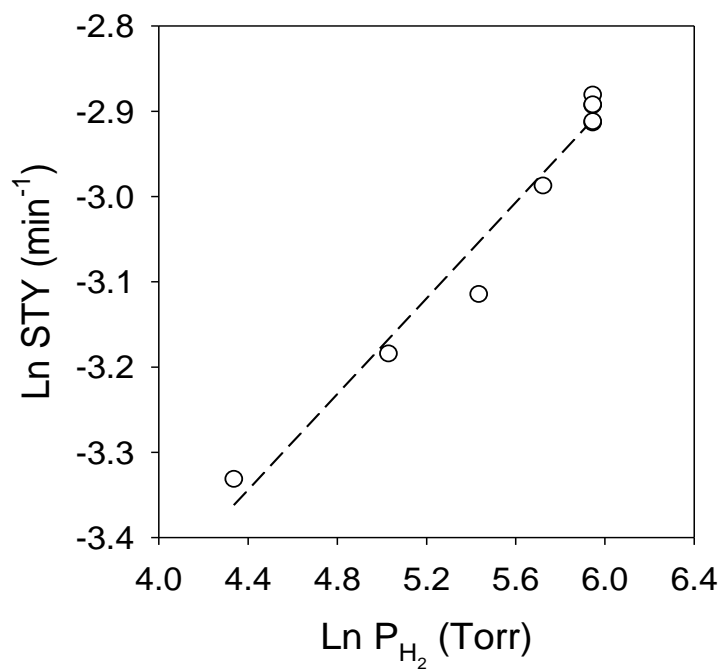
Figure 6.3: Effect of hydrogen partial pressure on methanation in a 1% CO and balance He stream at 489K.
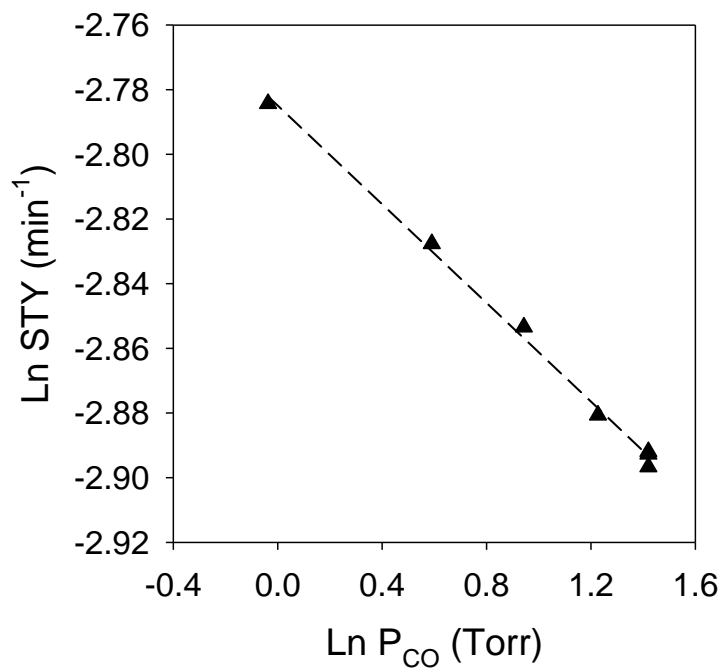
Figure 6.4: Effect of carbon monoxide partial pressure on methanation in a 50% H_2 and balance He stream at 489K.

Propanal

Figure 6.5 shows an Arrhenius plot of the propanal hydrogenation, from which the apparent activation barrier was found to be 15 kJ/mole ±3 kJ/mole. The low barrier from aldehyde hydrogenation is not atypical because it has been well accounted for in literature from experimental studies[19]. Propanal exhibited high rates of deactivation, this made it increasingly difficult to collect rates however since experiments involving propanol can follow the same pathways as propanal; more emphasis was placed on collecting propanol experiments because of how stable the Pt catalysts were during those experiments.
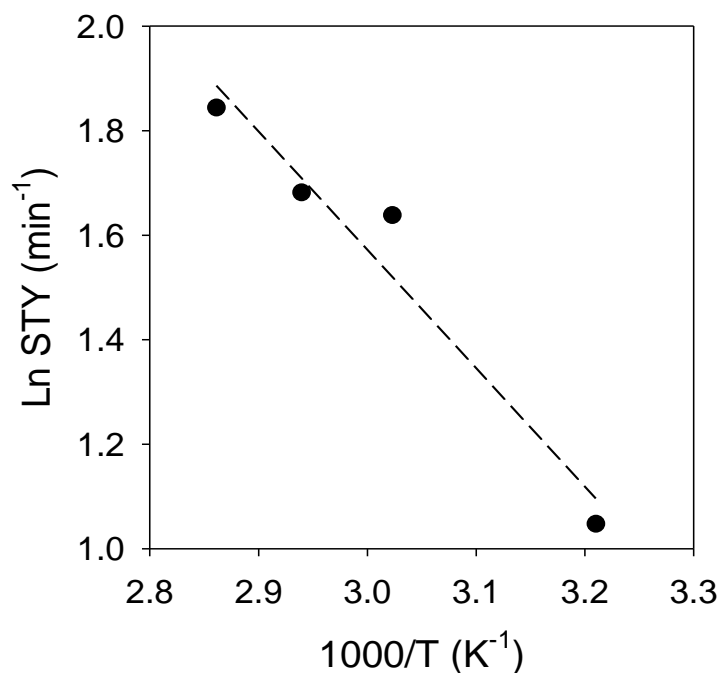
Figure 6.5: Arrhenius plot for propanal hydrogenation from 312 to 350 K at a propanal and hydrogen partial pressure of 2.5 and 757 torr respectively.

Propanol

There was suspicion that propanol and propanal are most likely controlled by equilibrium, it is important to be aware of this when attempting to extract kinetic parameters from propanol dehydrogenation. For further investigation, the theoretical equilibrium constant was calculated for each temperature and its ratio to the reaction quotient at different temperatures were observed as in Figure 6.6. It can be seen that kinetic control decreases as the temperature increases, all of the values for propanol dehydrogenation were far away from the theoretical equilibrium constant, this points towards the strong possibility that this reaction is kinetically controlled.
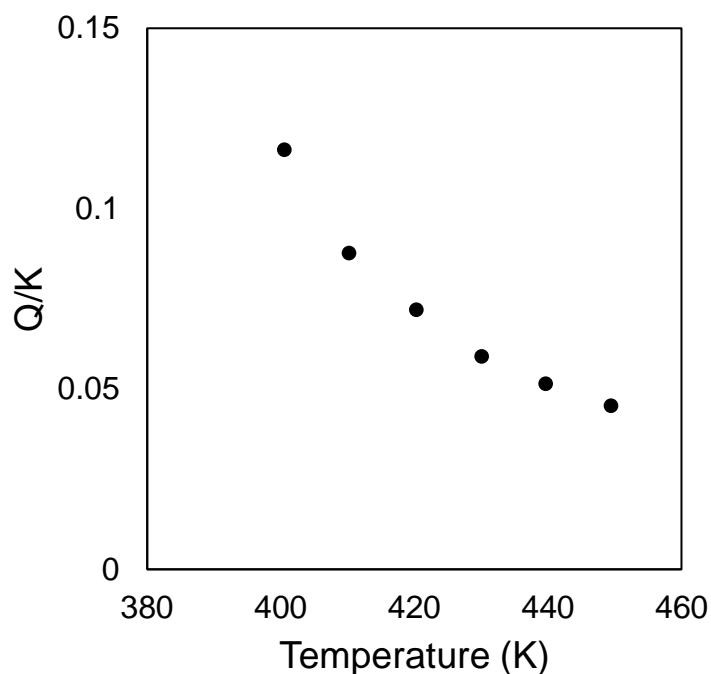
Figure 6.6: Testing kinetic control over the temperature study by comparing ratio of reaction quotient to theoretical equilibrium constant for dehydrogenation at propanol and hydrogen partial pressure of 5 and 755 torr respectively and at 458K.

Figure 6.7 is an Arrhenius plot of the data across all the temperatures from Figure 6.6. The dehydrogenation rates were calculated by taking into account that decarbonylation products are

only evolved through propanal, so an accurate apparent barrier for dehydrogenation had to include the rates from non-primary pathways. The apparent activation barrier of propanol dehydrogenation was found to be 88 kJ/mole ±6 kJ/mole from. There have not been any reliable values for this apparent barrier reported in the literature because previous studies have mainly focused on surface science and DFT simulations or over different metals[20,21]. Reports that did include experiments were not confident in reporting an apparent barrier because only the decarbonylation products were formed, there was uncertainty about whether decarbonylation occurred on the propanol or propanal since the latter product was not actually observed[22].
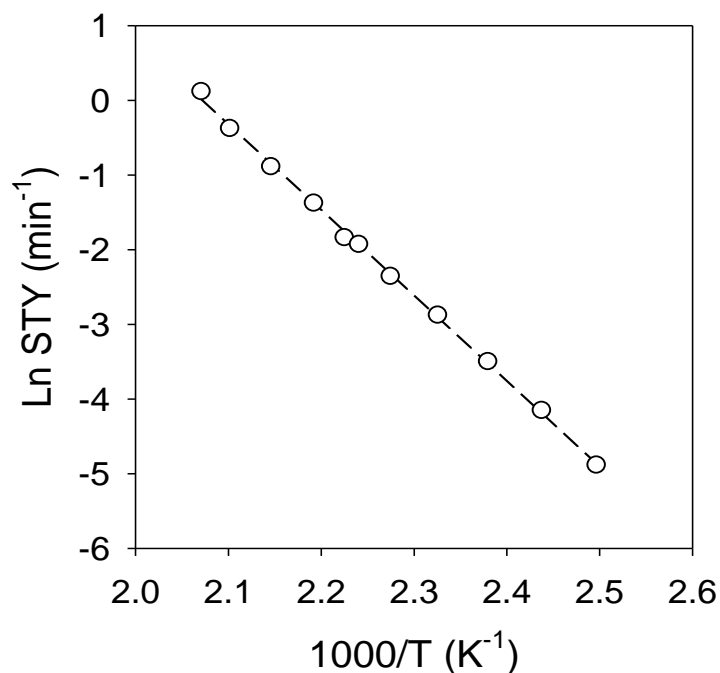
Figure 6.7: Arrhenius Plot for propanol dehydrogenation from 400 to 483 K at propanol and hydrogen partial pressure of 5 and 755 torr respectively.
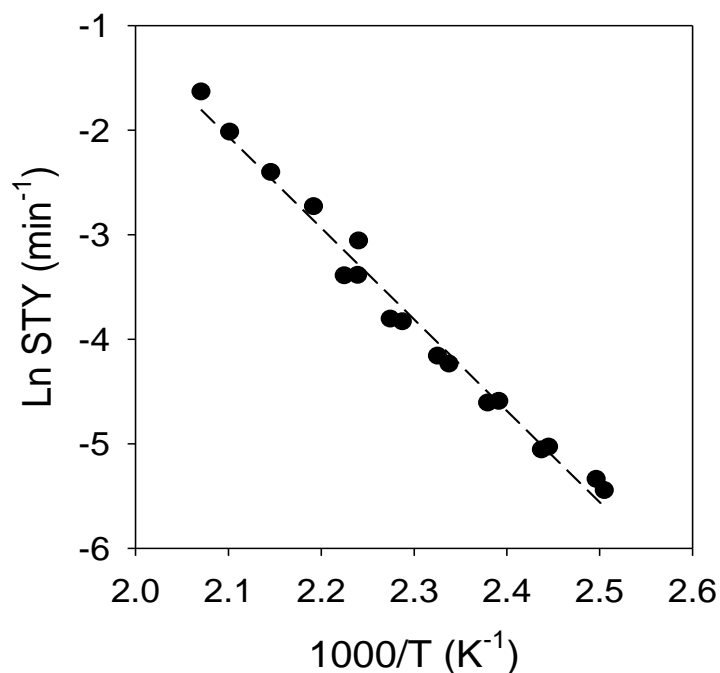
Figure 6.8: Arrhenius Plot for propanol hydrogenolysis from 400 to 483 K at propanol and hydrogen partial pressure of 5 and 755 torr respectively.

From Figure 6.8, the apparent activation energy for propanol hydrogenolysis is 73 kJ/mole $\pm$5 kJ/mole. Even though there have been no experimental values for kinetic parameters involving gas phase propanol hydrogenolysis over silica supported Pt catalysts, density functional theory (DFT) studies have reported barriers ranging from 65-105 kJ/mole[20]. Kinetic studies were reported for alumina supported Pt catalysts, which gave an apparent alcohol hydrogenation barrier of 71 kJ/mole[22]; assuming the support played little role, this barrier should be significantly comparable to 1-propanol hydrogenolysis because the C-O bond enthalpy in both isomers are the relatively close.
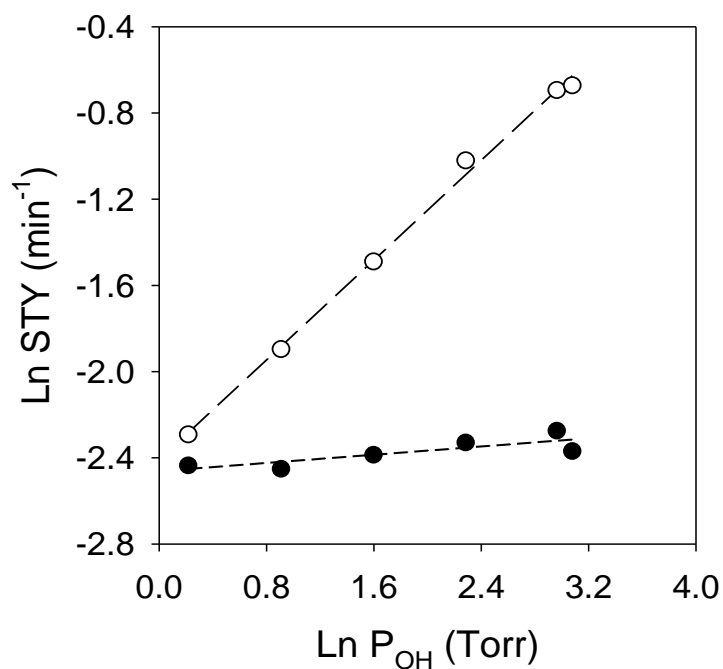
Figure 6.9: Effect of propanol partial pressure on the reaction pathways of hydrogenolysis (○) and dehydrogenation (○) and carbon monoxide (●) at 456 K.

The propanol-dependent reaction orders from pathways can be deduced from the plots in Figure 6.9 using power rate laws. Hydrogenolysis and dehydrogenation reaction orders were found to be 0.05 and 0.58 respectively. Reaction orders for the chemistries involved generally range from 0 to half order[21,22]; the numbers presented could have been affected by species on the surface competing for active sites.

Figure 6.10 shows the hydrogen dependent reaction orders for the different pathways involved in the experiment. The hydrogen-dependent reaction orders for hydrogenolysis, and dehydrogenation was 0.13 and -0.23 respectively, these are indicative of competition between hydrogen and adsorbed species.
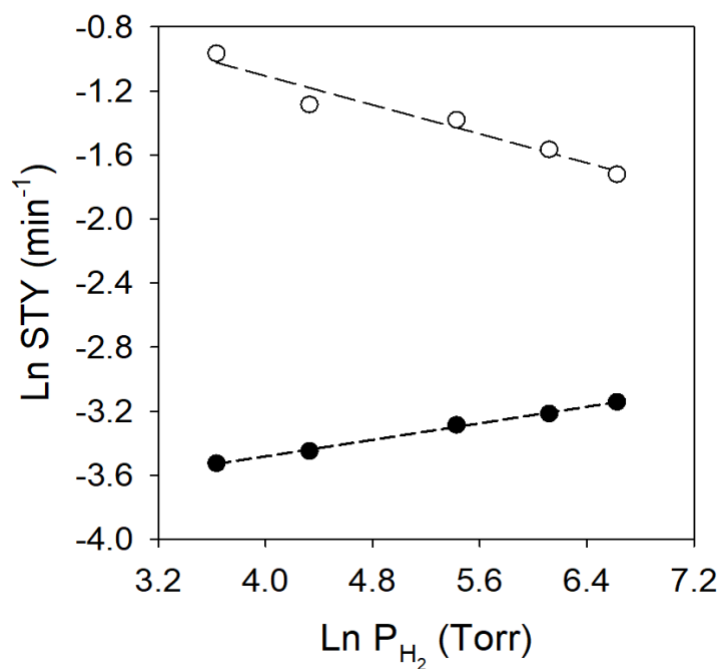
Figure 6.10: Effect of hydrogen partial pressure on the reaction pathways of hydrogenolysis (○) and dehydrogenation (○) and carbon monoxide (●) at 456 K.

6.3.2. Differential Reactor vs Integral Reactor

The choice of governing equations for simulating the packed bed reactor had to be chosen based on observations seen during propionic acid HDO. Typically, in a differential reactor, the conversions are kept small so that there is little or no change in rate, temperature and species concentration across the bed[23]. The fractional conversion should increase linearly with contact time over the catalyst bed in order to be characterized under differential conditions; Figure 6.11 shows that this only applies for very short contact times as the change in conversion decreases at higher contact time. Observing the rate of conversion across the fractional conversions in Figure 6.12, it shows that the rate decreases as fractional conversion increases, and in turn, the rate of conversion is decreasing at higher contact times. With all this being taken into consideration, the

185

packed bed reactor should be simulated as an integral reactor and also capture the effect of CO

formation on catalyst activity.
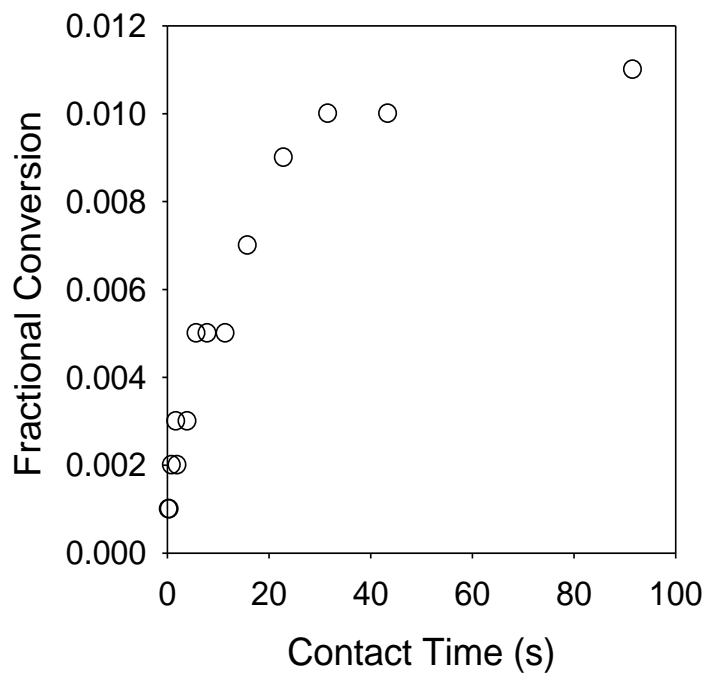
Figure 6.11: Fractional conversion across different contact times over Pt.
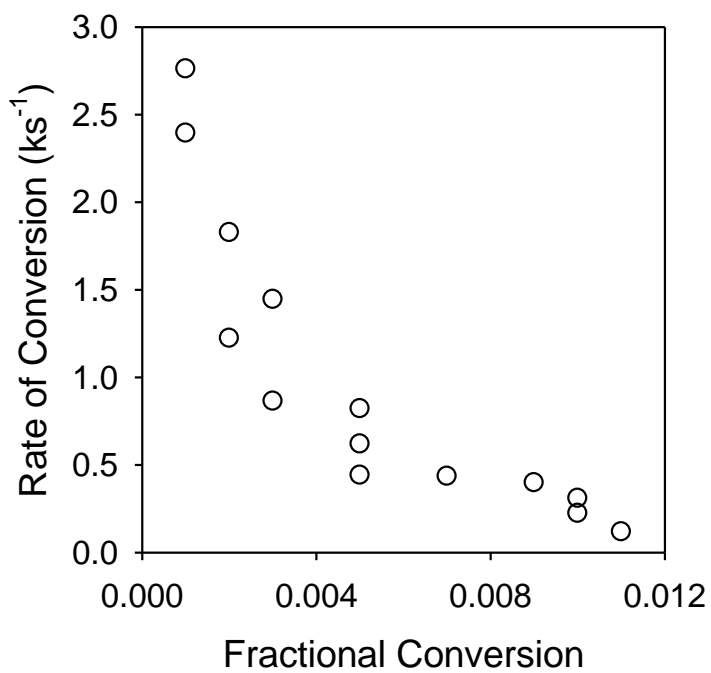
Figure 6.12: The rate of conversion at different fractional conversions over Pt.

6.3.3. Power Rate Laws

In general, one may use power law models to describe the rate of each macroscopic reaction as a function of kinetic parameters (rate constants, k_i) and the partial pressure (p_j) of the reacting species present in the gas phase. In this model, the rate is dependent on the partial pressure of each species in an unknown reaction order (α,β):

$$-r_A = kP_A^\alpha P_B^\beta$$

Unfortunately, with our particular data set, a complication prevents the use of a simple power law model. In an effort to isolate contributions from a range of primary, secondary, and tertiary reactions, we have operated our reactors over a very large range of reaction conditions. Apparent reaction orders (α,β) are generally constant only for narrow ranges in operating conditions such that this type of model has poor accuracy when examining a large range of temperatures, pressures, and compositions. In addition, the use of simple power-law models creates numerical instability under certain reaction conditions, which can prevent numerical solution of ODE systems that describe the catalytic reactor. Specifically, we observe that many reactions have a negative order in carbon monoxide, yet many experiments are performed at or near zero CO partial pressure. In this limit, rates for reactions that are assumed to have a fixed, negative order dependence on CO become infinitely large, which is both physically unrealistic and leads to numerical instability in the ODE solution. Similarly, alkane hydrogenolysis reactions have a strong negative order in hydrogen, yet their rate remains finite in the absence of hydrogen. The beauty of microkinetic solutions is that they are sufficiently robust to allow for variable reaction orders because they

model variations in surface coverage with reactant partial pressures. Ideally, we would like our model to be similarly robust; however, we presently lack sufficient insight into the elementary mechanisms, rate limiting steps, and kinetic parameters governing each overall reaction. Accordingly, we look towards a semi-empirical approach based on the conventions of Langmuir-Hinshelwood surface kinetics.

6.3.4. Macroscopic model

In this instance, we use the gas phase equations in Figure 6.1 to create a model that would not only capture the pathways presented, but also incorporate the product inhibition. For preliminary analysis, we have assumed that the rate of each reaction has a first order dependence on the *coverage* of the reactants that participate in the overall reaction. Species coverages are then computed by assuming that the adsorption/desorption of each stable, gas-phase reactant and/or is equilibrated. This allows us to broadly capture inhibitive effects of certain species while preventing computation of infinite reaction rates as inhibiting species approach zero partial pressure. Species production rates in this system are computed by modeling our experimental reactor as an idealized packed bed, which requires that we integrate species balances over the number of active sites present in a given reactor at a given set of experimental conditions.

The main governing equations of the model are as follows:

$$k_i = k_m \cdot e^{\frac{-E_A}{R\Delta T}}$$

$$K_j = K_m \cdot e^{\frac{-DH}{R\Delta T}}$$

$$\theta_* = \frac{1}{1 + \sum K_j \cdot p_j}$$

$$\theta_j = K_j \cdot p_j \cdot \theta_*$$

$$r_i = k_i \cdot \prod \theta_j$$

Where DH is the binding enthalpy, E_A is the activation energy, θ_j is the species coverage, k_m is the mean rate constant, K_m is the mean binding constant, K_j is the binding constant, k_i is the rate constant and r_i is the rate of the reaction. The mean rate constants and mean binding constants are use in order to regress the model parameters with experimental values. The parameters that undergo regression in order to fit the data include the activation energies, mean rate constants, and the mean binding constants and enthalpies for the non-terminal species.

The model included eight of the ten reactions proposed in Fig. 12, this was because while carbon dioxide had been reported as a product of water-gas shift and Boudouard reaction over Pt, the reactions were not observably active over the reaction conditions for which propionic acid HDO was carried out. This was also done because of the low selectivity of carbon dioxide over experimental conditions, especially since it is an undesirable product; it was not a necessity to explore all the possible pathways than can produce carbon dioxide. The equilibrium relationship between propanol and propanal was represented through two separate reactions in the MATLAB script (Equations 4 and 5).

1. $C_2H_5COOH + H_2 \rightarrow C_2H_5CHO + H_2O$

2. $C_2H_5COOH \rightarrow C_2H_6 + CO_2$

3. $C_2H_5COOH + H_2 \rightarrow C_2H_6 + CO + H_2O$

4. $C_2H_5CHO + H_2 \rightarrow C_3H_7OH$

5. $C_3H_7OH \rightarrow C_2H_5CHO + H_2$

6. $C_2H_5CHO \rightarrow C_2H_6 + CO$

7. $C_3H_7OH + H_2 \rightarrow C_3H_8 + H_2O$

8. $CO + 3H_2 \rightarrow CH_4 + H_2O$
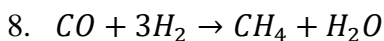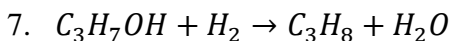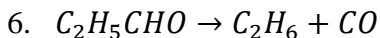
List of Equations used in MATLAB model.

The model was able to regress reaction rate constants as well as activation barriers for the different steps, it also provided upper and lower bounds for those parameters. Figure 6.13 shows a parity plot exhibiting the degree to which the model was able to match the experimental data collected with the theoretical calculations using the regressed parameters.
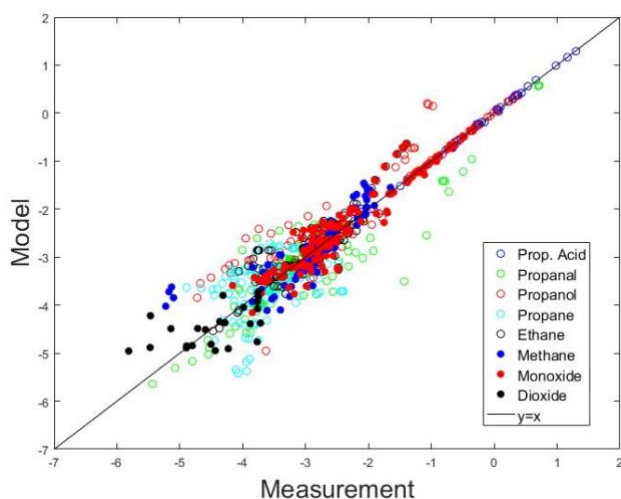
Figure 6.13: Parity plot of the natural logarithm of experimental rates versus theoretical rates for all species involved in reactions proposed.

Table 6.1 shows the values resolved from MATLAB as well as the lower and upper bounds of those values. A standout among all the parameters is the behavior of those involved in equation 3 from the proposed model; decarbonylation of propionic acid. Large uncertainty in parameters are indicative of the model not being able capture an accurate value to represent the data set. The uncertainty in propionic acid decarboxylation parameters is a result of the pathway having the lowest selectivity, carbon dioxide barely appears, and on appearance, it's quantities were too small

which created a lot of variability. There was also uncertainty in propanol hydrogenolysis parameters to form propane because of the product concentrations being the too small; even though appreciable propane concentrations were recorded in experiments using propanol as a feed, quantities collected using propionic acid as a feed were very small, which facilitated the limitations of detector sensitivity to have an influence on the parameter uncertainty. However, decarbonylation products represented a sizeable percentage of product selectivity using propionic acid feed, which led to the belief that equations 2 and 6 should be among the best fit. Instead, the parameters of propanal decarbonylation were far more precise than propionic acid decarbonylation; upon further inspection, the rate of acid decarbonylation was more than three orders of magnitude lower than that of aldehyde decarbonylation. While there can be debate on how well the macroscopic model captures trends, the biggest flaw is that 26 parameters were regressed using this model; over-parameterization was a high possibility as some of the values were not theoretically accurate, and in some instances, it did not follow the laws of thermodynamics. Also, there were occasions were the model regressed to different minimums, this is another result of too many parameters being regressed.

Table 6.1: Regressed parameters from the MATLAB model. 'Ea' is the activation barrier in kJ/mole and 'k' is the forward rate constant for the 8 equations

Parameter	Value	Lower Bound	Upper Bound
k1	2.31E-01	2.02E-01	2.65E-01
k2	4.47E-04	3.17E-04	6.29E-04
k3	3.32E-04	1.13E-04	9.72E-04
k4	5.61E+01	4.63E+01	6.80E+01
k5	1.21E-02	1.04E-02	1.42E-02
k6	1.68E+01	1.43E+01	1.98E+01
k7	2.76E-02	2.39E-02	3.19E-02
k8	1.93E-02	1.60E-02	2.33E-02
Ea1	164.88	153.33	177.30
Ea2	146.42	114.51	187.22
Ea3	3.38E-10	N/A	N/A
Ea4	0.31	0.25	0.38
Ea5	76.70	69.17	85.06
Ea6	56.19	49.51	63.77
Ea7	12.15	7.18	20.55
Ea8	84.20	74.99	94.54

6.3.5. A Microkinetic Approach

It may also not be accurate to think of a reaction schematic over a catalyst surface in terms of homogeneous equations. For example, propanal decarbonylation is one of the most facile chemistries tested over Pt, it is not implausible to hypothesize all the DCN products being formed through this pathway; however, the selectivity of DCN products in Figure 6.14 can be seen to have a non-zero selectivity towards zero conversion. While arguments can be made that this non-zero

selectivity can be as a result the rapid rates of propanal DCN, we postulate a reaction schematic

that considers all the observations, including those published in the literature[13-15,17-19,21,22,24-29].
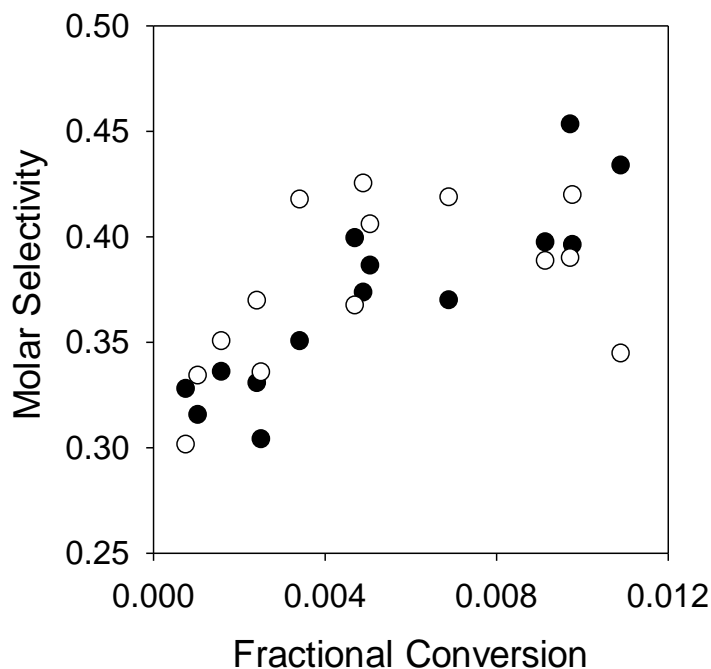
Figure 6.14: Effect of fractional conversion on the molar selectivity of DCN products ethane (○) and carbon monoxide (●) at propionic acid and hydrogen partial pressure of 5 and 755 torr respectively at 448K over Pt.

A propanol mechanism to form the observed products, in accordance with the literature proposed

over metal surfaces, can be envisioned as follows:

Alc-1) $H_{2(g)} \rightarrow 2H_{(a)}$

Alc-2) $C_2H_5CH_2OH_g \rightarrow C_2H_5CH_2OH_a$

Alc-3) $C_2H_5CH_2OH_a \rightarrow C_2H_5CH_{2_a} + OH_a$

Alc-4) $C_2H_5CH_{2_a} + H_a \rightarrow C_3H_{8_a}$

Alc-5) $C_3H_{8_a} \rightarrow C_3H_{8_g}$

Alc-6) $OH_a + H_a \rightarrow H_2O_a$

Alc-7) $H_2O_a \rightarrow H_2O_g$

Alc-8) $C_2H_5CH_2OH_a \rightarrow C_2H_5CH_2O_a + H_a$

Alc-9) $C_2H_5CH_2O_a \rightarrow C_2H_5CHO_a + H_a$

Alc-10) $C_2H_5CHO_a \rightarrow C_2H_5CHO_g$

Alc-11) $C_2H_5CHO_a \rightarrow C_2H_5CO_a + H_a$

Alc-12) $C_2H_5CO_a \rightarrow C_2H_{5a} + CO_a$

Alc-13) $C_2H_{5a} + H_a \rightarrow C_2H_{6a}$

Alc-14) $C_2H_{6a} \rightarrow C_2H_{6g}$

Alc-15) $CO_a \rightarrow CO_g$
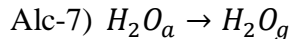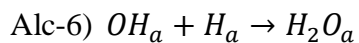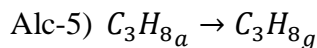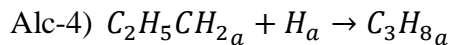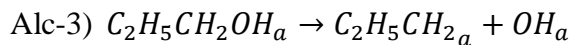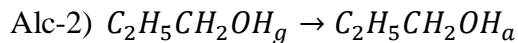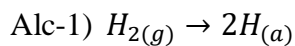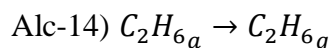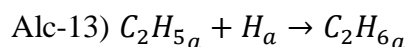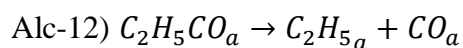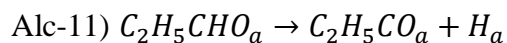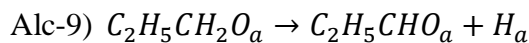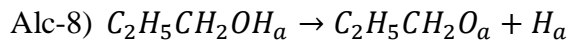
Equations Alc-3) – Alc-7) represents hydrogenolysis to form propane, dehydrogenation of propanol to form propanal is formed through equations Alc-8) – Alc-10). The carbonyl species formed at step Alc-9) is further dehydrogenated to an acyl species in Alc-11), this undergoes decarbonylation to form carbon monoxide and an ethyl compound that quickly forms ethane.

A mechanism for propanal reactivity into the observed products involves similar steps, except in the opposite direction for the hydrogenation pathways to propanol and propane:

Ald-1) $H_{2(g)} \rightarrow 2H_{(a)}$

Ald-2) $C_2H_5CHO_g \rightarrow C_2H_5CHO_a$

Ald-3) $C_2H_5CHO_a \rightarrow C_2H_5CO_a + H_a$

Ald-4) $C_2H_5CO_a \rightarrow C_2H_{5a} + CO_a$

Ald-5) $C_2H_{5a} + H_a \rightarrow C_2H_{6a}$

Ald-6) $C_2H_{6a} \rightarrow C_2H_{6g}$

Ald-7) $CO_a \rightarrow CO_g$

Ald-8) $C_2H_5CHO_a + 2H_a \rightarrow C_2H_5CH_2OH_a$

Ald-9) $C_2H_5CH_2OH_a \rightarrow C_2H_5CH_2OH_g$

Ald-10) $C_2H_5CH_2OH_a \rightarrow C_2H_5CH_{2_a} + OH_a$

Ald-11) $C_2H_5CH_{2_a} + H_a \rightarrow C_3H_{8_a}$

Ald-12) $C_3H_{8_a} \rightarrow C_3H_{8_g}$

Ald-13) $OH_a + H_a \rightarrow H_2O_a$

Ald-14) $H_2O_a \rightarrow H_2O_g$
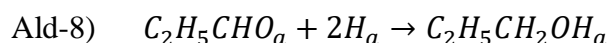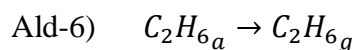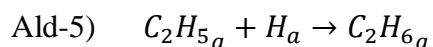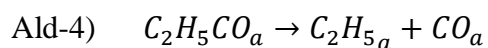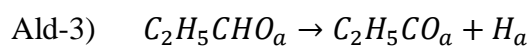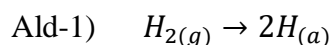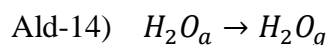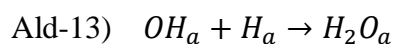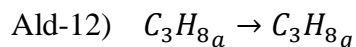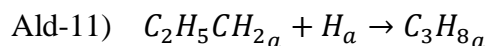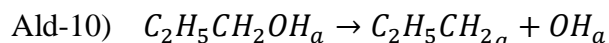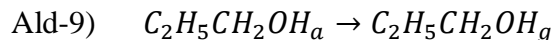
The presence of an acyl species, $R - CO_a$, has been also proposed as a key intermediate in carboxylic acid HDO over supported metals. Here, we make use of this intermediate, as well as the established mechanisms from propanol and propanal, to contribute a mechanism that hypothesizes reaction pathways in terms surface species; this avoids the oversimplification of using gas phase equations, which assume products definitively being evolved through specific pathways that may be considered primary, secondary etc. Here we look at the evolution of the main products propanal, propanal, ethane, carbon monoxide from propionic acid over Pt.

Acid-1) $H_{2(g)} \rightarrow 2H_{(a)}$

Acid-2) $C_2H_5COOH_g \rightarrow C_2H_5COOH_a$

Acid-3) $C_2H_5COOH_a \rightarrow C_2H_5CO_a + OH_a$

Acid-4) $C_2H_5CO_a + H_a \leftrightarrow C_2H_5CHO_a$

Acid-5) $C_2H_5CHO_a + H_a \leftrightarrow C_2H_5CH_2O_a$

Acid-6) $C_2H_5CH_2O_a + H_a \leftrightarrow C_2H_5CH_2OH_a$

Acid-7) $C_2H_5CO_a \rightarrow C_2H_{5_a} + CO_a$

Acid-8) $C_2H_{5_a} + H_a \rightarrow C_2H_{6_a}$

Acid-9) $OH_a + H_a \rightarrow H_2O_a$

Acid-10) $C_2H_5CHO_a \rightarrow C_2H_5CHO_g$

Acid-11) $C_2H_5CH_2OH_a \rightarrow C_2H_5CH_2OH_g$

Acid-12) $C_2H_{6_a} \rightarrow C_2H_{6_g}$

Acid-13) $CO_a \rightarrow CO_g$

Acid-14) $C_3H_{8_a} \rightarrow C_3H_{8_g}$

Acid-15) $H_2O_a \rightarrow H_2O_g$
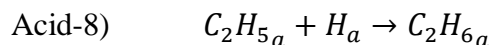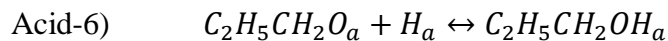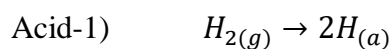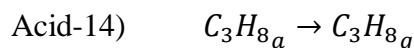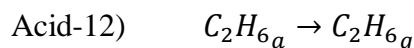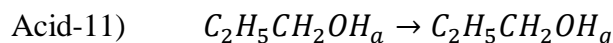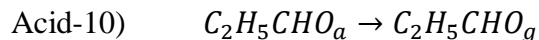
We can see that the C_2H_5CO acyl species that undergoes decarbonylation is an intermediate from both propionic acid and propanal as reactor inlets; this indicates the reason why it may be inaccurate to think of DCN as a secondary product from propanal. Since the acyl species is not stable in the gas phase, the gas phase products formed primarily through this species are observed as primary products during propionic acid HDO (Figure 6.13). The hydrogenation of the carbonyl species Acid-5) is relatively facile as seen during propanal hydrogenation experiments, this is explains why propanol is observed as a primary product during propionic acid HDO. The observation that may seem contradictory is the behavior of these *primary species* at higher conversion- the apparent consumption of HDO species and production of DCN species. One might be tempted to say this is because of secondary pathways, however, the caveat is that there is no observed product formed that reflects the amount of propanol that was consumed at higher conversions. Instead, we may think of the protons as being able to move reversibly in steps Acid-4) and Acid-5) without necessarily being in equilibrium, this is not the case for Acid-6) as it is highly unlikely that the decarbonylation of the acyl species is reversible.

While the propionic acid HDO steps proposed shows pathways to form the main products (propanal, propanol, carbon monoxide and ethane), here we present pathways to the remaining products observed. Propane can be formed from further reactions of propanol on the surface similar to equations Ald-10) - Ald-12) in the scheme presented for propanal activity, and equations Alc-3) – Alc-5) for propanol activity.

Methanation can occur from carbon monoxide on the surface through the following pathways:

Met-1.) $CO_a \rightarrow C_a + O_a$

Met-2.) $C_a + 4H_a \rightarrow CH_{4_a}$

Met-3.) $CH_{4_a} \rightarrow CH_{4_g}$

Met-4.) $O_a + H_a \rightarrow OH_a$

Met-5.) $OH_a + H_a \rightarrow H_2O_a$

Met-6.) $H_2O_a \rightarrow H_2O_g$
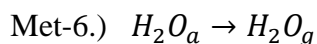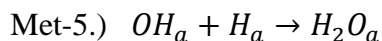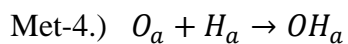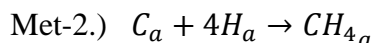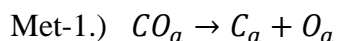
Because of the trace amounts of carbon dioxide, it was speculated that majority of this species were produced via water-gas shift and that the reaction was equilibrium controlled; this may explain why carbon dioxide is said to be a primary product. We postulate that decarboxylation products previously reported are artifacts of DCN and WGS (water-gas shift) happening on the surface, the carbon dioxide being evolved is most likely dependent on external conditions like partial pressures of hydrogen and water on the surface.

Taking this into consideration, carbon dioxide formation can be imagined to proceed through the following pathways:

WGS-1.) $CO_a + O_a \rightarrow CO_{2_a}$

WGS-2.) $CO_{2_a} \rightarrow CO_{2_G}$
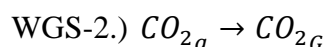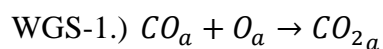
By using the proposed pathways for the formation of all the products observed during propionic acid HDO, we can approach finding a method to accurately model the mechanisms. During the propionic acid experiments, since carbon dioxide and methane were not observed for most of the reaction conditions, we may therefore disregard the microkinetic reactions of the formations of these products; this leaves all the acid equations to be used in the model. To avoid over-parameterization, we make the use of theoretical correlations in order to use fewer parameters. One such correlation is the bond order conservation approach put forth by Shustorovich, chemisorption was used to observe energy profiles of surface reactions[30-32].

For a reaction

$$A + B \rightarrow AB$$
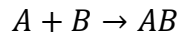
$$\Delta E^*_{A-B} = {Q_A Q_B}/{(Q_A + Q_B)}$$

Where ΔE^*_{A-B} is the activation barrier for the step and Q_i is the heat of chemisorption (this is also the binding energy) of species i. The pre-exponential factor was calculated using Plancks, h, and Boltzmann distribution constants, k_b, ideal gas constant , R, as well as the entropy of reaction, DS.

$$A = \frac{k_b T}{h} e^{DS/R}$$

The rate constant was calculated by using the Arrhenius equation:

$$k = A e^{-E_A/RT}$$

The reactions were kept within the laws of equilibrium by making use of the theoretical gibbs free energy of the reaction and its relationship with the forward/reverse rate constants:

$$K = e^{(DG/RT)}$$

$$k_r = {k_f}/{K}$$

All rate equations were hence represented in terms of a forward and reverse direction, where a_i is the activity of species i:

$$r = k_f a_A a_B - k_r a_C$$

Here we now have a model that only uses binding energies as the variable to be regressed, this greatly reduces the chances of establishing too many parameters. This work is ongoing as the model has not yet been used for regression.

6.4. Conclusion

A kinetic analysis of HDO activity over Pt requires a deep understanding of surface mechanisms. Homogeneous equations over Pt leads can lead to redundancy in extracting rate; while there may be multiple gas phase reactions that can occur, each of the reactions can be envisioned to pass through one pathway on a catalyst surface. In addition to a mandatory incorporation of surface species, a reaction model should also be able to take into account the species binding capabilities- the binding energies are directly correlated with the catalyst poisoning. The accuracy of a regression model is dependent on how parameters are used to constrain the model to experimental data, over-parameterization is common in these types of models, where values are distributed among parameters to attain a minimum that may not necessarily be the most accurate. A model was created taking advantage of theoretical correlations based on binding energies used to calculate activation barriers as well as the well established parameters such as enthalpies and entropies of formations; this left only binding energies of the species as the parameters left to be regressed. While the ordinary differential equations in the model converges, further investigation will be done towards carrying out actual regression to put forth accurate parameters.

6.5. References

1   Alonso, D. M., Wettstein, S. G. & Dumesic, J. A. Bimetallic catalysts for upgrading of biomass to fuels and chemicals. *Chemical Society Reviews* (2012).

2   Pritchard, J., Filonenko, G. A., Van Putten, R., Hensen, E. J. M. & Pidko, E. A. Heterogeneous and homogeneous catalysis for the hydrogenation of carboxylic acid derivatives: history, advances and future directions *Chemical Society Reviews* **44**, 3808 (2015).

3   Srifa, A., Faungnawakij, K., Itthibenchapong, V. & Assabumrungrat, S. Roles of monometallic catalysts in hydrodeoxygenation of palm oil to green diesel. *Chemical Engineering Journal 278*, 249-258 (2015).

4   Vardon, D. R. *et al.* Ru/Sn/Ac for the squeous phase reduction of succinic acidk to 1,4-butanediol under continuous process conditions. **7** (2017).

5   Haas, T., Jaeger, B., Weber, R., Mitchell, S. F. & King, C. F. Vol. 280 83-88 (Applied Catalysis A: General, 2005).

6   Lugo-José, Y. K., Monnier, J. R., Heyden, A. & Williams, C. T. Hydrodeoxygenation of propanoic acid over silica-supported palladium: effect of metal particle size. *Catalysis Science & Technology 4*, 3909-3916 (2014).

7   Lugo-José, Y. K., Monnier, J. R. & Williams, T. C. Gas-Phase, catalytic hydrodeoxygenation of propanoic acid, over supported group VIII noble metals: Metal and support effects. *Applied Catalysis A: General 469*, 410-418 (2014).

8   Behtash, S. *et al.* Solvation Effects in the Hydrodeoxygenation of Propanoic Acid over a Model Pd(211) Catalyst. *The Journal of Physical Chemistry* **120**, 2724-2736 (2016).

9   Primo, A., Concepción, P. & Corma, A. Synergy between the metal nanoparticles and the support for the hydrogenation of functionalized carboxylic acids to diols on Ru/TiO2. *Chemical Communications 47*, 3613-3615 (2011).

10   Maynar, H. G. *et al.* Highly selective and efficient hydrogenation of carboxylic acids to alcohols using titania supported Pt catalysts. *Chemical Communications 46*, 6279-6281 (2010).

11   Wang, S., Guo, Z., Cai, Q. & Guo, L. Vol. 45 138-143 (Biomass and Bioenergy 2012).

12   Chen, L. *et al.* Aqueous-phase hydrodeoxygenation of carboxylic acids to alcohols or alkanes over supported Ru catalysts. *Journal of Molecular Catalysis A: Chemical 351*, 217-227 (2011).

13   Gao, X., Heyden, A., Abdelrahman, O. A. & Bond, J. Q. Microkinetic analysis of acetone hydrogenation over Pt/SiO2. *Journal of Catalysis* **374**, 183-198 (2019).

14   Matera , S., Schneider , W. F., Heyden , A. & Savara, A. Progress in Accurate Chemical Kinetic Modeling, Simulations, and Parameter Estimation for Heterogeneous Catalysis. *ACS Catalysis* **9**, 6624-6647 (2019).

15   Lu, J., Faheem, M., Behtash, S. & Heyden, A. Theoretical investigation of the decarboxylation and decarbonylation mechanism of propanoic acid over a Ru(0001) model surface. *Journal of Catalysis* **324**, 14-24 (2015).

16   Lu, J., Behtash, S. & Heyden, A. Theoretical Investigation of the Reaction Mechanism of the Decarboxylation and Decarbonylation of Propanoic Acid of Pd(111) Model Surfaces. *Journal of Physical Chemistry C 116*, 14328-14341 (2012).

17   Wan , W. *et al.* Controlling reaction pathways of selective C–O bond cleavage of glycerol. *Nature Communications* **9**, 4612 (2018).

18   Vannice, M. A. & Sudhakar, C. A Model for the Metal-Support Effect Enhancing CO Hydrogenation Rates over Pt-Ti02. Catalysts. *Journal of Physical Chemistry* **88**, 2429-2432 (1984).

19   Vannice, M. A. The influence of MSI (metal-support interactions) on activity and selectivity in the hydrogenation of aldehydes and ketones. *Topics in Catalysis 4*, 241-248 (1991).

20   Sad, M. E., Neurock, M. & Iglesia, E. Formation of C–C and C–O Bonds and Oxygen Removal in Reactions of Alkanediols, Alkanols, and Alkanals on Copper Catalysts. *Journal of the American Chemical Society 133*, 20384–20398 (2011).

21   Gursahani, K. I., Alcalá, R., Cortright, R. D. & Dumesic, J. A. Reaction kinetics measurements and analysis of reaction pathways for conversions of acetic acid, ethanol, and ethyl acetate over silica-supported Pt. *Applied Catalysis: A General 222*, 369-392 (2001).

22   Peng, B. *et al.* Comparison of kinetics and reaction pathways for hydrodeoxygenation of C3 alcohols on Pt/Al2O3. *Catalysis Today 183*, 3-9 (2012).

23   Davis, M. E. & Davis, R. J. *Fundamentals of chemical reaction engineering*. (McGraw-Hill, 2002).

24   Rachmady, W. & Vannice, M. A. Acetic Acid Hydrogenation over Supported Platinum Catalysts. *Journal of Catalysis 192*, 322-334 (2000).

25   Mavrikakis, M. & Barteau, M. A. Oxygenate reaction pathways on transition metal surfaces. *Journal of Molecular Catalysis A: Chemical 131*, 135-147 (1998).

26   Alotaibi, M. A., Kozhevnikova, E. F. & Kozhevnikov, I. V. Deoxygenation of propionic acid on heteropoly acid and bifunctional metal-loaded heteropoly acid catalysts: Reaction pathways and turnover rates. *Applied Catalysis A: General 447-448*, 32-40 (2012).

27   Zhang, Y., Liu, D. & Chen, Z. Production of C2-C4 diols from renewable bioresources: new metabolic pathways and metabolic engineering strategies. *Biotechnology for biofuels* **10**, 299 (2017).

28   Abdelrahman, O. A., Heyden, A. & Bond, J. Q. Vol. 348   59-74 (Journal of Catalysis, 2017).

29   Ammal, S. C. & Heyden, A. Origin of the unique activity of Pt/TiO2 catalysts for the water–gas shift reaction. *Journal of Catalysis* **306**, 78-90 (2013).

30   Santen, v., R. A. On Shustorovich's bond-order conservation method as applied to chemisorption. *Recueil des Travaux Chimiques des Pays-Bas* **109**, 59-63 (1990).

31   Shustorovich, E. MAPPING OF SURFACE REACTIONS: A BOND-ORDER-CONSERVATION APPROACH. *Catalysis* (1987).

32   Shustorovich, E. Chemisorption phenomena: Analytic modeling based on perturbation theory and bond-order conservation. *Surface Science Reports* **6** (1986).

CHAPTER 7

Proposed Future Work

This dissertation highlighted the main issues associated with carboxylic acid hydrodeoxygenation over the supported noble metals, Pt and Ru, and also shown the avenues of future exploration. These metals in their supported monometallic states may never be able to transition into a practical large scale setting for succinic acid HDO towards targeted oxygenated products, but a strong foundation is essential for understanding these metals, and strategically improving its usefulness. Using bimetallic catalysts to improve oxygenate selectivity is not a new area of research, however, the understanding of why this takes place is not an area that has been fully developed. Upon meticulously comparing the activity of monometallic and bimetallic catalysts, more enhanced characterization techniques as well as the development of a microkinetic model are inevitable next step for demistifying the science behind adding promoter metals. We saw evidence of Sn having a large effect on the chemical adsorption capabilities of carbon monoxide on the platinum surface, this improved the selectivity of the catalyst, and it also improved then catalytic stability since it prevented the catalysts from being poisoned; in other words, the binding energies are what's truly affected which can only be resolved using microkinetic techniques[1]. Apart from a microkinetic model, the structure of the catalyst can also provide information on the nature of the metal-promoter interactions. High resultion TEM[2] as well as x-ray adsorption spectroscopy on a beamline light source[3] are techniques that have been popularly employed for probing the catalytst surface to observe how metals are adsorbed on a support as well as how different metals may interact.

Studies should then be done in aqueous media and observing the solvent effects on carboxylic HDO over bimetallic catalysts, work has already been done using aqueous phase hydrogenation of

levulinic acid[4] over monometallic Ru catalysts which highlighted reversible and irreversible deactivation of catalytic activity; it would be interesting to observe how these challenges would be affected by adding a promoter metal. Since we know that the oxophilic properties of the promoter metal is fundamentally behind its favorability, we are not confined to Sn as a promoter metal; other promoter metals may be explored with different particle size or charge strengths. Process optimization iterations would eventually lead to highly selective aqueous phase succinic acid HDO over bimetallic catalysts at low temperatures. This would eventually pave the way for a one pot method's of converting raw biofeedstocks directly to targed oxygenated products; anaerobic fermentation would convert the feedstocks to carboxylic acids, while the bimetallic catalysts would facilitate further transformation of the carboxylic acids to the desired compounds. This is the most practical scenatio for making bioderived chemicals faesible in the industrial landscape.

7.1. References

1   Matera , S., Schneider , W. F., Heyden , A. & Savara, A. Progress in Accurate Chemical Kinetic Modeling, Simulations, and Parameter Estimation for Heterogeneous Catalysis. *ACS Catalysis* **9**, 6624-6647 (2019).

2   Samad, J. E., Keels, J. & Regalbuto, J. R. A Comparison of Pt(II) and Pt(IV) Chloride Precursors for Strong Electrostatic Adsorption Synthesis of Pt/Alumina and Pt/Carbon Catalysts. **146**, 157-162 (2015).

3   Robert M. Palomino, E. S., Iradwikanari Waluyo, Yu-chen Karen Chen-Wiegart, Milinda Abeykoon, Jerzy T. Sadowski, Jose A. Rodriguez, Anatoly I. Frenkel & Sanjaya D. Senanayake. New In-Situ and Operando Facilities for Catalysis Science at NSLS-II: The Deployment of Real-Time, Chemical, and Structure-Sensitive X-ray Probes. *Synchrotron Radiation News* **30**, 30-37 (2017).

4   Omar Ali Abdelrahman, H. Y. L., Andreas Heyden, Yuriy Román-Leshkov, Jesse Q. Bond. Toward rational design of stable, supported metal catalysts for aqueous-phase processing: Insights from the hydrogenation of levulinic acid. *Journal of Catalysis* **329**, 10-21 (2015).

Vita

NAME OF AUTHOR:

Joshua Levi Emmanuel Judah Gopeesingh

PLACE OF BIRTH

Mount Hope, Trinidad and Tobago

DATE OF BIRTH

December 23, 1991

UNDERGRADUATE SCHOOLS ATTENDED

Hampton University, Hampton, Virginia USA

DEGREES AWARDED:

Bachelor of Science in Chemical Engineering 2014, Hampton University